Molecular responses of human lung epithelial cells to the toxicity of metal oxide nanoparticles

（金属酸化物ナノ粒子に対するヒト肺上皮細胞の毒性応答分子機構の解明）

Fei Zhuang

Graduate School of Life Science

Hokkaido University

September 2013

Molecular responses of human lung epithelial cells to the toxicity of metal oxide nanoparticles

（金属酸化物ナノ粒子に対するヒト肺上皮細胞の毒性応答分子機構の解明）

Fei Zhuang

A dissertation submitted in fulfillment of the requirement for the degree of
Doctor of Life Science

Graduate School of Life Science
Hokkaido University
北海道大学

September 2013

CONTENTS

Chapter 1 General Introduction

1.1 Health Risk of Particulate Matter

All the stories began from the occurrence of the London Smog and its a few precedents. The smog disaster led to 12 000 additional deaths over several days with the sharp increase in concentration of air pollutants in London in 1952 (GREAT LONDON SMOG) [1], similar pollution incidents resulted in 60 person deaths in the Meuse valley of Belgium in 1930 [2], and 20 person deaths in 1948 in the Donora and Webster Hollow area of United States [3]. These tragic events reshaped the view on air pollution, spurred the government regulatory agencies and scientific community to explore the potential lethal pollution, the immediate investigations confirmed associations between short-term exposure to suddenly increasing air pollution and the abnormal mortality, just as the "1954 Report" suggested that the SMOG impose adverse effects on the individuals who were on the brink of death already. However seldom assessments addressing the potential health risk of persisting suspend particulate matters exposure on the public health until 50 years later when the studies largely were able to rule out sulphur dioxide, NO_2 and ozone pollution as the cause of the observed deaths and the weak association between SO_2, NO_2 and the mortality is difficult to separate from the co-pollutant, the air borne particulate matters [4].

Though human beings have been exposed to airborne particulate matter (PM) throughout their evolution, the naturally happened particles such as volcanic lava, forest fire and smoke never had attracted so many concerns. Since the GREAT LONDON SMOG, studies have reported associations between the mortality and the air pollution concentrations in many locations [5]. However late to the end of the 20 century, extensive epidemiology studies on the relationship of daily mortality and the air pollution confirmed the consistent association between the mortality and the airborne particulate matters in the air even at low concentration [6-9], and even the contribution of the particles to the mortality in the GREAT SMOT was

identified by analyzing the archival autopsy lung tissues [10]. As reported by the Harvard School of public health, U.S. EPA, the Johns Hopkins University School of Hygiene and Public Health, the London school of Hygiene and tropical medicine and Brigham Young University, the particulate air pollutants were correlated with the mortality in DETROIT, Los Angeles, London, Czech, Utah Valley and Santa Clara, a bit independently with the acidity of the particles [11]. Also in the Harvard Six Cities Study, it was demonstrated that the residents in the cities with the lowest PM levels had a survival rate roughly 2 years longer than those living in the cities with the high PM levels [12]. These results were confirmed by the American Cancer Society cancer prevention study II with a much larger study population (1200 000 adults). Following the subsequent promulgation of a new national PM standard [U.S. Environmental Protection Agency (U.S. EPA)], and a challenge to that standard by the American Trucking Association (American Trucking Associations Inc.v. United States Environmental Protection Agency 1999), these results came under considerable scrutiny. Recent concerns focus upon epidemiological studies that show an increase in mortality of 0.2% (United States) to 0.6% (Europe) for each 10 $\mu g/m^3$ increase in PM10 [13].

1.2 Nanoparticles and Health Hazard

1.2.1 Classification of particulate matter

Particle size is a vital consideration when it comes to air pollution and health. Particles greater than 10 μm mean aerodynamic diameters have short atmospheric lifetime and are removed in the upper airways and are not the focus of health concerns. In practical terms, the particles smaller than 10 μm (PM10) in diameter can penetrate in to the lower respiratory system are called thoracic particles. As particle size decreases, deposition occurs deep in the respiratory tract. The particles smaller than 2.5 μm (PM2.5) can penetrate into the gas-exchange region of the lung are called respiratory particle; the particles smaller than 0.1 μm (PM0.1) are thought to be able to penetrate the air-blood barriers are called ultrafine particles, nanometer particles or nanoparticles.

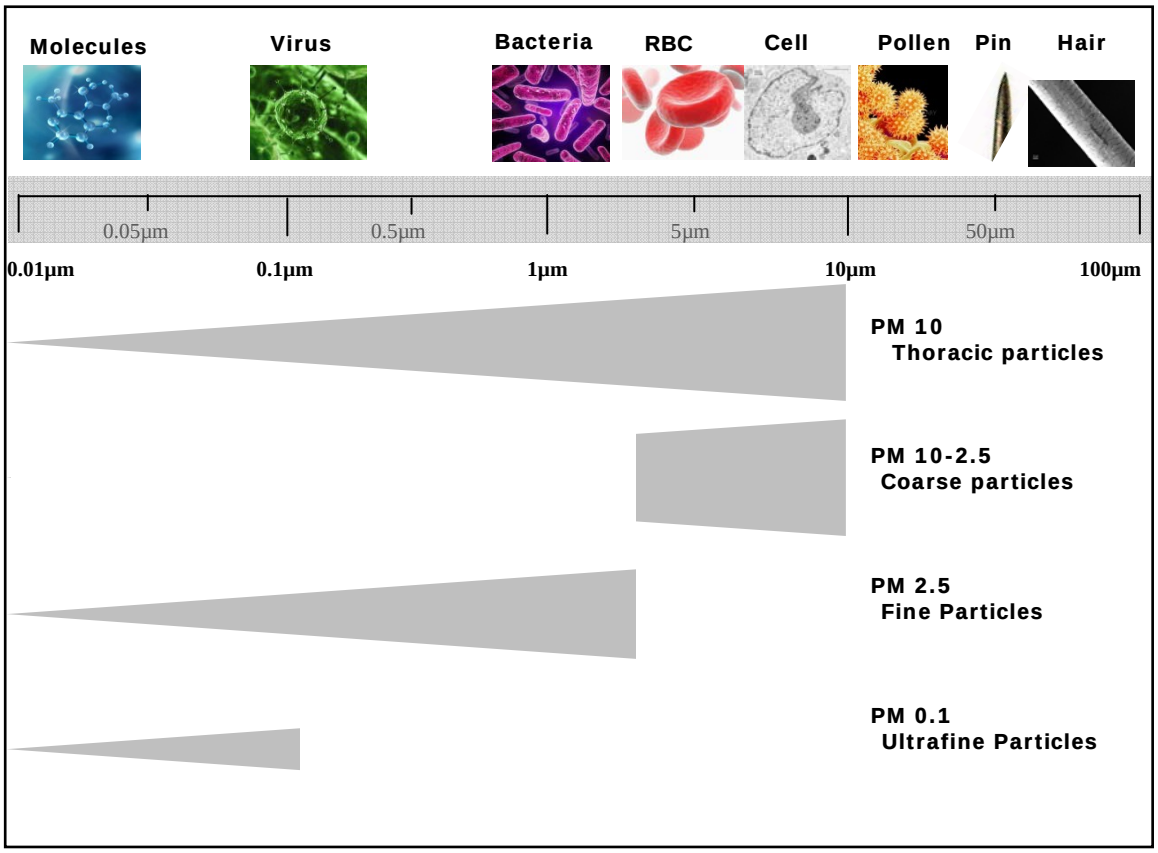

Figure 1.1 Classification of the airborne particles in terms of the particle diameters and the depth they can reach.

As the U.S. National Research Council reported that measuring the particles by weight without regard to particle size, has little utility for judging effects [14], the ultrafine particles contribute little to particle mass but are most abundant in terms of numbers and offer a very large surface area, with increasing degrees of lung penetration. While, ultrafine particles are found to a large extent in urban air as both singlet and aggregated particles, and indeed are the predominant particle size by number in urban PM10, although they contribute modestly to mass. For example, Wichmann et al. summarized the data of Erfurt area between 1995 and 1998, as followings [15]. It indicated whilst 97% of the particle mass was found in the components PM0.1, this constitutes only 12% of the particle numbers, while the ultrafine particle contribute to 88% of the particle number but just 3% of the particle mass.

Table 1.1 Number and mass contribution of different sized particles

Size (μm)	Contribution	
	Number	**Mass**
Ultrafine particles NC0.01-0.03 NC0.03-0.05 NC0.05-0.1	88%	3%
Fine particles MC0.1-0.5 MC0.5-1.0 MC1.0-2.5	12%	97%
Total ultrafine and fine particles 0.01-2.5	100%	100%
Coarse particles PM10-2.5 TSP-PM10	--- ---	20% 30%

The concentration of ultrafine and fine particles to number and mass in the size range of 0.01-2.5 μm and contribution of coarse particles to mass of total aerosol size distribution.

1.2.2 Term of "Nanoparticle"

The terms "ultrafine particles" was used by some aerosol scientists during a 1979 Workshop on Ultrafine Aerosols in Vienna. Ultrafine particles were defined at that time as those characterized by particle diameters < 0.1μm. The U.S. EPA used the term "ultrafine particles in a biological context" to characterize particle size distributions with mass median diameter below about 0.1μm (U.S. EPA, 1996).

Thus, the UFP and nanoparticles are concurrently used for a period of time to refer to the particle matter with diameter between 1 and 100 nanometers. The reason for this double name of the same object is that, during the 1970-80's, the first thorough fundamental studies with "nanoparticles" were underway in the USA and Japan [16], (within an ERATO Project) they were called "ultrafine particles (UFP) ".

However, with the production of nanostructure materials becoming an exciting new area for the materials industry, it is the topic of several recent symposia and workshops (e.g. Third International Conference on Nanostructured Materials, 1996: Joint NSF/JSPS U.S.-Japan Workshop on Nanoparticle Synthesis and Applications, 1996), bringing together researchers

from the aerosol and materials communities to investigate new production and evaluation methods. When the National Nanotechnology Initiative was launched in the USA, the new name, “nanoparticle” had become fashionable and the NNI adopt the term nanoparticles, further the new term nanoparticles were extensively used in toxicological and material science [17].

Hereafter we use the term “nanoparticles (NPs)” to refer to the airborne particulate matters whose diameters fall between 1 nm to 100 nm.

1.2.3 Health hazard of nanoparticles

Accompanying the concerns turning to the dominant proportion of the UFPs in the particulate pollutant and they were associated with adverse health effects reported in epidemiologic studies and *in vivo* researches, such as increased use of medication for asthma, attacks of asthma in patients with pre-existing asthma, attacks of chronic obstructive pulmonary disease, admission to hospital for cardiovascular causes, deaths from heart attacks, deaths from strokes, deaths from respiratory causes and else adverse health effects[18-22].

Early in 1990, Paula et al. reported the deposition of ultrafine particles in respiratory tract found in the subjects with obstructive or restrictive lung disease [23]. Yeh et al. also found that singlet particles with aerodynamic diameter down to 10 nm deposit readily in the air ways and centriacinar regions of the lung and those pathological changes in the lungs such as the airway narrowing found in COPD and asthma cause an increase in the efficiency of deposition of nanoparticles. Then Peters et al. reported that decrement in evening peak flow in a group of asthmatic patients was best associated with the ultrafine component of the airborne particles during an episode of severe air pollution [24].

Results on direct effects of nanoparticles and model UFPs have been reported from epidemiologic studies and controlled clinical studies in humans, inhalation/instillation studies in rodents, or in vitro cell culture systems. For example, several epidemiological studies have found associations of ambient UFPS with adverse respiratory and cardiovascular effects resulting in morbidity and mortality in susceptible parts of the population [15, 24-28], whereas other

epidemiological studies have not seen such associations [25, 29]. Controlled clinical studies evaluated deposition and effects of laboratory-generated UFPs. High deposition efficiencies in the total respiratory tract of healthy subjects were found, and deposition was even greater in subjects with asthma or chronic obstructive pulmonary disease. In addition, effects on the cardiovascular system, including blood markers of coagulation and systemic inflammation and pulmonary diffusion capacity, were observed after controlled exposures to carbonaceous UFPs [15, 23, 30-36].

Studies in animals using laboratory generated model UFPs or ambient UFPs showed that UFPs consistently induced mild yet significant pulmonary inflammatory responses as well as effects in extrapulmonary organs. Animal inhalation studies included the use of different susceptibility models in rodents, with analysis of lung lavage parameters and lung histopathology, effects on the blood coagulation cascade, and translocation studies to extrapulmonary tissues [37-54].

1.3 Lung Deposition and Clearance of Nanoparticles

The main mechanism for deposition of inhaled NPs in the respiratory tract is diffusion due to displacement when they collide with air molecules. Other deposition mechanisms of importance for larger particles, such as inertial impaction, gravitational settling, and interception, do not contribute to nanoparticles deposition and electrostatic precipitation occurs only in cases where nanoparticles carry significant electric charges.

The pulmonary deposition of particles matter has been simplified as follows: particulates with diameter more than 5 um will deposit in the upper airways (nose and trachea), smaller particles will also deposit deeper in the airways, and those with diameter less than 2.5 um can travel down to the alveoli. The deposition of nanoparticles has been found to be able to target all three regions of the respiratory tract. Particles with a size between 10 and 50 nm are deposited mainly in the alveoli, smaller and larger ones are more efficiently deposited in the

higher regions [55-57].

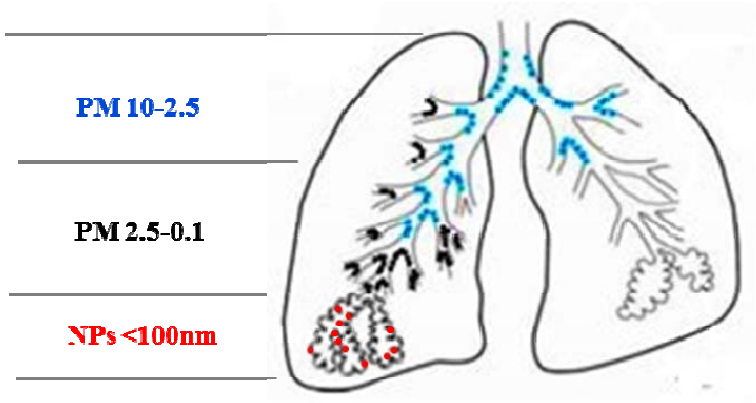

Figure 1.2 Deposition of particulate matter in the lungs.

The classical clearance of deposited particles in the respiratory tract depend on the chemical and physical two processes. The chemical dissolution is directed at biosoluble particles or components of particles that are either lipid soluble or soluble in intracellular and extracellular fluids. Solutes and soluble components can then undergo absorption and diffusion of binding to proteins and other subcellular structures and may be eventually cleared in to blood and lymphatic circulation.

The most prevalent mechanism for solid particle clearance in the alveolar region is mediated by alveolar macrophages, through phagocytosis of deposited particles. The success of macrophage-particle encounter appears to be facilliated by chemotactic attraction of alveolar macrophages to the site of particle depposion [58]. The chemotactic signal is most likely complement protein 5a (C5a), derived from activation of the complement cascade from serum proteins present on the alveolar surface [59-60]. In the case of acute exposure, the phagocytosis is followed by gradual movement of the macropages with internalized particles toward the mucociliary escalator. However in the long-term exposure, the phagocytosis results in activation of macrophages and induces the release of chemokines, cytokines, reactive oxygen species and

other mediators. Chronic stimulation of macrophages can result in sustained inflammation and progress to lung damage [61-62].

In vivo (rat) studies revealed only approximately 20% of nanosized 15-20 nm and 80 nm particles could be lavaged with the macrophages. It indicated that nanoparticles were in epithelial cells or had further translocated to the interstitium [38, 41, 43, 47, 50].

1.4 Translocation of Inhaled Nanoparticles

As discussed above, about 80% of the inhaled NPs appear to translocate readily to extra-pulmonary sites and reach other target organ by different transfer routes and mechanisms. The prevalent pathway involves transcytosis across epithelia of the respiratory tract into the interstitium and access to the blood circulation directly or via lymphatics, resulting in distribution throughout the body. Some studies also revealed another not generally recognized route, the uptake by sensory nerve endings embedded in airway epithelia, followed the translocation by axonal to ganglionic and CNS.

1.4.1 Translocation to lung interstitium

The studies (rat) with ultrafine PTFE fumes exposure revealed that the particles could be found in interstitial and submucosal sites of the airways as well as in the interstitium of the lung periphery. Thus Oberdorster et al. supposed that instead phagocytosis, once deposited, most of nanoparticles were expected to interact with the epithelial cells [38]. Instead of the inefficient nanoparticles phagocytosis the interstitium translocation also was seemed to be another inflammation eliminating of the alveolar space, while it shifted the inflammation to the interstitium sites [47]. Because the interstitium traslocation of nanoparticles also was identified in dogs, nonhuman primates than in rodents the high translocation of nanoparticles in human was also assumed reasonable [63].

1.4.2 Translocation to circulatory system

The uptake into the blood circulation and lymphatic pathways can be inferred on the basis of the reports on the interstitium translocation. Early in 1977 Berry et al. [64] found large amounts of 30 nm gold particles in platelets of pulmonary capillaries 30 min later they instilled into the rat, the researchers suggest induce to platelet aggregation with formation of microthrombi athermanous plaques. Since then, a number of studies with different particle types have confirmed the existence of this translocation pathway, and indicated that particle size and surface chemistry (coating), and possibly charge, govern translocation across epithelial and endothelial cell layers [43, 65-67].

The transcytosis involved in the circulatory translocation was reported mediated by an albumin-binding protein, named caveolin-1 and a phospholipid named lecithin by many studies [65-66, 68-69]. Therefore, the albumin and phospholipids in alveolar epithelial lining fluid may be important for facilitating epithelial cell uptake of nanoparticles after deposition in the alveolar space. Rejman [70] supposed that this facilitating mechanism is especially important for the nonphagocytic cells in the nanoparticles uptake, in which case the caveolae became the predominant pathway. The nanoparticles uptake mechanism was in agreement with that of biological nanoparticles, the viruses [71], the knowledge from virology was then expected to shed light on the further nanoparticles research.

The studies in humans showed more complicated translocation mechanisms of inhaled nanoparticles [45]: found rapid appearance in the blood and significant accumulation of 20 nm carbon particles; whereas Brown et al. [31] reported the contrary results with the same particles. It was explained as that except for the particle size, the extrapulmonary translocation is highly governed by particle surface characteristics/chemical.

The circulation translocation and the following system distribution through the circulation also make the nanoparticles come under the suspicion of adverse effect on the other organs, such as heart, liver, spleen and even CNS. Translocation to the blood circulation could

provide an explanation for epidemiologic findings of cardiovascular effects associated with inhaled ambient UFPs and for the results of clinical studies showing vascular responses to inhaled UFPs [36, 72]. Except the lung-close heart, also the spleen, bone marrow and CNS are the target of the nanoparticles [73-78]. The surface modifications can facilitate the target-specific properties, which made engineered nanoparticles be a promising drug delivery method [79-81].

1.4.3 Neuronal uptake and translocation

That the 30 nm polio virus bio-nanopparticles was neuronal uptake and translocation by sensory nerve endings of the olfactory and the trigeminus nerves and an intricate network of sensory nerve endings in the he nasal and tracheobronchial regions was described about 60 years ago by the toxicologists [82].

Intranasal instilled 50 nm nanoparticles were observed to translocate in the axons of the olfactory nerves to the olfactory bulbs, even cross synapses in the olfactory glomerulus to reach mitral cell dendrites in squirrel monkeys [83]. The results of recent studies also support that the olfactory and trigeminus nerve should be considered a portal of entry to the CNS for humans under conditions of environmental and occupational exposures to airborne nanoparticles [84-91].

These studies also explain the potential mechanism of CNS effects of airborne particulate pollutant, especially the nanoparticles. Both Campbell and Calderon [92-93] found increase inflammatory or neurodegenerative changes in the olfactory muscosa, olfactory bulb and cortical and subcortical brain structures in animal experiments.

1.5 New Challenges from Engineered Nanoparticles

We have discussed the evolution of the toxicity research on airborne nanoparticles during the past 60 years, from the events brought about the original concern on the health risk of air pollution, to the findings indicating that the airborne nanoparticles in the air pollution was identified as a determinant of the adverse health effects, and their local deposition and systemic distribution. All these specific properties and the extra risks of nanoparticles than their bulk

counterpart are thought as conferred by the small size and corresponding large specific surface area.

The importance of surface area becomes evident when considering that surface atoms or molecules properties [94]; the ratio of surface to total atoms or molecules increases exponentially with decreasing particle size. Increased surface reactivity predicts that nanoparticles exhibit greater biological activity per given mass compared with larger particles, should they be taken up into living organisms and provided they are solid rather than solute particles. This increased biologic activity can be either positive or desirable (e.g. antioxidant activity, carrier capacity for therapeutics, penetration of cellular barriers for drug delivery) or negative and undesirable (e.g. toxicity, induction of oxidative stress or of cellular dysfunction) or a mix of both. Not only may adverse effects be induced, but interactions of nanoparticles with cells and subcellular structures and their bio-kinetics are likely to be very different from those of larger-sized particles. For example, more than 60 years ago virologists described the translocation of 30 to 50 nm sized virus particles along axons and dendrites of neurons and across epithelia [82], whereas first reports about increased inflammatory activity and epithelial translocation of manmade 20 and 30 nm solid particles appeared only more recently [95-96].

The characteristic bio-kinetic behaviors of nanoparticles are attractive qualities for promising applications in medicine as diagnostic and therapeutic devices and as tools to investigate and understand molecular processes and structures in living cells [72, 79, 97-98]. For example, targeted drug delivery to tissues that are difficult to reach (e.g., central nervous system CNS), nanoparticles for the fight against cancer, intravascular nano-sensor and nano-robotic devices, nanoparticles for diagnostic and imaging procedures are presently under development. The discipline of nano-medicine defined as medical application of nanotechnology and related research has arisen to design, test and optimize these applications so that they can eventually be used routinely by physicians [99].

However, in apparent contrast to the many efforts aimed at exploiting desirable

properties of nanoparticles for improving human health are the limited attempts to evaluate potential undesirable effects of NPs when administered intentionally for medicinal purposes or after unintentional exposure during manufacture or processing for industrial applications. The same properties that make NPs so attractive for development in nano-medicine and for specific industrial processes could also prove deleterious when NPs interact with cells. Thus, evaluating the safety of NPs should be of highest priority given their expected worldwide distribution for industrial applications and the likelihood of human exposure, directly or through release into the environment (air, water and soil).

Though in the same size scale (1-100 nm), the engineered nanoparticles have their specific properties compared with the conventional air borne pollutant nanoparticles. The traditional air borne nanoparticles produces by the fossil fuel and the combustions, they always have a carbon core coating by the organic chemical components with different sizes, while the engineered nanoparticle of one genre share the same component and size.

Table 1.2 Comparison of naturally occurred ultrafine particles and engineered nanoparticls.

	Nano dimension	**Chemical /physical characterization**	**Exposure pathway**	**potential toxicological mechanism**
Ultrafine particles	Sharing the many similarities on the extensive specific surface area and hydrokinetics	Chemical heterogeneity Physical polydisperse	Respiratory tract	Organic carbon and polycyclic aromatic hydrocarbon (PAH) content impose oxidative stress to biological system, and the finer is the particle, the higher is the content of organic carbon and PAH, the more toxic.
Engineered nanomaterials		Chemical homogeneity Physical mondisperse	Respiratory Skin Injection Digestive tract Intervention operation And so on	The extensive surface area provide bioactivity reactive surface, the residue exposed on the surface reacte with the residue of plasma membrane or other active biomolecular.

The detail comparison is summarized in the Table 2. In the sense of chemical components and physical disperse, once exposed to the engineered nanoparticles, it means much higher concentration exposure than the combustion and higher bioactivity risk. However in the sense of genre, the airborne pollutant nanoparticles have limited genre the engineered nanoparticles have been developed many genres with the development of nanotechnology. Also, due to the multifarious properties, the engineered nanoparticles can be inferred to have the specific toxicology mechanism respectively. The recent achievements on the nanotoxicities are summaries according to the particles genres.

1.6 Health Risk of Widely Applied Nanoparticles

Carbon nanoparticles, with their unique one-dimensional hollow nanostructure and unusual properties, are emerging as an important new class of multifunctional building blocks for the development of nanotechnology. The number of industrial scale facilities for the relatively low-cost production of multi-walled carbon nanotubes (MWCNTs) continues to grow, and therefore, professional and public exposure to MWCNTs is expected to increase significantly in the coming years.

Several research groups have examined the uptake and potential hazards of CNTs, particularly MWCNTs, to humans and other biological systems. Dumortier et al. [100] demonstrated that water-soluble CNTs functionalized with polyethylene glycol chains did not have toxic effects when tested in a wide variety of immune system cells. However, it has been demonstrated that CNTs can induce inflammatory and apoptosis responses in human T cells [101-103]. Gene expression analysis by Ding et al. [101] indicated that MWCNTs activated genes involved in cellular transport, metabolism, cell cycle regulation and stress response in human skin fibroblasts. Magrez et al. [104] found evidence of cytotoxicity for carbon nanoparticle, although MWCNTs were the least toxic among the carbon nanotubes. Zhu et al. [105] found that MWNTs could accumulate and induce apoptosis in mouse embryonic stem cells and activate the

tumor suppressor protein p53 up-regulated the expression of base excision repair protein, double strand break repair protein. Jia et al. [105-106] suggested that the cytotoxicity apparently follows a sequence on a mass basis: SWCNTs > MWCNTs > quartz > C60 in *in vitro* study.

Siliva et al. [107] demonstrated that ultrafine carbon particles show greater lung penetration and are able to cross the blood-brain barrier and impact on the central nervous system rather than release clotting agents from the lungs. Lam et al. [108] have reported the SWCNT clump together into bundles and produce pulmonary inflammation together in mice.

Quantum dots (QDs) are nanocrystals containing 1 000 to 100 000 atoms. With unique optical and electrical properties, QDs are promising in optimal fluorophores for biomedical imaging [109-116].

Zhang et al. [117] have shown that skin penetration is one of the major routes into biological system for QDs. Lovric [118] found that Mercaptopropionic acid coated CdTe QDs in less toxic than its non-coated counterpart. However Trolox et al. [119] though that the cytoxicity should be attributed to the coating materials rather than the core metalloid complexitself. Shiohara et al. [120] have also observed the QD-induced cytotoxicity. Deufus et al. [121] think the cytotoxicity of CdSe-core QDs is conditional. Additionally, recent researches concluded that the cytotoxicity of QDs can be modulated by processing parameters during synthesis, exposure to ultraviolet light, and surface coating and that cytotoxicity correlates with the liberation of free Cd^{2+} ions due to deterioration of the CdSe lattice.

Each individual type of QD possesses its own unique physicochemical properties, which in turn determines its potential toxicity and as a result, there are discrepancies in the current literature regarding the toxicity of QDs7-87 [117-119, 121-129]. Rouse et al.[125] also have investigated the effects of applied strain on QDs uptake by human epidermal keratinocytes (HEK). Mortensen et al. [130] furtherlly demonstrated QDs skin penetration by employing an in vivo semiconductor QDs model system. Gopee et al. [129] have demonstrated that regional lymph nodes, liver, kidney and spleen are sentinel organs for the detection of QDs skin penetration.

Metallic nanoparticles are among the most widely used types of engineered nanomaterials; however, little is known about their environmental fate and effects.

Chithrani et al. [131] demonstrated that kinetics and saturation concentrations of gold nanoparticles are highly dependent on the physical dimensions of the nanoparticles. Connor et al. [132] Goodman et al. [133] reported that gold nanoparticles with a variety of surface modifiers are not inherently toxic to human cells, despite being taken up into cells. Wang et al. investigated shape and size dependent cellular uptake and cytotoxicity of gold nanomaterials on human skin HaCaT keratinocytes [134]. Gold nanomaterials can penetrate through human skin HaCaT keratinocytes easily and can accumulate in the cell nucleus. Pernodet et al. [135] suggested though without cytotoxicity, the particles did apparently promote the formation of abnormal actin filaments, which led to decreases in cell proliferation, adhesion and motility as discussed.

Carlson et al. [136] reported size dependent cellular interactions of silver nanoparticles mediated, which is thought to be mediated through oxidative stress. Lu et al. [137] found no difference in cell viability between cells treated or not treated with silver nanoparticles of different sizes to human skin keratinocyte cells. However Griffitt et al. [138] and Asharani et al. [139] found the cytotoxicity of silver nanoparticles in zebrafish, daphnids, and an algal species. The studies of Benn et al. [140] suggest that the potential toxicity of nano silver in brough about by the released silver ions.

What have to be taken into consider in research on the metal nanoparticles is the coating articles. Wang et al. [141] have demonstrated the Hexadecylcetyltrimethylammonium bromide (CTAB), a coating materials of nanometal was highly cytotoxic. Similarly, the coating material, poly-ethylene glycol also was demonstrated toxic by Niidome et al [142].

Metal oxide nanomaterials are important industrial materials widely used as additives in cosmetics, pharmaceuticals and food colorants and humans are more likely to be exposed occupationally or via consumer products and the environment.

Grassian et al. [143] reported inhalation TiO_2 nanoparticles exposure study in mice, and the results indicated anoparticles aggregate to form aerosol particles in the exposure chamber and showed a significant but modest inflammatory response. Jin et al. [144] demonstrated after exposed to TiO_2, there is a significant increase in oxidative stress in L929 cells. Park et al. [145] reported the cytotoxicity of TiO_2 nanoparticles with the induction of ROS in cultured BEAS-2B cells and the expressions of oxidative stress-related genes including heme oxygenase-1 or inflammation-related genes including IL-8 were increased.

Cozzoli et al. [146] evaluated a human mesothelioma and a rodent fibroblast cell line for in vitro cytotoxicity tests using seven industrially important nanoparticles. The result shows nanoparticle-specific cytotoxic mechanism for uncoated iron oxide and partial detoxification or recovery after treatment with zirconia, ceria or titania. The investigation of Karlsson et al. [147] on CuO, TiO_2, ZnO, $CuZnFe_2O_4$, Fe_3O_4 and Fe_2O_3 showed that there was a high variation among different nanoparticles concerning their ability to cause toxic effects. CuO nanoparticles were the most potent regarding cytotoxicity and DNA damage. ZnO showed effects on cell viability as well as DNA damage, whereas the TiO_2 particles (a mixture of rutile and anatase) only caused DNA damage. For iron oxide particles (Fe_3O_4, Fe_2O_3), no or low toxicity was observed, but $CuZnFe_2O_4$ particles were rather potent in inducing DNA lesions. Xia et al. [148] reported that ZnO induced toxicity in, leading to the generation of ROS, oxidant injury, excitation of inflammation and cell death. In contrast, CeO_2 nanoparticles were taken up by BEAS-2B and RAW 264.7 cells, without inflammation or cytotoxicity. CeO_2 also suppressed ROS production and induced cellular resistance to exogenous source of oxidative stress.

1.7 Research Objective

The rapidly developing field of nanotechnology is likely to become another source for human exposures to nanoparticles-engineered nanoparticles mainly by the route of inhalation (respiratory tract). The small size and corresponding large specific surface area of solid nanoparticles confer specific properties of them, for example, making them desirable as catalysts for chemical reactions. The ratio of surface to total atoms or molecules increases exponentially with decreasing particle size. Increased surface reactivity predict that nanoparticles exhibit greater biologic activity per given mass compared with larger particles, should they be taken up into living organisms and provided they are solid rather than solute particles. This increased biologic activity can be either positive or desirable (e.g., antioxidant activity, carrier capacity for therapeutics and penetration of cellular barriers for drug delivery) or negative and undesirable (e.g., toxicity and induction of oxidative stress or of cellular dysfunction) or a mix of both. Not only may adverse effects be induced, but interactions of nanoparticles with cells and subcellular structures and their biokinetics are likely to be very different from those of larger-sized particles.

A popular hypothesis on the toxicological mechanism of nanoparticles suggested that ROS can be used as the evaluating standard of engineered nanoparticles, since it has been demonstrated as the predominant toxicant production of combustion and diesel exhaust in the health hazard. But there are great discrepancies on the mechanism of engineered nanoparticles for the different chemical components and different morphology though the same component. This study is to identify the role of ROS in the toxicity of metal oxide nanoparticles. We examined a series of metal oxide nanoparticles, and found copper oxide nanoparticles are the toxic one among them and zinc oxide nanoparticles have the most complicated toxic behavior. Thus, we use the global gene analysis technology to examine the whole gene change in the exposure to the CuO-NPs and ZnO-NPs, to clarify the toxicological mechanism of them.

1.8 References

1. Bell M. L.; Davis D. L. Reassessment of the lethal London fog of 1952: Novel indicators of acute and chronic consequences of acute exposure to air pollution. *Environ Health Perspect* **2001**, *109*, 389-394.

2. Nemery B.; Hoet P. H. M.; Nemmar A. The Meuse Valley fog of 1930: an air pollution disaster. *Lancet* **2001**, *357*, 704-708.

3. Air pollution in Donora. *Jama-J Am Med Assoc* **1949**, *139*, 1122-1122.

4. Sawyer R. F. Science based policy for addressing energy and environmental problems. *P Combust Inst* **2009**, *32*, 45-56.

5. Mazumdar S.; Schimmel H.; Higgins I. T. Relation of daily mortality to air pollution: an analysis of 14 London winters, 1958/59-1971/72. *Arch Environ Health* **1982**, *37*, 213-20.

6. Pope C. A.; Burnett R. T.; Thun M. J.; Calle E. E.; Krewski D.; Ito K.; Thurston G. D. Lung cancer, cardiopulmonary mortality, and long-term exposure to fine particulate air pollution. *Jama-J Am Med Assoc* **2002**, *287*, 1132-1141.

7. Araujo J. A. Particulate air pollution, systemic oxidative stress, inflammation, and atherosclerosis. *Air Qual Atmos Health* **2010**, *4*, 79-93.

8. Donaldson K.; Gilmour M. I.; Macnee W. Asthma and PM10. *Respir Res* **2000**, *1*, 12-5.

9. Panis L. I.; De Geus B.; Vandenbulcke G.; Willems H.; Degraeuwe B.; Bleux N.; Mishra V.; Thomas I.; Meeusen R. Exposure to particulate matter in traffic: A comparison of cyclists and car passengers. *Atmos Environ* **2010**, *44*, 2263-2270.

10. Hunt A.; Abraham J. L.; Judson B.; Berry C. L. Toxicologic and epidemiologic clues from the characterization of the 1952 London smog fine particulate matter in archival autopsy lung tissues. *Environ Health Perspect* **2003**, *111*, 1209-1214.

11. Samet J. M.; Dominici F.; Curriero F. C.; Coursac I.; Zeger S. L. Fine particulate air pollution and mortality in 20 US cities, 1987-1994. *New Engl J Med* **2000**, *343*, 1742-1749.

12. Dockery D. W.; Pope C. A.; Xu X. P.; Spengler J. D.; Ware J. H.; Fay M. E.; Ferris B. G.; Speizer F. E. An association between air-pollution and mortality in 6 United-States cities. *New Engl J Med* **1993**, *329*, 1753-1759.

13. Dominici F.; Mcdermott A.; Zeger S.; Samet J.; Bell M. Time-series analysis of ozone and mortality in 95 US cities using a Bayesian hierarchical model. *Epidemiology* **2004**, *15*, S60-S60.

14. Dockery D. W.; Pope C. A. Acute respiratory effects of particulate air-pollution. *Annu Rev Publ Health* **1994**, *15*, 107-132.

15. Wichmann H. E.; Spix C.; Tuch T.; Wolke G.; Peters A.; Heinrich J.; Kreyling W. G.; Heyder J. Daily mortality and fine and ultrafine particles in Erfurt, Germany part I: role of particle number and particle mass. *Res Rep Health Eff Inst* **2000**, 5-86; discussion 87-94.

16. Granqvist C. G.; Buhrman R. A. Log-normal size distributions of ultrafine metal particles. *Solid State Commun* **1976**, *18*, 123-126.

17. Kiss L. B.; Soderlund J.; Niklasson G. A.; Granqvist C. G. New approach to the origin of lognormal size distributions of nanoparticles. *Nanotechnology* **1999**, *10*, 25-28.

18. Donaldson K.; Stone V.; Seaton A.; Macnee W. Ambient particle inhalation and the cardiovascular system: Potential mechanisms. *Environ Health Perspect* **2001**, *109*, 523-527.

19. Riedl M. A. The effect of air pollution on asthma and allergy. *Curr Allergy Asthm R* **2008**, *8*, 139-146.

20. Peden D. B. The epidemiology and genetics of asthma risk associated with air pollution. *J Allergy Clin Immun* **2005**, *115*, 213-219.

21. Patel M. M.; Miller R. L. Air pollution and childhood asthma: recent advances and future directions. *Curr Opin Pediatr* **2009**, *21*, 235-242.

22. Li N.; Harkema J. R.; Lewandowski R. P.; Wang M. Y.; Bramble L. A.; Gookin G. R.; Ning Z.; Kleinman M. T.; Sioutas C.; Nel A. E. Ambient ultrafine particles provide a strong adjuvant effect in the secondary immune response: implication for traffic-related asthma flares. *Am J Physiol-Lung C* **2010**, *299*, L374-L383.

23. Anderson P. J.; Wilson J. D.; Hiller F. C. Respiratory-tract deposition of ultrafine particles in subjects with obstructive or restrictive lung-disease. *Chest* **1990**, *97*, 1115-1120.

24. Peters A.; Doring A.; Wichmann H. E.; Koenig W. Increased plasma viscosity during an air pollution episode: A link to mortality? *Lancet* **1997**, *349*, 1582-1587.

25. Pekkanen J.; Timonen K. L.; Ruuskanen J.; Reponen A.; Mirme A. Effects of ultrafine and fine particles in urban air on peak expiratory flow among children with asthmatic symptoms. *Environ Res* **1997**, *74*, 24-33.

26. Peters A.; Wichmann H. E.; Tuch T.; Heinrich J.; Heyder J. Respiratory effects are associated with the number of ultrafine particles. *Am J Resp Crit Care* **1997**, *155*, 1376-1383.

27. Penttinen P.; Timonen K. L.; Tiittanen P.; Mirme A.; Ruuskanen J.; Pekkanen J. Ultrafine particles in urban air and respiratory health among adult asthmatics. *Eur Respir J* **2001**, *17*, 428-35.

28. Von Klot S.; Wolke G.; Tuch T.; Heinrich J.; Dockery D. W.; Schwartz J.; Kreyling W. G.; Wichmann H. E.; Peters A. Increased asthma medication use in association with ambient fine and ultrafine particles. *Eur Respir J* **2002**, *20*, 691-702.

29. Tiittanen P.; Timonen K. L.; Ruuskanen J.; Mirme A.; Pekkanen J. Fine particulate air pollution, resuspended road dust and respiratory health among symptomatic children. *Eur Respir J* **1999**, *13*, 266-273.

30. Pekkanen J.; Peters A.; Hoek G.; Tiittanen P.; Brunekreef B.; De Hartog J.; Heinrich J.; Ibald-Mulli A.; Kreyling W. G.; Lanki T.; Timonen K. L.; Vanninen E. Particulate air pollution and risk of ST-segment depression during repeated submaximal exercise tests among subjects with coronary heart disease - The exposure and risk assessment for fine and ultrafine particles in ambient air (ULTRA) study. *Circulation* **2002**, *106*, 933-938.

31. Brown J. S.; Zeman K. L.; Bennett W. D. Ultrafine particle deposition and clearance in the healthy and obstructed lung. *Am J Resp Crit Care* **2002**, *166*, 1240-1247.

32. Chalupa D. C.; Morrow P. E.; Oberdorster G.; Utell M. J.; Frampton M. W. Ultrafine particle deposition in subjects with asthma. *Environ Health Perspect* **2004**, *112*, 879-882.

33. Henneberger A.; Zareba W.; Ibald-Mulli A.; Ruckerl R.; Cyrys J.; Couderc J. P.; Mykins B.; Woelke G.; Wichmann H. E.; Peters A. Repolarization changes induced by air pollution in ischemic heart disease patients. *Environ Health Perspect* **2005**, *113*, 440-446.

34. Jaques P. A.; Kim C. S. Measurement of total lung deposition of inhaled ultrafine particles in healthy men and women. *Inhal Toxicol* **2000**, *12*, 715-731.

35. Brauner E. V.; Forchhammer L.; Moller P.; Simonsen J.; Glasius M.; Wahlin P.; Raaschou-Nielsen O.; Loft S. Exposure to ultrafine particles from ambient air and oxidative stress-induced DNA damage. *Environ Health Perspect* **2007**, *115*, 1177-1182.

36. Pietropaoli A. P.; Frampton M. W.; Hyde R. W.; Morrow P. E.; Oberdorster G.; Cox C.; Speers D. M.; Frasier L. M.; Chalupa D. C.; Huang L. S.; Utell M. J. Pulmonary function, diffusing capacity, and inflammation in healthy and asthmatic subjects exposed to ultrafine particles. *Inhal Toxicol* **2004**, *16*, 59-72.

37. Oberdorster G.; Sharp Z.; Atudorei V.; Elder A.; Gelein R.; Kreyling W.; Cox C. Translocation of inhaled ultrafine particles to the brain. *Inhal Toxicol* **2004**, *16*, 437-445.

38. Oberdorster G. Toxicology of ultrafine particles: in vivo studies. *Philos T Roy Soc A* **2000**, *358*, 2719-2739.

39. Nemmar A.; Hoylaerts M. F.; Hoet P. H. M.; Dinsdale D.; Smith T.; Xu H. Y.; Vermylen J.; Nemery B.; Nemery B. Ultrafine particles affect experimental thrombosis in an *in vivo* hamster model. *Am J Resp Crit Care* **2002**, *166*, 998-1004.

40. Elder A. C. P.; Gelein R.; Azadniv M.; Frampton M.; Finkelstein J.; Oberdorster G. Systemic effects of inhaled ultrafine particles in two compromised, aged rat strains. *Inhal Toxicol* **2004**, *16*, 461-471.

41. Ferin J.; Oberdorster G.; Soderholm S. C.; Gelein R. Pulmonary tissue access of ultrafine particles. *J Aerosol Med* **1991**, *4*, 57-68.

42. Ferin J.; Oberdorster G.; Penney D. P. Pulmonary retention of ultrafine and fine particles in rats. *Am J Resp Cell Mol* **1992**, *6*, 535-542.

43. Kreyling W. G.; Semmler M.; Erbe F.; Mayer P.; Takenaka S.; Schulz H.; Oberdorster G.; Ziesenis A. Translocation of ultrafine insoluble iridium particles from lung epithelium to extrapulmonary organs is size dependent but very low. *J Toxicol Env Heal A* **2002**, *65*, 1513-1530.

44. Nemmar A.; Delaunois A.; Nemery B.; Dessy-Doize C.; Beckers J. F.; Sulon J.; Gustin P. Inflammatory effect of intratracheal instillation of ultrafine particles in the rabbit: Role of C-fiber and mast cells. *Toxicol Appl Pharm* **1999**, *160*, 250-261.

45. Nemmar A.; Hoet P. H. M.; Vanquickenborne B.; Dinsdale D.; Thomeer M.; Hoylaerts M. F.; Vanbilloen H.; Mortelmans L.; Nemery B. Passage of inhaled particles into the blood circulation in humans. *Circulation* **2002**, *105*, 411-414.

46. Nemmar A.; Hoylaerts M. F.; Hoet P. H. M.; Vermylen J.; Nemery B. Size effect of intratracheally instilled particles on pulmonary inflammation and vascular thrombosis. *Toxicol Appl Pharm* **2003**, *186*, 38-45.

47. Oberdorster G.; Ferin J.; Gelein R.; Soderholm S. C.; Finkelstein J. Role of the alveolar macrophage in lung injury - studies with ultrafine particles. *Environ Health Perspect* **1992**, *97*, 193-199.

48. Oberdorster G.; Gelein R. M.; Ferin J.; Weiss B. Association of particulate air-pollution and acute mortality - involvement of ultrafine particles. *Inhal Toxicol* **1995**, *7*, 111-124.

49. Oberdorster G.; Sharp Z.; Atudorei V.; Elder A.; Gelein R.; Lunts A.; Kreyling W.; Cox C. Extrapulmonary translocation of ultrafine carbon particles following whole-body inhalation

exposure of rats. *J Toxicol Env Heal A* **2002**, *65*, 1531-1543.

50. Semmler M.; Seitz J.; Erbe F.; Mayer P.; Heyder J.; Oberdorster G.; Kreyling W. G. Long-term clearance kinetics of inhaled ultrafine insoluble iridium particles from the rat lung, including transient translocation into secondary organs. *Inhal Toxicol* **2004**, *16*, 453-459.

51. Elder A. C. P.; Gelein, R.; Finkelstein, J. N.; Cox, C.; Oberdorster, G. Pulmonary inflammatory response to inhaled ultrafine particles is modified by age, ozone exposure, and bacterial toxin. *Inhal Toxicol* **2000**, *12 (suppl 4)*, 227-246.

52. Elder A.C.P.; Gelein, R.; Azadniv, M.; Frampton, M.; Finkelstein, J.; Oberdorster, G.. Systemic interactions between inhaled ultrafine particles and endotoxin. *Ann Occup Hyp* **2002**, *46 (suppl1)*, 231-234.

53. Li X. Y.; Brown D.; Smith S.; Macnee W.; Donaldson K. Short-term inflammatory responses following intratracheal instillation of fine and ultrafine carbon black in rats. *Inhal Toxicol* **1999**, *11*, 709-731.

54. Zhou Y. M.; Zhong C. Y.; Kennedy I. M.; Leppert V. J.; Pinkerton K. E. Oxidative stress and NFkappaB activation in the lungs of rats: a synergistic interaction between soot and iron particles. *Toxicol Appl Pharmacol* **2003**, *190*, 157-69.

55. Oberdorster G.; Ferin J.; Lehnert B. E. Correlation between particle-size, *in-vivo* particle persistence, and lung injury. *Environ Health Perspect* **1994**, *102*, 173-179.

56. Oberdorster G.; Maynard A.; Donaldson K.; Castranova V.; Fitzpatrick J.; Ausman K.; Carter J.; Karn B.; Kreyling W.; Lai D.; Olin S.; Monteiro-Riviere N.; Warheit D.; Yang H. Principles for characterizing the potential human health effects from exposure to nanomaterials: elements of a screening strategy. *Part Fibre Toxicol* **2005**, *2*, 8.

57. Cormier S. A.; Lomnicki S.; Backes W.; Dellinger B. Origin and health impacts of emissions of toxic by-products and fine particles from combustion and thermal treatment of hazardous wastes and materials. *Environ Health Perspect* **2006**, *114*, 810-7.

58. Warheit D. B.; Overby L. H.; George G.; Brody A. R. Pulmonary macrophages are attracted to inhaled particles through complement activation. *Exp Lung Res* **1988**, *14*, 51-66.

59. Warheit D. B.; Hartsky M. A. Role of alveolar macrophage chemotaxis and phagocytosis in pulmonary clearance responses to inhaled particles: comparisons among rodent species. *Microsc Res Tech* **1993**, *26*, 412-22.

60. Warheit D. B.; Hill L. H.; George G.; Brody A. R. Time course of chemotactic factor generation and the corresponding macrophage response to asbestos inhalation. *Am Rev Respir Dis* **1986**, *134*, 128-33.

61. Donaldson K.; Brown D.; Clouter A.; Duffin R.; Macnee W.; Renwick L.; Tran L.; Stone V. The pulmonary toxicology of ultrafine particles. *J Aerosol Med* **2002**, *15*, 213-220.

62. Seaton A.; Macnee W.; Donaldson K.; Godden D. Particulate air-pollution and acute health-effects. *Lancet* **1995**, *345*, 176-178.

63. Nikula K. J.; Avila K. J.; Griffith W. C.; Mauderly J. L. Lung tissue responses and sites of particle retention differ between rats and cynomolgus monkeys exposed chronically to diesel exhaust and coal dust. *Fund Appl Toxicol* **1997**, *37*, 37-53.

64. Berry J. P.; Arnoux B.; Stanislas G.; Galle P.; Chretien J. A microanalytic study of particles transport across the alveoli: role of blood platelets. *Biomedicine* **1977**, *27*, 354-7.

65. Mehta D.; Bhattacharya J.; Matthay M. A.; Malik A. B. Integrated control of lung fluid balance. *Am J Physiol-Lung C* **2004**, *287*, L1081-L1090.

66. Kato T.; Yashiro T.; Murata Y.; Herbert D. C.; Oshikawa K.; Bando M.; Ohno S.; Sugiyama Y. Evidence that exogenous substances can be phagocytized by alveolar epithelial cells and transported into blood capillaries. *Cell Tissue Res* **2003**, *311*, 47-51.

67. Konig M. F.; Lucocq J. M.; Weibel E. R. Demonstration of pulmonary vascular perfusion by electron and light-microscopy. *J Appl Physiol* **1993**, *75*, 1877-1883.

68. Heckel K.; Kiefmann R.; Dorger M.; Stoeckelhuber M.; Goetz A. E. Colloidal gold particles as a new in vivo marker of early acute lung injury. *Am J Physiol-Lung C* **2004**, *287*, L867-L878.

69. Simionescu N.; Siminoescu M.; Palade G. E. Permeability of muscle capillaries to small heme-peptides. Evidence for the existence of patent transendothelial channels. *J Cell Biol* **1975**, *64*, 586-607.

70. Rejman J.; Oberle V.; Zuhorn I. S.; Hoekstra D. Size-dependent internalization of particles via the pathways of clathrin-and caveolae-mediated endocytosis. *Biochem J* **2004**, *377*, 159-169.

71. Smith A. E.; Helenius A. How viruses enter animal cells. *Science* **2004**, *304*, 237-242.

72. Akerman M. E.; Chan W. C. W.; Laakkonen P.; Bhatia S. N.; Ruoslahti E. Nanocrystal targeting *in vivo*. *Proc Natl Acad Sci U S A* **2002**, *99*, 12617-12621.

73. Cagle D. W.; Kennel S. J.; Mirzadeh S.; Alford J. M.; Wilson L. J. *In vivo* studies of fullerene-based materials using endohedral metallofullerene radiotracers. *Proc Natl Acad Sci U S A* **1999**, *96*, 5182-5187.

74. Bazile D. V.; Ropert C.; Huve P.; Verrecchia T.; Marlard M.; Frydman A.; Veillard M.; Spenlehauer G. Body distribution of fully biodegradable [C-14] poly (lactic acid) nanoparticles coated with albumin after parenteral administration to rats. *Biomaterials* **1992**, *13*, 1093-1102.

75. Gibaud S.; Andreux J. P.; Weingarten C.; Renard M.; Couvreur P. Increased bone-marrow toxicity of doxorubicin bound to nanoparticles. *Eur J Cancer* **1994**, *30A*, 820-826.

76. Gibaud S.; Demoy M.; Andreux J. P.; Weingarten C.; Gouritin B.; Couvreur P. Cells involved in the capture of nanoparticles in hematopoietic organs. *J Pharm Sci* **1996**, *85*, 944-950.

77. Gibaud S.; Rousseau C.; Weingarten C.; Favier R.; Douay L.; Andreux J. P.; Couvreur P. Polyalkylcyanoacrylate nanoparticles as carriers for granulocyte-colony stimulating factor (G-CSF). *J Control Release* **1998**, *52*, 131-139.

78. Ballou B.; Lagerholm B. C.; Ernst L. A.; Bruchez M. P.; Waggoner A. S. Noninvasive imaging of quantum dots in mice. *Bioconjug Chem* **2004**, *15*, 79-86.

79. Kreuter J. Nanoparticulate systems for brain delivery of drugs. *Adv Drug Deliver Rev* **2001**, *47*, 65-81.

80. Kreuter J. Influence of the surface properties on nanoparticle-mediated transport of drugs to the brain. *J Nanosci Nanotechno* **2004**, *4*, 484-488.

81. Kreuter J.; Shamenkov D.; Petrov V.; Ramge P.; Cychutek K.; Koch-Brandt C.; Alyautdin R. Apolipoprotein-mediated transport of nanoparticle-bound drugs across the blood-brain barrier. *J Drug Target* **2002**, *10*, 317-325.

82. Howe H. A.; Bordian, D.. Portals of entry of poliomyelitis virus in the chimpanzee. *Proc Soc Exp Biol Med* **1940**, *43*, 718-721.

83. De Lorenzo A. J.. The olfactory neuron and the blood-brain barrier. In *TASTE AND SMELL IN VERTEBRATES*. Wolstenholme G.; Knight J., Ed. Churchill: London, 1970; 151-176.

84. Oberdorster E. Manufactured nanomaterials (fullerenes, C60) induce oxidative stress in the brain of juvenile largemouth bass. *Environ Health Perspect* **2004**, *112*, 1058-62.

85. Kennedy P. G. E.; Chaudhuri A. Herpes simplex encephalitis. *J Neurol Neurosur Ps* **2002**, *73*, 237-238.

86. Hunter D. D.; Dey R. D. Identification and neuropeptide content of trigeminal neurons innervating the rat nasal epithelium. *Neuroscience* **1998**, *83*, 591-599.

87. Hunter D. D.; Undem B. J. Identification and substance P content of vagal afferent neurons innervating the epithelium of the guinea pig trachea. *Am J Resp Crit Care* **1999**, *159*, 1943-1948.

88. Utell M. J.; Frampton M. W.; Zareba W.; Devlin R. B.; Cascio W. E. Cardiovascular effects associated with air pollution: Potential mechanisms and methods of testing. *Inhal Toxicol* **2002**, *14*, 1231-1247.

89. Feikert T.; Mercer, P.; Corson, N.;Gelein, R.; Opanashuk, L.; Elder, A.. Inhaled solid ultrafine particles (UFP) are efficiently translocated via neuronal naso-olfactory pathways. *Toxicologist* **2004**, *78 (suppl 1)*, 435-436.

90. Fechter L. D.; Johnson D. L.; Lynch R. A. The relationship of particle size to olfactory nerve uptake of a non-soluble form of manganese into brain. *Neurotoxicology* **2002**, *23*, 177-83.

91. Terasaki S.; Kameyama T.; Yamamoto S. A case of zoster in the 2nd and 3rd branches of the trigeminal nerve associated with simultaneous herpes labialis infection-a case report. *Kurume Med J* **1997**, *44*, 61-6.

92. Campbell A.; Oldham M.; Becaria A.; Bondy S. C.; Meacher D.; Sioutas C.; Misra C.; Mendez L. B.; Kleinman A. Particulate matter in polluted air may increase biomarkers of inflammation in mouse brain. *Neurotoxicology* **2005**, *26*, 133-140.

93. Calderon-Garciduenas L.; Azzarelli B.; Acuna H.; Garcia R.; Gambling T. M.; Osnaya N.; Monroy S.; Mr D. E. L. Tizapantzi; Carson J. L.; Villarreal-Calderon A.; Rewcastle B. Air pollution and brain damage. *Toxicol Pathol* **2002**, *30*, 373-89.

94. Amato I.. Making the right stuff. *Sci News* **1989**, *136*, 108-110.

95. Ferin J.; Oberdorster G.; Penney D. P.; Soderholm S. C.; Gelein R.; Piper H. C. Increased pulmonary toxicity of ultrafine particles 1. Particle clearance, translocation, morphology. *J Aerosol Sci* **1990**, *21*, 381-384.

96. Oberdorster G.; Ferin, J.; Finkelstein, J.; Wade, P.; Corson, N.. Increased pulmonary toxicity of ultrafine particles? II. Lung lavage studies. *J Aerosol Sci* **1990**, *21*, 384-387.

97. Foley S.; Crowley C.; Smaihi M.; Bonfils C.; Erlanger B. F.; Seta P.; Larroque C. Cellular localisation of a water-soluble fullerene derivative. *Biochem Bioph Res Co* **2002**, *294*, 116-119.

98. Li N.; Sioutas C.; Cho A.; Schmitz D.; Misra C.; Sempf J.; Wang M.; Oberley T.; Froines J.; Nel A. Ultrafine particulate pollutants induce oxidative stress and mitochondrial

damage. *Environ Health Perspect* **2003**, *111*, 455-60.

99. Freitas R. A. Jr., Basic capabilities. In *Nanomedicine* Landes Bioscience: Georgetown, TX, 1999; Vol. I.

100. Dumortier H.; Lacotte S.; Pastorin G.; Marega R.; Wu W.; Bonifazi D.; Briand J. P.; Prato M.; Muller S.; Bianco A. Functionalized carbon nanotubes are non-cytotoxic and preserve the functionality of primary immune cells. *Nano Lett* **2006**, *6*, 1522-1528.

101. Ding L. H.; Stilwell J.; Zhang T. T.; Elboudwarej O.; Jiang H. J.; Selegue J. P.; Cooke P. A.; Gray J. W.; Chen F. Q. F. Molecular characterization of the cytotoxic mechanism of multiwall carbon nanotubes and nano-onions on human skin fibroblast. *Nano Lett* **2005**, *5*, 2448-2464.

102. Monteiro-Riviere N. A.; Nemanich R. J.; Inman A. O.; Wang Y. Y. Y.; Riviere J. E. Multi-walled carbon nanotube interactions with human epidermal keratinocytes. *Toxicol Lett* **2005**, *155*, 377-384.

103. Bottini M.; Bruckner S.; Nika K.; Bottini N.; Bellucci S.; Magrini A.; Bergamaschi A.; Mustelin T. Multi-walled carbon nanotubes induce T lymphocyte apoptosis. *Toxicol Lett* **2006**, *160*, 121-126.

104. Magrez A.; Kasas S.; Salicio V.; Pasquier N.; Seo J. W.; Celio M.; Catsicas S.; Schwaller B.; Forro L. Cellular toxicity of carbon-based nanomaterials. *Nano Lett* **2006**, *6*, 1121-1125.

105. Zhu L.; Chang D. W.; Dai L. M.; Hong Y. L. DNA damage induced by multiwalled carbon nanotubes in mouse embryonic stem cells. *Nano Lett* **2007**, *7*, 3592-3597.

106. Jia G.; Wang H. F.; Yan L.; Wang X.; Pei R. J.; Yan T.; Zhao Y. L.; Guo X. B. Cytotoxicity of carbon nanomaterials: Single-wall nanotube, multi-wall nanotube, and fullerene. *Environ Sci Technol* **2005**, *39*, 1378-1383.

107. Silva V. M.; Corson N.; Elder A.; Oberdorster G. The rat ear vein model for investigating in vivo thrombogenicity of ultrafine particles (UFP). *Toxicol Sci* **2005**, *85*, 983-989.

108. Lam C. W.; James J. T.; Mccluskey R.; Hunter R. L. Pulmonary toxicity of single-wall carbon nanotubes in mice 7 and 90 days after intratracheal instillation. *Toxicol Sci* **2004**, *77*, 126-134.

109. Alivisatos P. The use of nanocrystals in biological detection. *Nat Biotechnol* **2004**, *22*, 47-52.

110. Gao X. H.; Cui Y. Y.; Levenson R. M.; Chung L. W. K.; Nie S. M. *In vivo* cancer targeting and imaging with semiconductor quantum dots. *Nat Biotechnol* **2004**, *22*, 969-976.

111. Wu X. Y.; Liu H. J.; Liu J. Q.; Haley K. N.; Treadway J. A.; Larson J. P.; Ge N. F.; Peale F.; Bruchez M. P. Immunofluorescent labeling of cancer marker Her2 and other cellular targets with semiconductor quantum dots. *Nat Biotechnol* **2003**, *21*, 41-46.

112. Chan W. C. W.; Maxwell D. J.; Gao X. H.; Bailey R. E.; Han M. Y.; Nie S. M. Luminescent quantum dots for multiplexed biological detection and imaging. *Curr Opin Biotech* **2002**, *13*, 40-46.

113. Chen F. Q.; Gerion D. Fluorescent CdSe/ZnS nanocrystal-peptide conjugates for long-term, nontoxic imaging and nuclear targeting in living cells. *Nano Lett* **2004**, *4*, 1827-1832.

114. Dubertret B.; Skourides P.; Norris D. J.; Noireaux V.; Brivanlou A. H.; Libchaber A. *In vivo* imaging of quantum dots encapsulated in phospholipid micelles. *Science* **2002**, *298*, 1759-1762.

115. Lidke D. S.; Nagy P.; Heintzmann R.; Arndt-Jovin D. J.; Post J. N.; Grecco H. E.; Jares-Erijman E. A.; Jovin T. M. Quantum dot ligands provide new insights into erbB/HER receptor-mediated signal transduction. *Nat Biotechnol* **2004**, *22*, 198-203.

116. Michalet X.; Pinaud F. F.; Bentolila L. A.; Tsay J. M.; Doose S.; Li J. J.; Sundaresan G.; Wu A. M.; Gambhir S. S.; Weiss S. Quantum dots for live cells, *in vivo* imaging, and diagnostics. *Science* **2005**, *307*, 538-544.

117. Zhang L. W.; Monteiro-Riviere N. A. Assessment of quantum dot penetration into intact, tape-stripped, abraded and flexed rat skin. *Skin Pharmacol Phys* **2008**, *21*, 166-180.

118. Lovric J.; Bazzi H. S.; Cuie Y.; Fortin G. R. A.; Winnik F. M.; Maysinger D. Differences in subcellular distribution and toxicity of green and red emitting CdTe quantum dots. *J Mol Med-Jmm* **2005**, *83*, 377-385.

119. Hoshino A.; Hanaki K.; Suzuki K.; Yamamoto K. Applications of T-lymphoma labeled with fluorescent quantum dots to cell tracing markers in mouse body. *Biochem Bioph Res Co* **2004**, *314*, 46-53.

120. Shiohara A.; Hoshino A.; Hanaki K.; Suzuki K.; Yamamoto K. On the cyto-toxicity caused by quantum dots. *Microbiol Immunol* **2004**, *48*, 669-675.

121. Derfus A. M.; Chan W. C. W.; Bhatia S. N. Probing the cytotoxicity of semiconductor quantum dots. *Nano Lett* **2004**, *4*, 11-18.

122. Zhang L. W.; Yu W. W.; Colvin V. L.; Monteiro-Riviere N. A. Biological interactions of quantum dot nanoparticles in skin and in human epidermal keratinocytes. *Toxicol Appl Pharm* **2008**, *228*, 200-211.

123. Guo G. N.; Liu W.; Liang J. G.; He Z. K.; Xu H. B.; Yang X. L. Probing the cytotoxicity of CdSe quantum dots with surface modification. *Mater Lett* **2007**, *61*, 1641-1644.

124. Li H. C.; Zhou Q. F.; Liu W.; Yan B.; Zhao Y.; Jiang G. B. Progress in the toxicological researches for quantum dots. *Sci China Ser B* **2008**, *51*, 393-400.

125. Rouse J. G.; Haslauer C. M.; Loboa E. G.; Monteiro-Riviere N. A. Cyclic tensile strain increases interactions between human epidermal keratinocytes and quantum dot nanoparticles. *Toxicol in Vitro* **2008**, *22*, 491-497.

126. Tang M. L.; Xing T. R.; Zeng J.; Wang H. L.; Li C. C.; Yin S. T.; Yan D.; Deng H. M.; Liu J.; Wang M.; Chen J. T.; Ruan D. Y. Unmodified CdSe quantum dots induce elevation of cytoplasmic calcium levels and impairment of functional properties of sodium channels in rat primary cultured hippocampal neurons. *Environ Health Perspect* **2008**, *116*, 915-922.

127. Yang R. S.; Chang L. W.; Wu J. P.; Tsai M. H.; Wang H. J.; Kuo Y. C.; Yeh T. K.; Yang C. S.; Lin P. Persistent tissue kinetics and redistribution of nanoparticles, quantum dot 705, in mice: ICP-MS quantitative assessment. *Environ Health Perspect* **2007**, *115*, 1339-43.

128. Zhang Y. B.; Chen W.; Zhang J.; Liu J.; Chen G. P.; Pope C. *In vitro* and *in vivo* toxicity of CdTe nanoparticles. *J Nanosci Nanotechno* **2007**, *7*, 497-503.

129. Gopee N. V.; Roberts D. W.; Webb P.; Cozart C. R.; Siitonen P. H.; Warbritton A. R.; Yu W. W.; Colvin V. L.; Walker N. J.; Howard P. C. Migration of intradermally injected quantum dots to sentinel organs in mice. *Toxicol Sci* **2007**, *98*, 249-257.

130. Mortensen L. J.; Oberdorster G.; Pentland A. P.; Delouise L. A. *In vivo* skin penetration of quantum dot nanoparticles in the murine model: The effect of UVR. *Nano Lett* **2008**, *8*, 2779-2787.

131. Chithrani B. D.; Ghazani A. A.; Chan W. C. W. Determining the size and shape dependence of gold nanoparticle uptake into mammalian cells. *Nano Lett* **2006**, *6*, 662-668.

132. Connor E. E.; Mwamuka J.; Gole A.; Murphy C. J.; Wyatt M. D. Gold nanoparticles are taken up by human cells but do not cause acute cytotoxicity. *Small* **2005**, *1*, 325-327.

133. Goodman C. M.; Mccusker C. D.; Yilmaz T.; Rotello V. M. Toxicity of gold nanoparticles functionalized with cationic and anionic side chains. *Bioconjugate Chem* **2004**, *15*, 897-900.

134. Wang B.; Feng W. Y.; Wang M.; Wang T. C.; Gu Y. Q.; Zhu M. T.; Ouyang H.; Shi J. W.; Zhang F.; Zhao Y. L.; Chai Z. F.; Wang H. F.; Wang J. Acute toxicological impact of nano- and submicro-scaled zinc oxide powder on healthy adult mice. *J Nanopart Res* **2008**, *10*, 263-276.

135. Pernodet N.; Fang X. H.; Sun Y.; Bakhtina A.; Ramakrishnan A.; Sokolov J.; Ulman A.; Rafailovich M. Adverse effects of citrate/gold nanoparticles on human dermal fibroblasts. *Small* **2006**, *2*, 766-773.

136. Carlson C.; Hussain S. M.; Schrand A. M.; Braydich-Stolle L. K.; Hess K. L.; Jones R. L.; Schlager J. J. Unique cellular interaction of silver nanoparticles: Size-dependent generation of reactive oxygen species. *J Phys Chem B* **2008**, *112*, 13608-13619.

137. Senapati D.; Lu W. T.; Ray P. C. COLL 317-Shape dependent cellular uptake and toxic effects of silver nanomaterials. *Abstr Pap Am Chem S* **2009**, *238*.

138. Griffitt R. J.; Luo J.; Gao J.; Bonzongo J. C.; Barber D. S. Effects of particle composition and species on toxicity of metallic nanomaterials in aquatic organisms. *Environ Toxicol Chem* **2008**, *27*, 1972-1978.

139. Asharani P. V.; Wu Y. L.; Gong Z. Y.; Valiyaveettil S. Toxicity of silver nanoparticles in zebrafish models. *Nanotechnology* **2008**, *19*.

140. Benn T. M.; Westerhoff P. Nanoparticle silver released into water from commercially available sock fabrics. *Environ Sci Technol* **2008**, *42*, 4133-4139.

141. Wang S. G.; Lu W. T.; Tovmachenko O.; Rai U. S.; Yu H. T.; Ray P. C. Challenge in understanding size and shape dependent toxicity of gold nanomaterials in human skin keratinocytes. *Chem Phys Lett* **2008**, *463*, 145-149.

142. Niidome T.; Yamagata M.; Okamoto Y.; Akiyama Y.; Takahashi H.; Kawano T.; Katayama Y.; Niidome Y. PEG-modified gold nanorods with a stealth character for in vivo applications. *J Control Release* **2006**, *114*, 343-347.

143. Grassian V. H.; O'shaughnessy P. T.; Adamcakova-Dodd A.; Pettibone J. M.; Thorne P. S. Inhalation exposure study of titanium dioxide nanoparticles with a primary particle size of 2 to 5 nm. *Environ Health Perspect* **2007**, *115*, 397-402.

144. Jin C. Y.; Zhu B. S.; Wang X. F.; Lu Q. H. Cytotoxicity of titanium dioxide nanoparticles in mouse fibroblast cells. *Chem Res Toxicol* **2008**, *21*, 1871-1877.

145. Park E. J.; Yi J.; Chung Y. H.; Ryu D. Y.; Choi J.; Park K. Oxidative stress and apoptosis induced by titanium dioxide nanoparticles in cultured BEAS-2B cells. *Toxicol Lett* **2008**, *180*, 222-229.

146. Cozzoli P. D.; Curri M. L.; Agostiano A.; Leo G.; Lomascolo M. ZnO nanocrystals by a non-hydrolytic route: Synthesis and characterization. *J Phys Chem B* **2003**, *107*, 4756-4762.

147. Karlsson H. L.; Cronholm P.; Gustafsson J.; Moller L. Copper oxide nanoparticles are highly toxic: A comparison between metal oxide nanoparticles and carbon nanotubes. *Chem Res Toxicol* **2008**, *21*, 1726-1732.

148. Xia T.; Kovochich M.; Liong M.; Madler L.; Gilbert B.; Shi H. B.; Yeh J. I.; Zink J. I.; Nel A. E. Comparison of the mechanism of toxicity of zinc oxide and cerium oxide nanoparticles based on dissolution and oxidative stress properties. *Acs Nano* **2008**, *2*, 2121-2134.

Chapter 2 *in Vitro* Toxicity Mechanism of Zinc Oxide Nanoparticles

2.1 Introduction

ZnO-NPs have been extensively applied in electronics, optoelectronics, gas sensors, sunscreens and antibacterial coating due to their unique properties arising from the quantum confinement, such as antibacterial, antifungal, ultraviolet filtering properties, high catalytic, photochemical activity and so on [1-4]. But the epidemiological and *in vivo* studies have lagged behind the speed of the mass production of the ZnO-NPs and the escalating human exposure risks to them [5-6]. Unfortunately, ZnO-NPs are more and more reported to be toxic to the environment including the aquatic organisms, the terrestrial animals and plants and the microorganism [7-10]. The *in vitro* studies also revealed that ZnO-NPs were toxic to various human cell lines, such as lung epithelial cells, aortic endothelial cells, epidermal cells, bronchial epithelial cells, lymphoblastoid cells, lung mesothelioma cell and fibroblast cells [11-18].

To this day, the concerns have focused on whether the solid particles *per se* or the released zinc is the real toxicant in the ZnO-NPs cytotoxicity. On one hand, some findings indicated that the solid particles played an important role: Moos et al. found that the contact of particles with the cells was required for ZnO-NPs cytotoxicity [14]; Gojova et al. concluded that the internalization of nanoparticles by the cells was necessary for the ZnO-NPs cytotoxicity [13-14]. Furthermore, the ZnO-NPs cytotoxicity was well reported to be resulted from the increase of intracellular reactive oxygen species (ROS) brought about by the solid particles via a special interface chemical activity [12, 17, 19]. On the contrary, Franklin et al. fully discussed the importance of the solubility of the ZnO-NPs for the toxicity on microalga [20]. Brunner also found that the solubility of ZnO-NPs was very important for cytotoxicity [18]. Additionally, there was another compromised hypothesis that the particles were internalized by the cells and intracellular released zinc was the real toxicant in

ZnO-NPs cytotoxicity [21]. Xia and co-researchers found the accumulation of fluorexcein isothiocyanate (FITC) labeled ZnO-NPs in human bronchial epithelial cells, and concluded the intracellular dissolution of them was important for the cytotoxicity [22]. However, Gojova et al did not detect the uptake of ZnO-NPs though they found the presence of the solid particles was pre-requisite for the cytotoxicity [13-14].

The objective of this study was to identify the respective contributions of the solid particles and the released zinc to the ZnO-NPs cytotoxicity. Thus we prepared three kinds of exposure medium; they were ZnO-NPs suspension in the medium, their extractions collected via centrifugation, and the medium containing zinc chloride ($ZnCl_2$), which could release same zinc concentration as ZnO-NPs suspension in the culture medium. A549 cell line was used in this study, since nano-particles are well reported to be capable of reaching the alveoli and causing pulmonary inflammation [23-24], A549 cell line is derived from human lung adenocarcinoma and has an extensive application history in the airborne particle toxicity study [12, 25-27], because it keeps most of the characteristics of type II alveolar epithelial cells [28], which play important roles in responding to the lung damage and contribute to various pulmonary immunology and inflammatory activity [29].

2.2 Materials and Methods

2.2.1 Preparing and characterizing the exposure mediums

The ZnO-NPs were purchased from Sigma-Aldrich (MO, USA), the $ZnCl_2$ was purchased from WAKO, Ltd., and we prepared three kinds of exposure medium with them. One was the suspension: ZnO-NPs were dispersed into sterilized MiliQ water with sonication for 30min, diluted with Dulbecco's Modified Eagle Medium containing 10% fetal bovine serum (hereafter referred to as supplemented DMEM or medium) to 25, 50, 75 and 100 μg/mL，respectively. The hydrodynamic diameter distribution of the ZnO-NPs suspension was measured with a laser diffraction particle size

analyzer (DLS6000AL, Otsuka, Japan). The second was the extraction: the ZnO-NPs suspensions were incubated in a 37 ℃, 5% CO_2 incubator for 24 h, then the solid particles were removed with 150 000 g centrifugation for 1 h at 4 ℃, and the extractions was collected. The third was $ZnCl_2$ medium: $ZnCl_2$ was dissolved in the sterilized MiliQ water and then diluted with the medium to the desired concentration. The concentration of the released zinc in the extractions and the $ZnCl_2$ medium were determined with the zinc colorimetric assay kit (AKJ Global Technology., Ltd).

2.2.2 Cell culture and cytotoxicity assay

A549 cells were seeded in culture vessels with the density of 8 000/cm^2 and incubated for 48 h in 37 ℃, 5% CO_2 incubator. The culture medium was then replaced with the three kinds of exposure mediums. After 24 h of exposure, the cytotoxicity was assayed through morphology observation with Cell Double Staining Kit (Dojindo, Japan) and WST cell viability assay with Cell Counting Kit-8 (CCK-8, Dojindo company, Japan), and LDH leakage assay with CytoTox96® Non-radioactive Cytotoxicity Assay Kit (Promega Corporation). The assays were conducted according to the corresponding kit protocols.

2.2.3 Global gene expression analysis

The total RNA of cells surviving the exposure was extracted with ISOGEN (NIPPON GENE. Co. Ltd) and purified from the protein and DNA ingredients with Recombinant DNaseI (Takara-bio, Inc.). Amino Allyl MessageAmp II Arna Amplification Kit (Ambion, TX, USA) was used for the subsequent sample preparation for microarray analysis. We published the sample preparation and scanning procedure previously [30]. Finally, locally weighted scatter plot smoothing (LOWESS) adjustment was applied, and the expression situation of the global genes was transited into corresponding numerical value. Function analysis was conducted via PANTHER's Gene Ontology (GO) biological process categories database (www.pantherdb.org/tools/

genexAnalysis.jsp), and the regulated genes were classified into three broad function categories including the “biological process”, “cellular function” and the “molecular function”. Each broad category had a hierarchical structure and the corresponding genes could be further classified in more detail function categories. The function annotation of each gene was calculated with Fisher’s exact test to determine the *p*-value, which represented the statistical significance of the concordance rate between each category and the functional annotation of each gene [31]. Unless the *p*-value was less than 10^{-4} ($p < 0.0001$), the regulated genes were not considered as the inevitable response to the stress.

2.2.4 Inhibiting the expression of metallothionein gene with siRNA

Lipofectamine™ RNAiMAX (InvitrogenTM) was used as transfection reagent. The transfection mixture was prepared, stand at room temperature for 20 min and then was treated to the cells with the exposure medium. After 24 h of incubation, the cells were collected and used for the subsequent cytotoxicity assay or reverse transcription polymerase chain reaction (RT-PCR) assay. For RT-PCR, the total RNA of the cells was collected with ISOGENE (NIPPON GENE. Co. Ltd), purified with Recombinant DNaseI (Takara-bio, Inc.), reverse-transcribed into cDNA with PrimerScript RT reagent kit (Takara-bio, Inc.), and finally stained with LightCycler Fast Start DNA Master SYBR Green I (Roche Applied Science Corporation). The fluorescence intensity was scanned with lightCycler (CAROUSEL, Roche) and analyzed with corresponding software.

2.2.5 Detecting intracellular ROS

OxiSelect™ Intracellular ROS Assay Kit (Green Fluorescence) was purchased from Cell Biolab, Inc. The assay kit employed the cell-permeable fluorogenic probe DCFH-DA, a well-established reagent for detecting the intracellular ROS [32-34]. The exposed cells in opaque 96-well plate were washed twice with DPBS and then incubated in the medium containing 100 μM

of DCFH-DA in 37 ℃, 5% CO_2 incubator for 60 min. Then the fluorescence intensity was determined with a microplate reader at an excitation of 485 nm and an emission of 530 nm. N-acetyl-L-cysteine (NAC, Sigma) was used to confirm the contribution of ROS to the cytotoxicityis since it was a precursor of intracellular cysteine and could transform into glutathione in the cells to enhance the intracellular reduction state by increasing the GSH/GSSG rate [35]. A549 cells were pretreated with 10 mM of NAC for 2 h and then the medium was replaced with exposure medium. After another 24 h exposure, the cell viability was assayed with the CCK-8.

2.2.6 Experimental design and statistics analysis

The cells without exposure were used as the negative control. Each experiment was conducted with three parallel samples and repeated independently three times. The results were analyzed with two-tailed Student's t-test. The results were considered significantly different from the control group if $p<0.05$ or evidently different with the control group if $p<0.01$.

2.3 Results

2.3.1 Characterizations of ZnO-NPs suspension in supplemented DMEM

We previously reported that he pristine dimensions of ZnO-NPs were less than 60 nm, which were consistent with the nominal dimension determined by the supplier [36]. When the concentration of the ZnO-NPs suspension were from 25 to 100 μg/mL, the mean hydrodynamic diameter of the freshly prepared suspensions were 394.7 nm to 529.3 nm, and the mean hydrodynamic diameter were 352.2 to 591.8 nm after the incubation for 24 h (Table 2.1). The concentration of the released zinc in the suspensions were determined with their corresponding extractions and were 6.09 to 9.18 μg/mL; and when the particle concentration was more than 75 μg/mL, the released zinc reached the saturation concentration, about 9.18 μg/mL (Table 2.2).

Table 2.1 Mean hydrodynamic diameter of ZnO-NPs in supplemented DMEM.

Concentration of ZnO-NPs (μg/mL)	Mean Hydrodynamic Diameter (nm)	
	Freshly prepared Medium	24h-Incubated Medium
25	525.3	591.8
50	529.3	431.4
75	394.7	449.5
100	406.1	352.2

Table 2.2 Concentration of released zinc in ZnO-NPs suspension.

ZnO-NPs (μg/mL)	Released Zinc (μg/mL)
25	6.09
50	7.85
75	9.18
100	9.18

2.3.2 Cytotoxicity of ZnO-NPs suspensions, extractions and $ZnCl_2$ medium

After A549 cells were exposed to the 50, 75, and 100 μg/mL of ZnO-NPs suspensions for 24 h, the cell viability decreased to approximately 20%, 30%, and 60% respectively, while no evident change in case of exposure to 25 μg/mL of ZnO-NPs suspensions (Figure 2.1a, b). In addition, the LDH leakage assay revealed the exposure to the 50, 75, and 100 μg/mL of ZnO-NPs suspensions also resulted in the in integrity loss of the plasma membrane (Figure 2.1c). By contrast, Zn released from ZnO-NPs showed neither reduction in cell viability nor the adverse effects on cell number or plasma membrane (Figure 2.2a-c).

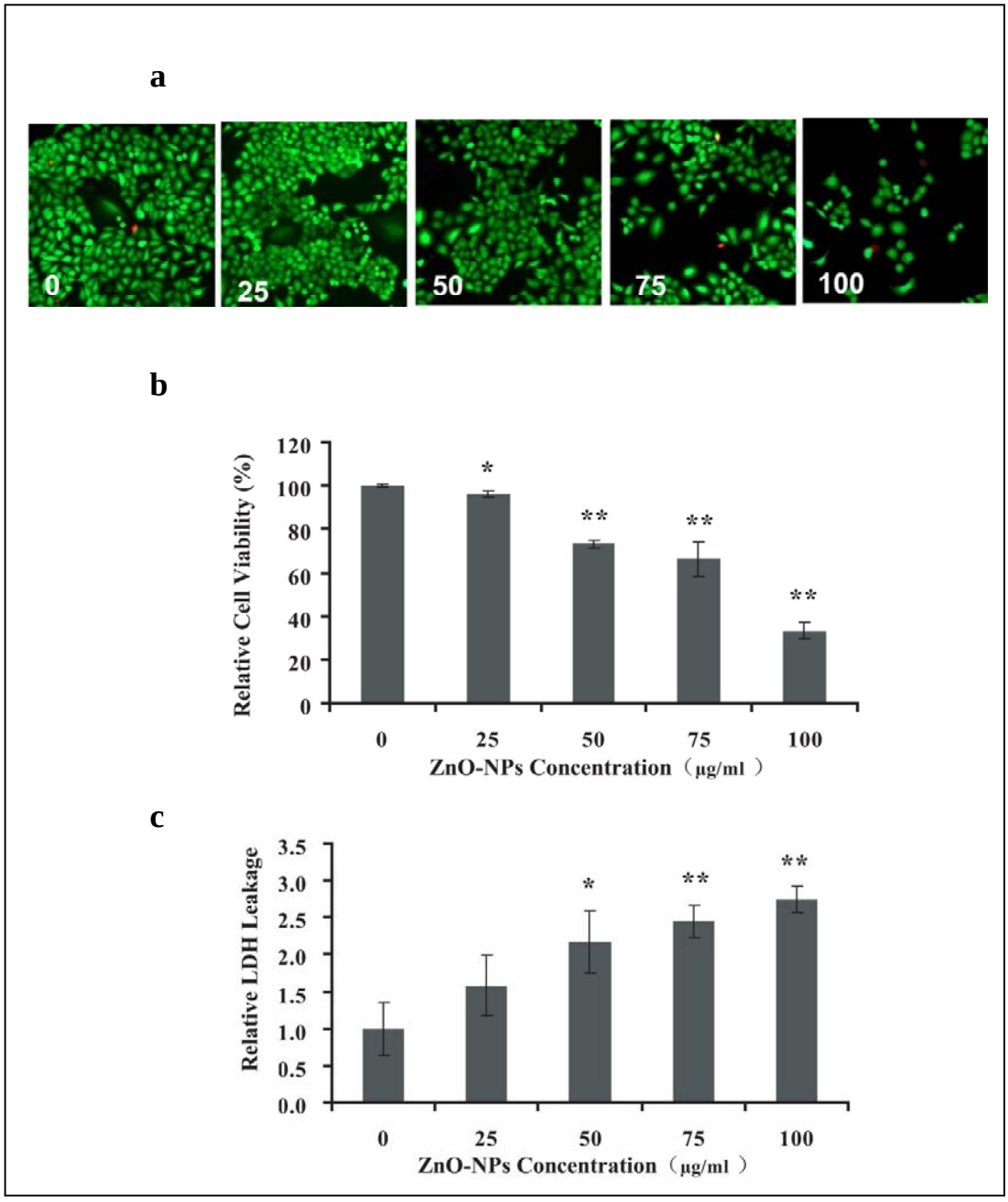

Figure 2.1 Cytotoxicity induced by ZnO-NPs suspension. A549 cells were exposed to 25, 50, 75 and 100 μg/mL of ZnO-NPs suspension respectively for 24 h, and the cell viability was assayed with (a) cell staining, (b) WST and (c) LDH leakage assay. $^{**}\ p < 0.01$, $^{*}\ p < 0.05$

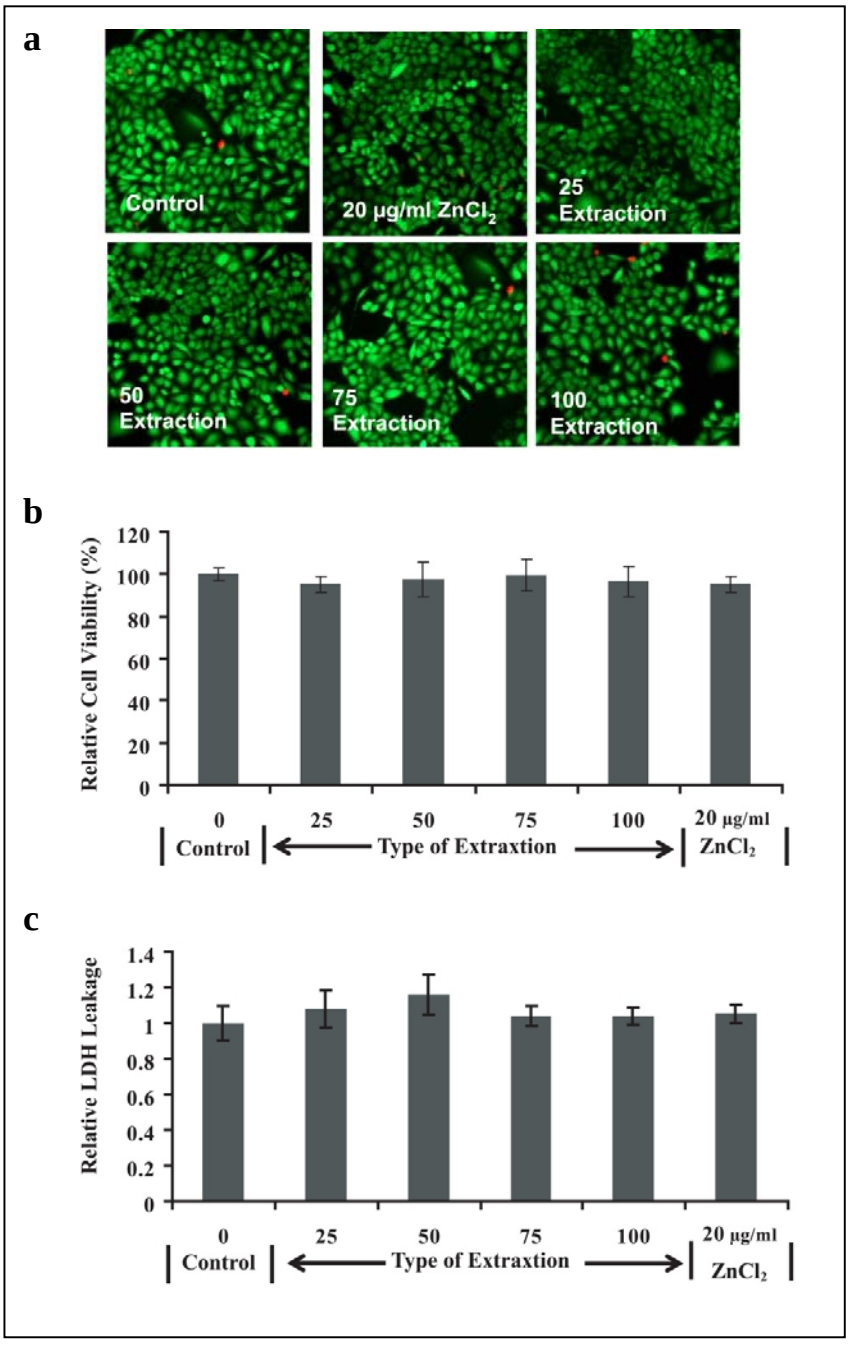

Figure 2.2 Cytotoxicity induced by the 20 μg/mL of $ZnCl_2$ and the ZnO-NPs extractions. A549 cells were exposed to the 20 μg/mL $ZnCl_2$ and the extractions of the 25, 50, 75 and 100 μg/mL of ZnO-NPs suspension respectively for 24 h, and the cell viability was assayed with a) cell staining, b) WST, and c) LDH leakage assay.** $p<0.01$; * $p<0.05$

2.3.3 Global gene expression analysis

To identify the gene functional category in response of ZnO-NPs and their released zinc respectively, we conducted a cDNA microarray assay on the cells exposed to the 100 μg/mL of ZnO-NPs suspension and 20 μg/mL of $ZnCl_2$. We used 20 μg/mL of $ZnCl_2$ as the released zinc control in absence of the solid particles to avoid the possible interference from the released impurities in the extractions, also because we found 20 μg/mL of $ZnCl_2$ medium contained about 10 μg/mL of released zinc (data not shown), which was equivalent to that of 100 μg/mL of ZnO-NPs suspension. A549 cells up-regulated 206 genes and down-regulated 113 genes in response of the 100 μg/mL of ZnO-NPs suspension; and up-regulated 29 genes, down-regulated 37 genes in response of the 20 μg/mL of $ZnCl_2$ medium (Table 2.3 and Table S1~S4 of reference 37**)** [37] . Through the subsequent data mining on the regulated genes via PANTHER's GO biological process categories database, the same one functional gene category, "cadmium ion binding category", was identified in response not only of the ZnO-NPs but also of the $ZnCl_2$. The "cadmium ion binding category" consisted of five MT isomer genes, MT1F, MT1A, MT1B, MT1E and MT1L. The fold change of the MTs' expression was summarized in the Table 2.4. Among the down regulated genes, no significantly changed functional category was identified.

Table 2.3 Numbers of the regulated genes.

	ZnO-NPs Medium 100 μg/mL	**$ZnCl_2$ Medium 20 μg/mL**
Up-regulated genes	206	29
Down-regulated genes	113	37

Table 2. 4 Cadmium ion binding category in response of the exposures.

Gene Name	Fold Change	
	100 µg/mL of ZnO-NPs	20 µg/mL of $ZnCl_2$
MT1F	5.02	3.53
MT1A	4.90	1.45
MT1B	3.74	1.09
MT1E	3.73	<1.00
MT1L	2.73	<1.00

2.3.4 Cytotoxicity in absence of MT over expression

We inhibited the MT expression with the corresponding siRNA during 24 h exposure. The control group cells were transfected with random siRNA sequence. MT expression of the treatment group was calculated to be the portion of the control group. In the case of exposure to ZnO-NPs, the siRNA transfection inhibited the MT expression to about 1.4% of the corresponding control; in the case of the $ZnCl_2$ exposure, the siRNA transfection inhibited the MT expression to about 1.1% of the corresponding control group (Table 2.5). Then we assayed the cell viability: inhibiting MTs expression resulted in the decrease of cell viability to about 88%, 80%, and 53% of the control in 50, 75 and 100 µg/mL ZnO-NPs suspensions respectively but had no effect on the viability of cells exposed to the extractions and the $ZnCl_2$ medium (Figure 2.3).

Table 2.5 Relative mRNA expression of MT.

	Medium Control	100 µg/mL ZnO-NPs	20 µg/mL $ZnCl_2$
Cell control	1 [a]	1573.76	359.538
Reagent control[b]	0.858	1448.155	250.732
Randam RNA[c]	0.846	1060.11	242.19
siRNA treatment	0.607	15.348	2.657

a) The MT expression of A549 cells in normal medium was used as 1; b) The MT expression of A549 cells in medium containing the trasfiction reagen without siRNA. The inhibition efficiency was evaluated through comparing the reagent control with the siRNA transfected sample in present study; c) The MT expression of A549 cells in medium containing the trasfiction reagen and random siRNA, to detects whether there was any unexpected effects on the result just because of the non-specific RNA sequence.

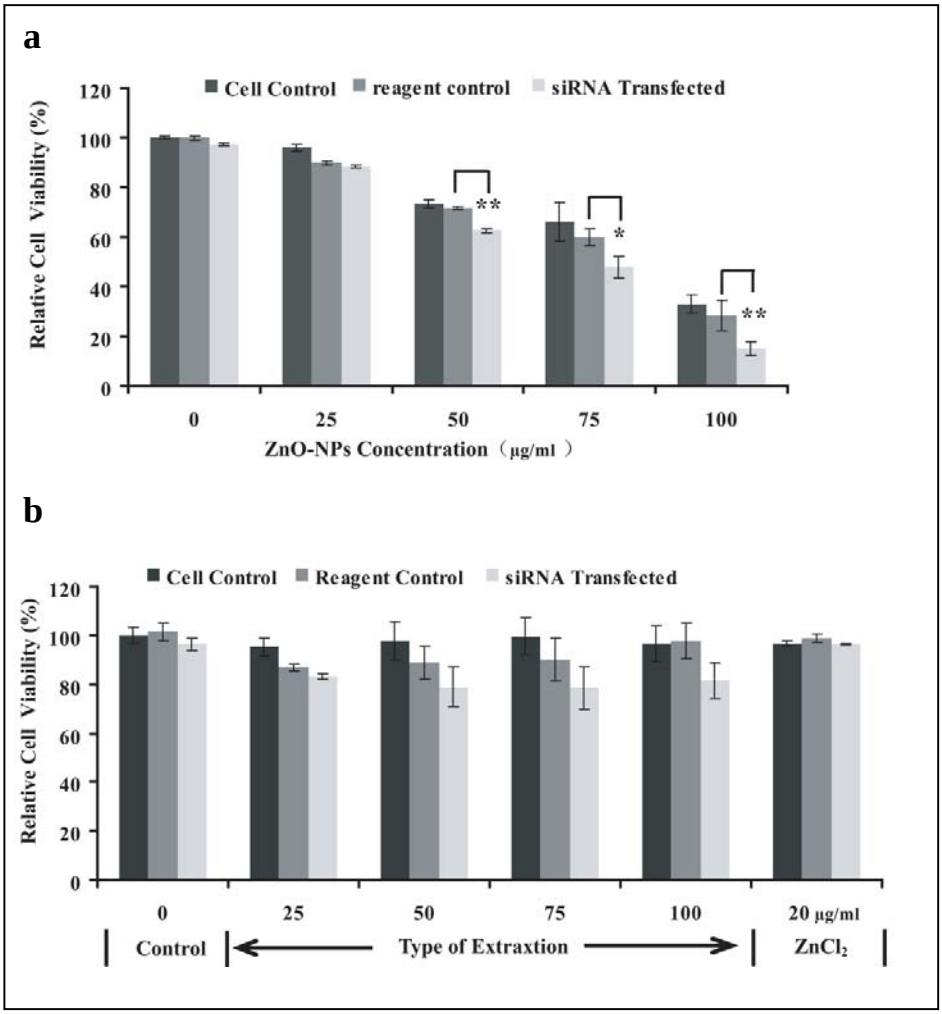

Figure 2.3 Function of MTs in response of the exposures. The MT expression of A549 cells was inhibited with the corresponding siRNA during the exposure to (a) the suspension of 25, 50, 75 and 100 μg/mL of ZnO-NPs, (b) their extraction and 20 μg/mL of $ZnCl_2$ respectively for 24 h . The cell viability was assayed with CCK-8. The statistical significance was analyzed by comparing the siRNA transfected cells with the corresponding reagent control. $^{**}\ p < 0.01$ $^{*}\ p < 0.05$

2.3.5 Intracellular ROS

The intracellular ROS was detected when ZnO-NPs were more than 50 μg/mL; however, no ROS generation was observed in the cells exposed to $ZnCl_2$ (Figure 2.4). To examine whether ROS induced by ZnO-NPs is involved in cytotoxicity, cells were pre-treated with NAC before exposed to ZnO-NPs. As shown in Figure 2.5, the cell viability was partially recovered by NAC treatment in 50 μg/mL and 75 μg/mL ZnO-NPs. However, in the case of 100 μg/mL ZnO-NPs suspension, NAC pre-treatment had no effect on the cell viability.

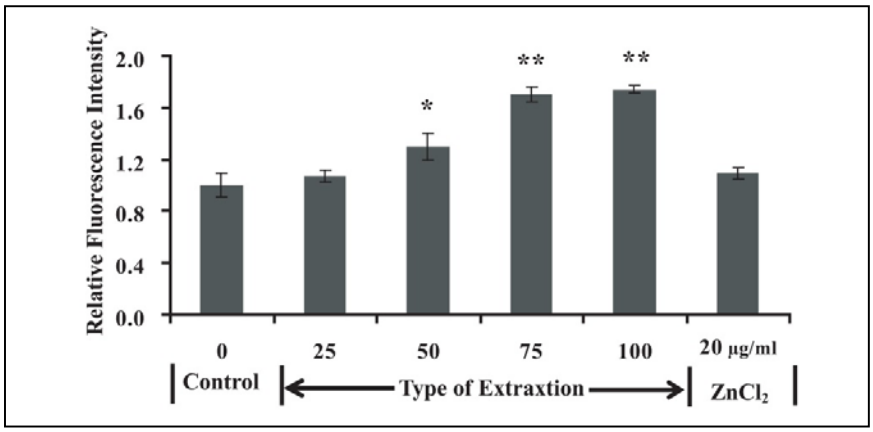

Figure 2.4 Intracellular ROS assay with DCFH-DA. The fluorescence intensity is directly proportional to the Intracellular ROS. ** $p<0.01$; * $p<0.05$

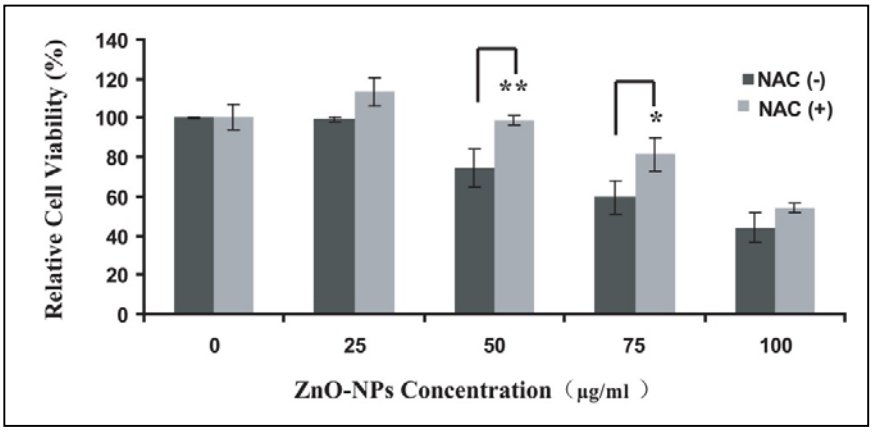

Figure 2.5 Change of cell viability after NAC pre-incubation. After pre-incubated with NAC for 2 h, A549 cells were exposed to ZnO-NPs for another 24 h and the cell viability was assayed with WST. ** $p<0.01$, * $p<0.05$

2.3.6 Synergic toxicity of ROS and zinc

We incubated the A549 cells in the exposure medium containing $ZnCl_2$ and/or H_2O_2 for 24 h. According to the concentration of H_2O_2, the exposure medium were designed as 0 mM, 0.5 mM, and 1 mM of H_2O_2 group respectively; and in each group, the concentration of $ZnCl_2$ were from 0 to 50 μg/mL. The cell viability was assayed after 24 h incubation; the viability of the cells exposed to 0 μg/mL $ZnCl_2$ of each group were used as 100% and the viability of the cells exposed to $ZnCl_2$ was rectified to be the percentage of the 0 μg/mL $ZnCl_2$ of the corresponding group. For example, in the 0.5 mM H_2O_2 group, the viability of the cells exposed to 0 μg/mL of $ZnCl_2$ was used as 100%; and the cell viability of the cells exposed to 10, 20, 30, 40 and 50 μg/mL of $ZnCl_2$ in this group were calculated to be the percentage of the 100% respectively, so that we could isolate the toxicity of $ZnCl_2$ from that of H_2O_2. As shown in Figure 2.6, in absence of H_2O_2 (0 mM H_2O_2 group), 20 μg/mL of $ZnCl_2$ had no effects on the cell viability; however in presence of 1 mM of H_2O_2 (0.5 mM and 1 mM H_2O_2 groups), 20 μg/mL of $ZnCl_2$ reduced the cell viability to about 83% and 50% of the control. In the case of 30 μg/mL of $ZnCl_2$, there was no change of the cell viability in absence of H_2O_2, while in presence of 0.5 mM and 1mM of H_2O_2 (0.5 mM and 1mM H_2O_2 groups) the cell viability decreased to 75% and 10%. And 40 μg/mL of $ZnCl_2$ resulted in that the relative cell viability decreased to 0 in presence of 1mM H_2O_2 (1 mM H_2O_2 group) but just decreased the cell viability by about 15% in absence of H_2O_2 (0 mM H_2O_2 group), and about 40% decrease in the presence of 0.5 mM of H_2O_2 (0.5 mM H_2O_2 group).

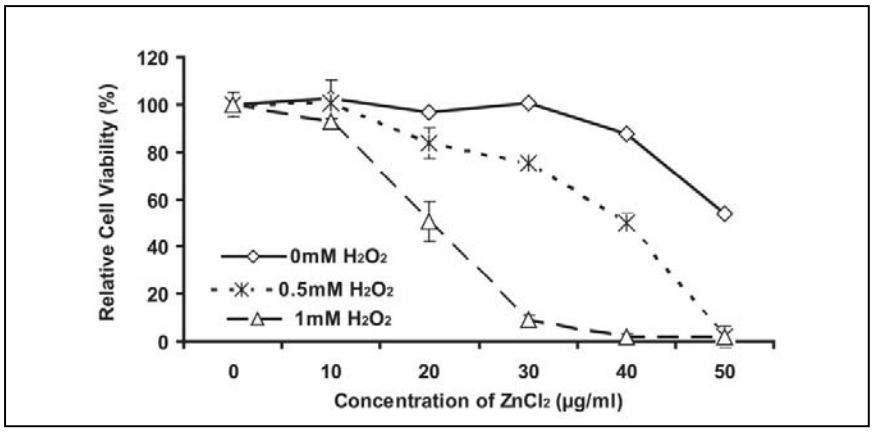

Figure 2.6 Synergic effects of H_2O_2 and zinc. The results were rectified to be the percentage of the control of the corresponding group. The statistical significance of the change of cell viability was analyzed by comparing with the control series.

2.4 Discussion

2.4.1 Exposure design

The dissolution of zinc oxide is well known and occurs over a wide range of pHs [38]. In water at pH 7.5, the overall dissolution reaction of zinc oxide can be shortly written as following: ZnO (s) $=Zn^{2+}$ (aq) + OH (aq) [39-40]. Franklin et al. fully discussed the importance of water solubility of ZnO-NPs in the toxicity study on microalga [20]. However in the previous studies, the solubility and saturation of ZnO-NPs in different culture medium were rarely taken into the consideration, which resulted in that the ZnO-NPs cytotoxicity was compared with the toxicity of the zinc salt, which consisted of the equivalent mole zinc, but was not compared with the zinc salt with the same capability to release zinc in the same solvent [18, 22, 41]. This brought about the risk deviating from real exposure status and the possibility of over- or under-estimation on the effects of the released zinc. Since the objective of this study was to identify the respective contributions of the released zinc and the solid particles to the cytotoxicity of ZnO-NPs, we used the ZnO-NPs extractions as the control of the released zinc of the ZnO-NPs suspension in the cytotoxicity assay.

For the global gene expression analysis, we used the $ZnCl_2$ medium as the released zinc control to avoid the possible impurities interference in the extractions. We measured the concentration of released zinc in the ZnO-NPs suspension and $ZnCl_2$ medium with a zinc specific chelator [42], and found the released zinc in 100 μg/mL of ZnO-NPs suspension reached saturation concentration, about 9.18 μg/mL (Table 2.2), which was equivalent to the zinc concentration of 20 μg/mL of $ZnCl_2$ medium. Therefore the 20 μg/mL of $ZnCl_2$ medium was used as control of the released zinc of 100 μg/mL ZnO-NPs suspension in gene expression analysis. Additionally, with the usage of saturation zinc concentration of the ZnO-NPs, we could avoid the possible interference of "bound zinc/free zinc" ratio induced by different solubility since this issue had not been studied clearly [43-45]. The bound zinc and free zinc are the different forms of the released zinc in the supplemented DMEM. The zinc binding capacity of DMEM has garnered concerns in *in vitro* studies. Part of the total zinc is localized by zinc-ligand in DMEM, therefore the total released zinc can be separated into two groups, one is free zinc, and the other is bound-zinc binding to protein components in the medium [46-47]. In this study the total released zinc is determined with the zinc specific chelator. We are also working on this issue since the effects of free zinc and bound zinc in *in vitro* toxicity have not been studied clearly [17] .

2.4.2 Both of solid particles and released zinc contribute to cyototoxicity

With the above modification, we found that the ZnO-NPs suspension reduced the cell viability, damaged the plasma membrane integrity and induce the deteriorative cell morphologies (Figure 2.1), but neither their extractions nor $ZnCl_2$ medium showed adverse effects on A549 cells (Figure 2.2). This findings indicates the importance of the solid particles for the ZnO-NPs cytotoxicity, as Moos et al. predicted that the presence of the solid particles was necessary for the ZnO-NPs cytotoxicity [14].

The subsequent global gene expression analysis revealed that the same one functional category, "cadmium ion binding" category, was up-regulated to respond not only to the $ZnCl_2$ but also to the ZnO-NPs, though they show directly opposite effects on the exposed cells, nontoxic and toxic respectively. The "cadmium ion binding" category consist of metallothioneins (Table 2.4) which belongs to a well-studied cysteine-rich metalloprotein family. MTs play important role in keeping the intracellular homeostasis of the heavy metals via binding, exchanging and transporting the heavy metals, such as zinc, cadmium and copper with their cysteine residuals [48-49]. For example, when cells are suddenly exposed to high levels of zinc, apo-MTs capture the excessive intracellular zinc to a nontoxic level, meanwhile the cells up-regulate the expression of MTs via metal regulatory transcription factor 1 (MTF1) mediated feedback[50]. Additionally, MTs are also reported to act as an intracellular antioxidant to quench the ROS in some special cases [51]. We exposed A549 cells to the medium containing H_2O_2 and found no change in MTs' expression (Table 2.5). Accordingly, we could rule out of the possibility that the over expression of MTs was in response of the ROS and proposed that A549 cells up-regulated MTs to respond the released zinc generated by ZnO-NPs and $ZnCl_2$, though the ZnO-NPs were well reported to produce ROS [12, 16-17, 22]. To identify the role of the released zinc in the exposures, we inhibited the MTs expression with the corresponding siRNA (Table 2.5), and found the toxicity of 100 μg/mL ZnO-NPs suspension was accentuated when the MTs expression was inhibited (Figure 2.3). This result indicates the released zinc contributes to the ZnO-NPs cytotoxicity. The cytotoxicity of the excessive zinc has been well reported such as inhibiting cellular respiration [52-53], the key enzymes in the glycolytic pathway and leading to ATP depletion in cells [54-55].

2.4.3 Synergic toxicity of solid particles and released zinc

However, inhibiting MT expression made no difference in the viability of the cells exposed to the extractions and the 20 μg/mL $ZnCl_2$ (Figure 2.3), this meant that the released zinc could not impose substantial effect on the cells in the absence of the solid particles.

About the role of the solid particles in the ZnO-NPs, there is a "Trojan-horse" theory: nanoparticles bring zinc ions into cells along with the particle internalization by cells, like the Greeks are brought into the city of Troy by the wooden horses, and lead to the adverse effects and even cell death [21, 41]. Though there is report on the internalization of ZnO-NPs by A549 cells [12], but no data can demonstrate the proportional correlation of the uptake and the cytotoxicity. We also observe the exposed cells and rarely find the endocytosis of the particles by A549 cells in this study (data not shown). The other possibility is that the particles generate ROS, since ROS is thought to be the most important mechanism of nanotoxicity [56]. With DCFH we detected intracellular ROS in the ZnO-NPs exposure, but not in cells exposed to the $ZnCl_2$ medium (Figure 2.3). Further, when we pretreated A549 cells with NAC, a precursor of intracellular antioxidant, the cell viability was recovered as opposed to the cells without NAC treatment (Figure 2.5). Thus we concluded that ROS contributed to the ZnO-NPs cytotoxicity via the solid particles.

In the case of the nanoparticles of transient metal oxides, such as copper oxide (CuO-NPs) and iron oxide, ROS is thought to be produced by the dissolved metal ions via Fenton's reaction [21-22]. However, the divalent zinc is not redox reactive and usually it is not thought to cause the Fenton reaction [19, 57]. In a previous study we also demonstrated the different toxic behavior of the typical transient metal oxide, CuO-NPs, and the semi-conduct material, ZnO-NPs [36]. The oxidation potential of ZnO nanomaterial has been attributed to the unique surface properties resulting from the quantum size [1, 58-60]. We propose the special surface reactivity of ZnO-NPs is the reason for the necessity of the solid particles for ZnO-NPs cytotoxicity.

To demonstrate the relation of the ROS and the released zinc in the cytotoxicity, we exposed A549 cells to $ZnCl_2$ and H_2O_2 simultaneously. We found the toxicity of the released zinc was exacerbated by H_2O_2 (Figure 2.6), as Heng et al. reported that the cytotoxicity of ZnO-NPs was aggravated by exogenous ROS [15]. Zhang explained the mechanism as that the ROS could incapacitate MTs via oxidation of sulfhydryl groups, led the increase of the intracellular free zinc into toxic level [61]. We propose that the solid particles produced the ROS via the special surface activity, and then the ROS can incapacitate the MTs, the most important intracellular zinc homeostasis keeping protein, and finally lead the intracellular free zinc into toxic level.

2.5 Conclusions

The findings of this study indicated that both of the solid particles and the released zinc contribute to the cytotoxicity of ZnO-NPs but the released zinc cannot arouse substantial toxicity to A549 cells in absence of the solid particles. Also we propose synergic toxicity of the released zinc and the solid particles as followings: to respond the excessive released zinc generated by ZnO-NPs, A549 cells up-regulate the expression of MTs; the solid particles produce the ROS via the special surface chemical reaction, disable the MTs, lead to the breakdown of the defense against the excessive intracellular free zinc (Figure 2.7).

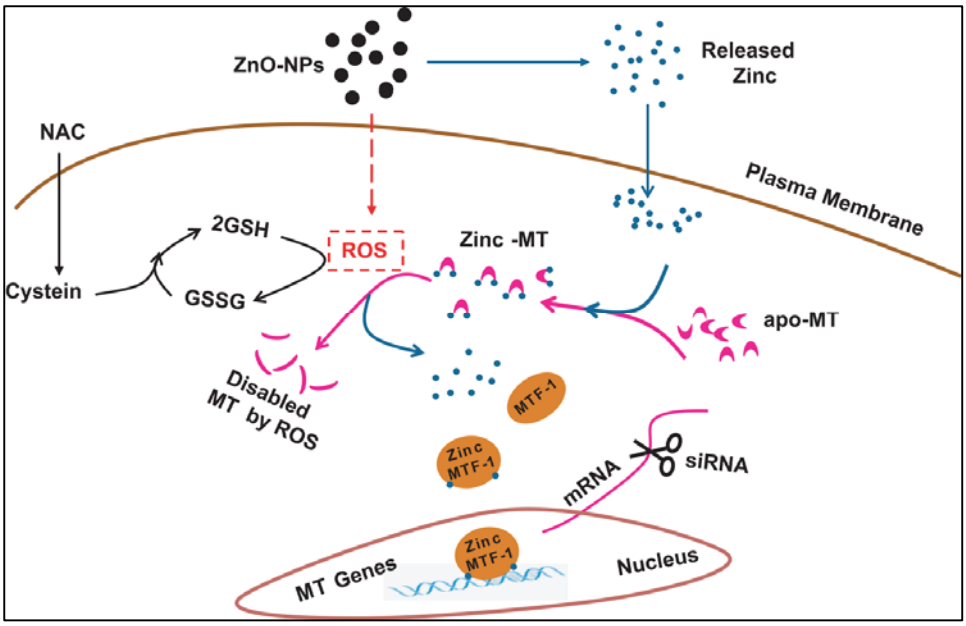

Figure 2.7 Synergic toxicity of solid particles and released zinc of ZnO-NPs to A549 cells. Once dispersed into cell culture medium, ZnO-NPs release zinc and generate ROS. To keep the homeostasis of the intracellular free zinc, A549 cells up-regulate the expression of apo-MTs (the pink crescent) via the increased zinc-MTF1 complex. ROS not only destroy the intracellular redox status, they also oxidize the MTs and result in the zinc defense breakdown.

Nowadays, human exposure to engineered nanoparticles is inevitable since nanoparticles are more and more widely used. The previous knowledge on the airborne pollutant particles, such as diesel exhaust, provides the most important knowledge on the toxicology of ultrafine particles (<100 nm), especially established the ROS model for toxicological mechanism of particulate materials [62]. However, unlike the similarity of the airborne pollutant particles, the engineered nanomaterials have distinct physicochemical properties from each other for their different chemical compositions. We have to take the real situation of exposure materials and exposed biological systems into the toxicity study case by case, which is very important in evaluating the toxicity potential and in improving the engineered nanomaterials. We suggest that both the nano-scaled superficial properties and the dissolved chemical composition of the nano-sized metal oxide should be characterized fully and the synergic effects of them deserve more concerns in the latter studies.

2.6 References

1. Fan Z.; Lu J. G. Zinc oxide nanostructures: synthesis and properties. *J Nanosci Nanotechnol* **2005**; 5: 1561-73.

2. Djurisic A. B.; Leung Y. H. Optical properties of ZnO nanostructures. *Small* **2006**, *2,* 944-961.

3. Banerjee D.; Lao J. Y.; Wang D. Z.; Huang J. Y.; Steeves D.; Kimball B.; Ren Z. F. Synthesis and photoluminescence studies on ZnO nanowires. *Nanotechnology* **2004**, *15,* 404-409.

4. De Berardis B.; Civitelli G.; Condello M.; Lista P.; Pozzi R.; Arancia G.; Meschini S. Exposure to ZnO nanoparticles induces oxidative stress and cytotoxicity in human colon carcinoma cells. *Toxicol Appl Pharmacol* **2010**, *246*, 116-127.

5. Ostrowski A. D.; Martin T.; Conti J.; Hurt I.; Harthorn B. H. Nanotoxicology: Characterizing the scientific literature, 2000-2007. *J Nanopart Res* **2009**, *11,* 251-257.

6. OECD, Guidance manual for the testing of manufactured nanomaterials: OECD's sponsorship programme. In **2009**.

7. Zhu X. S.; Zhu L.; Duan Z. H.; Qi R. Q.; Li Y.; Lang Y. P. Comparative toxicity of several metal oxide nanoparticle aqueous suspensions to Zebrafish (Danio rerio) early developmental stage. *J Environ Sci Heal A* **2008**, *43,* 278-284.

8. Wiench K.; Wohlleben W.; Hisgen V.; Radke K.; Salinas E.; Zok S.; Landsiedel R. Acute and chronic effects of nano- and non-nano-scale TiO_2 and ZnO particles on mobility and reproduction of the freshwater invertebrate Daphnia magna. *Chemosphere* **2009**, *76,* 1356-1365.

9. Lin D. H.; Xing B. S. Phytotoxicity of nanoparticles: Inhibition of seed germination and root growth. *Environ Pollut* **2007**, *150,* 243-250.

10. Jones N.; Ray B.; Ranjit K. T.; Manna A. C. Antibacterial activity of ZnO nanoparticle suspensions on a broad spectrum of microorganisms. *Fems Microbiol Lett* **2008**, *279,* 71-76.

11. Jeng H. A.; Swanson J. Toxicity of metal oxide nanoparticles in mammalian cells. *J Environ Sci Heal A* **2006**, *41,* 2699-2711.

12. Lin W. S.; Xu Y.; Huang C. C.; Ma Y. F.; Shannon K. B.; Chen D. R.; Huang Y. W. Toxicity of nano- and micro-sized ZnO particles in human lung epithelial cells. *J Nanopart Res* **2009**, *11,* 25-39.

13. Gojova A.; Guo B.; Kota R. S.; Rutledge J. C.; Kennedy I. M.; Barakat A. I. Induction of inflammation in vascular endothelial cells by metal oxide nanoparticles: Effect of particle composition. *Environ Health Perspect* **2007**, *115,* 403-409.

14. Moos P. J.; Chung K.; Woessner D.; Honeggar M.; Cutler N. S.; Veranth J. M. ZnO Particulate matter requires cell contact for toxicity in human colon cancer cells. *Chem Res Toxicol* **2010**, *23,* 733-739.

15. Heng B. C.; Zhao X. X.; Xiong S. J.; Ng K. W.; Boey F. Y. C.; Loo J. S. C. Toxicity of zinc oxide (ZnO) nanoparticles on human bronchial epithelial cells (BEAS-2B) is accentuated by oxidative stress. *Food Chem Toxicol* **2010**, *48,* 1762-1766.

16. Sharma V.; Shukla R. K.; Saxena N.; Parmar D.; Das M.; Dhawan A. DNA damaging potential of zinc oxide nanoparticles in human epidermal cells. *Toxicol Lett* **2009**, *185,* 211-218.

17. Yin H.; Casey P. S.; Mccall M. J.; Fenech M. Effects of surface chemistry on cytotoxicity, genotoxicity, and the generation of reactive oxygen species induced by ZnO nanoparticles. *Langmuir* **2010**, *26,* 15399-15408.

18. Brunner T. J.; Wick P.; Manser P.; Spohn P.; Grass R. N.; Limbach L. K.; Bruinink A.; Stark W. J. *In vitro* cytotoxicity of oxide nanoparticles: Comparison to asbestos, silica, and the effect of particle solubility. *Environ Sci Technol* **2006**, *40,* 4374-4381.

19. Eigen M. Fast elementary steps in chemical reaction mechanisms. *Pure Appl Chem* **1963**, *6,* 97-116.

20. Franklin N. M.; Rogers N. J.; Apte S. C.; Batley G. E.; Gadd G. E.; Casey P. S. Comparative toxicity of nanoparticulate ZnO, bulk ZnO, and $ZnCl_2$ to a freshwater microalga (Pseudokirchneriella subcapitata): The importance of particle solubility. *Environ Sci Technol* **2007**, *41,* 8484-90.

21. Limbach L. K.; Wick P.; Manser P.; Grass R. N.; Bruinink A.; Stark W. J. Exposure of engineered nanoparticles to human lung epithelial cells: Influence of chemical composition and catalytic activity on oxidative stress. *Environ Sci Technol* **2007**, *41,* 4158-4163.

22. Xia T.; Kovochich M.; Liong M.; Madler L.; Gilbert B.; Shi H. B.; Yeh J. I.; Zink J. I.; Nel A. E. Comparison of the mechanism of toxicity of zinc oxide and cerium oxide nanoparticles based on dissolution and oxidative stress properties. *Acs Nano* **2008**, *2,* 2121-2134.

23. Heyder J. Deposition of inhaled particles in the human respiratory tract and consequences for regional targeting in respiratory drug delivery. *Proc Am Thorac Soc* **2004**, *1,* 315-20.

24. Muhlfeld C.; Rothen-Rutishauser B.; Blank F.; Vanhecke D.; Ochs M.; Gehr P. Interactions of nanoparticles with pulmonary structures and cellular responses. *Am J Physiol Lung Cell Mol Physiol* **2008**, *294,* L817-29.

25. Singh S.; Shi T.; Duffin R.; Albrecht C.; Van Berlo D.; Hohr D.; Fubini B.; Martra G.; Fenoglio I.; Borm P. J.; Schins R. P. Endocytosis, oxidative stress and IL-8 expression in human lung epithelial cells upon treatment with fine and ultrafine TiO2: role of the specific surface area and of surface methylation of the particles. *Toxicol Appl Pharmacol* **2007**, *222,* 141-51.

26. Kim J. S.; Yoon T. J.; Yu K. N.; Noh M. S.; Woo M.; Kim B. G.; Lee K. H.; Sohn B. H.; Park S. B.; Lee J. K.; Cho M. H. Cellular uptake of magnetic nanoparticle is mediated through energy-dependent endocytosis in A549 cells. *J Vet Sci* **2006**, *7,* 321-6.

27. Stringer B.; Kobzik L. Environmental particulate-mediated cytokine production in lung epithelial cells (A549): Role of preexisting inflammation and oxidant stress. *J Toxicol Env Heal A* **1998**, *55,* 31-44.

28. Foster K. A.; Oster C. G.; Mayer M. M.; Avery M. L.; Audus K. L. Characterization of the A549 cell line as a type II pulmonary epithelial cell model for drug metabolism. *Exp Cell Res* **1998**, *243,* 359-366.

29. Thompson A. B.; Robbins R. A.; Romberger D. J.; Sisson J. H.; Spurzem J. R.; Teschler H.; Rennard S. I. Immunological functions of the pulmonary epithelium. *Eur Respir J* **1995**, *8,* 127-149.

30. Hanagata N.; Zhuang F.; Connolly S.; Li J.; Ogawa N.; Xu M. S. Molecular responses of human lung epithelial cells to the toxicity of cpper oxide nanoparticles inferred from whole genome expression analysis. *Acs Nano* **2011**, *5,* 9326-9338.

31. Hosack D. A.; Dennis G.; Sherman B. T.; Lane H. C.; Lempicki R. A. Identifying biological themes within lists of genes with EASE. *Genome Biol* **2003**, *4*.

32. Keller A.; Mohamed A.; Drose S.; Brandt U.; Fleming I.; Brandes R. P. Analysis of dichlorodihydrofluorescein and dihydrocalcein as probes for the detection of intracellular reactive oxygen species. *Free Radical Res* **2004**, *38,* 1257-1267.

33. Halliwell B.; Whiteman M. Measuring reactive species and oxidative damage *in vivo* and in cell culture: how should you do it and what do the results mean? *Brit J Pharmacol* **2004**, *142,* 231-255.

34. Wang H.; Joseph J. A. Quantifying cellular oxidative stress by dichlorofluorescein assay using microplate reader. *Free Radic Biol Med* **1999**, *27,* 612-616.

35. Kowaltowski A. J.; Vercesi A. E. Mitochondrial damage induced by conditions of oxidative stress. *Free Radic Biol Med* **1999**, *26,* 463-71.

36. Xu M. S.; Fujita D.; Kajiwara S.; Minowa T.; Li X. L.; Takemura T.; Iwai H.; Hanagata N. Contribution of physicochemical characteristics of nano-oxides to cytotoxicity. *Biomaterials* **2010**, *31,* 8022-8031.

37. Zhuang F.; Hanagata N.. Synergic toxicity of solid particles and released zinc of zinc oxide nanoparticles to human lung epithelial cells. *Nano Biomedicine* **2012**, *4,* 90-112.

38. Bian S. W.; Mudunkotuwa I. A.; Rupasinghe T.; Grassian V. H. Aggregation and dissolution of 4 nm ZnO nanoparticles in aqueous environments: Influence of pH, ionic strength, size, and adsorption of humic acid. *Langmuir* **2011**, *27,* 6059-6068.

39. Yamabi S.; Imai H. Growth conditions for wurtzite zinc oxide films in aqueous solutions. *J Mater Chem* **2002**, *12,* 3773-3778.

40. Degen A.; Kosec M. Effect of pH and impurities on the surface charge of zinc oxide in aqueous solution. *J Eur Ceram Soc* **2000**, *20,* 667-673.

41. Deng X. Y.; Luan Q. X.; Chen W. T.; Wang Y. L.; Wu M. H.; Zhang H. J.; Jiao Z. Nanosized zinc oxide particles induce neural stem cell apoptosis. *Nanotechnology* **2009**, *20*, 115101.

42. Makino T.; Saito M.; Horiguchi D.; Kina K. A highly sensitive colorimetric determination of serum zinc using water-soluble pyridylazo dye. *Clin Chim Acta* **1982**, *120,* 127-135.

43. Bai W.; Zhang Z. Y.; Tian W. J.; He X.; Ma Y. H.; Zhao Y. L.; Chai Z. F. Toxicity of zinc oxide nanoparticles to zebrafish embryo: a physicochemical study of toxicity mechanism. *J Nanopart Res* **2010**, *12,* 1645-1654.

44. Nel A. E.; Madler L.; Velegol D.; Xia T.; Hoek E. M. V.; Somasundaran P.; Klaessig F.; Castranova V.; Thompson M. Understanding biophysicochemical interactions at the nano-bio interface. *Nat Mater* **2009**, *8,* 543-557.

45. Cedervall T.; Lynch I.; Lindman S.; Berggard T.; Thulin E.; Nilsson H.; Dawson K. A.; Linse S. Understanding the nanoparticle-protein corona using methods to quantify exchange rates and affinities of proteins for nanoparticles. *Proc Natl Acad Sci U S A* **2007**, *104,* 2050-2055.

46. Lu J.; Stewart A. J.; Sadler P. J.; Pinheiro T. J. T.; Blindauer C. A. Albumin as a zinc carrier: properties of its high-affinity zinc-binding site. *Biochem Soc Trans* **2008**, *36,* 1317-1321.

47. Bozym R. A.; Chimienti F.; Giblin L. J.; Gross G. W.; Korichneva I.; Li Y. A.; Libert S.; Maret W.; Parviz M.; Frederickson C. J.; Thompson R. B. Free zinc ions outside a narrow concentration range are toxic to a variety of cells in vitro. *Exp Biol Med* **2010**, *235,* 741-750.

48. Guan Y. S. Comments to metallothionein as an anti-inflammatory mediator. *Mediat Inflamm* **2009**, *2009*, 426214.

49. Inoue K. I.; Takano H.; Shimada A.; Satoh M. Metallothionein as an anti-inflammatory mediator. *Mediat Inflamm* **2009**, *2009 suppl.1*, 101659.

50. Gyulkhandanyan A. V.; Lee S. C.; Bikopoulos G.; Dai F. H.; Wheeler M. B. The Zn^{2+}-transporting pathways in pancreatic β-cells. *J Biol Chem* **2006**, *281,* 9361-9372.

51. Vliagoftis A.; Schwingshackl A.; Milne C. D.; Duszyk M.; Hollenberg M. D.; Wallace J. L.; Befus A. D.; Moqbel R. Proteinase-activated receptor-2-mediated matrix metalloproteinase-9 release from airway epithelial cells. *J Allergy Clin Immun* **2000**, *106,* 537-545.

52. Sensi S. L.; Yin H. Z.; Carriedo S. G.; Rao S. S.; Weiss J. H. Preferential Zn^{2+} influx through Ca^{2+}-permeable AMPA/kainate channels triggers prolonged mitochondrial superoxide production. *Proc Natl Acad Sci U S A* **1999**, *96,* 2414-2419.

53. Frazzini V.; Rockabrand E.; Mocchegiani E.; Sensi S. L. Oxidative stress and brain aging: is zinc the link? *Biogerontology* **2006**, *7,* 307-314.

54. Dineley K. E.; Votyakova T. V.; Reynolds I. J. Zinc inhibition of cellular energy production: implications for mitochondria and neurodegeneration. *J Neurochem* **2003**, *85,* 563-570.

55. Gazaryan I. G.; Krasinskaya I. P.; Kristal B. S.; Brown A. M. Zinc irreversibly damages major enzymes of energy production and antioxidant defense prior to mitochondrial permeability transition. *J Biol Chem* **2007**, *282,* 24373-24380.

56. Nel A.; Xia T.; Madler L.; Li N. Toxic potential of materials at the nanolevel. *Science* **2006**, *311,* 622-627.

57. Nakamura M.; Shishido N.; Nunomura A.; Smith M. A.; Perry G.; Hayashi Y.; Nakayama K.; Hayashi T. Three histidine residues of amyloid-beta peptide control the redox activity of copper and iron. *Biochemistry* **2007**, *46,* 12737-43.

58. Chiou J. W.; Kumar K. P. K.; Jan J. C.; Tsai H. M.; Bao C. W.; Pong W. F.; Chien F. Z.; Tsai M. H.; Hong I. H.; Klauser R.; Lee J. F.; Wu J. J.; Liu S. C. Diameter dependence of the electronic structure of ZnO nanorods determined by x-ray absorption spectroscopy and scanning photoelectron microscopy. *Appl Phys Lett* **2004**, *85,* 3220-3222.

59. Wang X. D.; Ding Y.; Summers C. J.; Wang Z. L. Large-scale synthesis of six-nanometer-wide ZnO nanobelts. *J Phys Chem B* **2004**, *108,* 8773-8777.

60. Kukreja L. M.; Barik S.; Misra P. Variable band gap ZnO nanostructures grown by pulsed laser deposition. *J Cryst Growth* **2004**, *268,* 531-535.

61. Zhang B.; Georgiev O.; Hagmann M.; Gunes C.; Cramer M.; Faller P.; Vasak M.; Schaffner W. Activity of metal-responsive transcription factor 1 by toxic heavy metals and H_2O_2 in vitro is modulated by metallothionein. *Mol Cell Biol* **2003**, *23,* 8471-8485.

62. Li N.; Sioutas C.; Cho A.; Schmitz D.; Misra C.; Sempf J.; Wang M.; Oberley T.; Froines J.; Nel A. Ultrafine particulate pollutants induce oxidative stress and mitochondrial damage. *Environ Health Perspect* **2003**, *111,* 455-60.

Chapter 3 Molecular Response to Copper Oxide Nanoparticle

3.1 Introduction

As a result of recent advances in nanotechnology, the industrial use of nanomaterials is increasing. Although the size, shape, surface area, and surface activity of nanomaterials are attractive for many different applications, concern exists that these properties may contribute to the toxicity of nanomaterials. For example, their small size could allow them to easily enter the body through respiratory passages or wounds and affect various tissues. However, clear safety standards have not been established for nanomaterials.

Previously, we demonstrated that copper oxide nanoparticles (CuO-NPs) are the most toxic metal oxide nanoparticles [1-2]. CuO-NPs are used in textiles for their antibacterial effects [3]. They are also being developed for use in catalysts, gas sensors, microelectronic materials, and cosmetics [4-5]. Furthermore, CuO-NPs are added as materials to ink, plastics, lubricants, metallurgical coatings, and cosmetics for the skin [6]. Although SiO_2-NPs (15-25 nm), CeO_2-NPs (20 nm), and Al_2O_3- NPs (15-50 nm) are not toxic to A549 cells, ZnO-NPs (20-60 nm) are cytotoxic to a lesser extent than CuO-NPs [1-2].

These findings suggest that the toxicity of metal oxide nanoparticles is not due to their size but their chemical composition. Specifically, metal oxide nanoparticles suchas CuO-NPs and ZnO-NPs that release metal ions are most likely to be cytotoxic. In addition to CuO-NPs and ZnO-NPs, Ag-NPs are highly cytotoxic to HeLa cervical cancer cells, and Ag ions that are released into the culture medium are responsible for much of the toxicity [7]. However, until recently, the nanoparticles themselves, rather than released Cu ions, have been suggested to cause CuO-NP cytotoxicity [8-9]. The uptake of CuO-NPs into cells and subsequent generation of intracellular reactive oxygen species (ROS) have been reported to cause cytotoxicity and genotoxicity [8, 10], but the molecular basis of CuO-NP toxicity has not been clarified.

Human lung epithelial A549 cells were used in this study because we have a greater

chance of inhaling nanoparticles in the workplace rather than taking them up through the skin, ingestion, and injection. A549 cells that were derived from carcinoma tissue are classified as type I pneumocytes, which cover >95% of the internal surface that provides a barrier function and gas exchange in the lung. We used DNA microarrays to analyze the effects of CuO-NPs on the global gene expression of A549 cells. First, we identified genes affected by exposure to CuO-NPs and inferred functional changes of cells using gene ontology (GO) analysis, in which affected genes were classified into functional categories. Next, we performed global gene expression analysis of cells exposed to Cu ions released from CuO-NPs into medium and identified genes that were regulated by both CuO-NPs and released Cu ions.These analyses revealed the contribution of released Cu ions to the toxicity of CuO-NPs at the molecular level. Furthermore, we examined the gene expression of cells exposed to different concentrations of $CuCl_2$ to confirm the contribution of Cu ions released from CuO-NPs. Our results suggest that the in vitro cytotoxicity of CuO-NPs is primarily due to the effects of Cu ions that are released into the culture medium and absorbed into cells.

3.2 Materials and Methods

3.2.1 CuO nanoparticles

CuO nanoparticles (CuO-NPs) were purchased from Sigma-Aldrich (MO, USA). The average diameter of these particles was 50 nm. The mean aggregate size of the particles after dispersal in a medium was assessed using a laser diffraction particle size analyzer (DLS6000AL, Otsuka, Japan) at a concentration of 25 μg/mL.

3.2.2 Preparing medium containing CuO-NPs and medium containing released Cu

To prepare the medium containing CuO-NPs, CuO-NPs were first dispersed in water sterilized with ultrasonic waves for 15 min. Next, CuO-NPs were added to high-glucose Dulbecco's modified Eagle's medium supplemented with 10% fetal bovine serum, 100 units/mL penicillin, and 100 μg/mL streptomycin (hereafter referred to as DMEM) to obtain a

concentration of 25 μg/mL CuO-NPs. This medium was prepared just prior to its use. To prepare the medium containing released Cu ions, the medium containing CuO-NPs was incubated in a rotary shaker 37 ℃ for 24 h. The CuO-NP suspension was then centrifuged at 150 000 g for 1 h to eliminate the NPs. The upper portion of supernatant was collected and used as medium containing Cu ions released from CuO-NPs.

To measure the concentration of Cu in the supernatant, the supernatant was ashed using nitric acid and perchloric acid and then diluted with water. The concentration was then measured using coupled plasma optical emission spectrometry (ICP-OES; SPS1700HVR, Seiko Instruments Inc., Chiba, Japan).

To study CuO-NPs in the cell culture medium, a grid for transmission electron microscopy (TEM) was immersed in the CuO-NP suspension (25 μg/mL) for 24 h and then dried in air. To confirm the removal of NPs by centrifugation, a TEM grid was immersed in the supernatant for 24 h and dried in air. The darkfield TEM images, elemental mapping, and energy-dispersive spectroscopy (EDS) spectrum were obtained by JEM-2100F (JEOL, Tokyo, Japan). The size of Cu-NPs after incubation for 24 h was examined scanning electron microscope (SEM) (S-4800, Hitachi High-Technology, Tokyo Japan).

3.2.3 Cell culture

Carcinoma-derived human lung epithelial A549 cells were seeded in culture dishes and plates with DMEM at a concentration of 5 000 cells/cm^2. Normal human small airway epithelial cells (SAEC, TaKaRa Bio, Tokyo, Japan) were seeded in basal medium (SAGM BulletKit, TaKaRa Bio) at a concentration of 2 500 cells/cm^2. After culturing in medium at 37 ℃ in a 5% CO_2 humidified environment for 48 h, the cell concentration of this culture reached about 70% confluence. Next, the medium used to culture the cells was replaced with media containing CuO-NPs, released Cu ions, or $CuCl_2$. After culturing the cells for another 24 h, the cellular toxicity of the culture was evaluated. Six-well culture plates were used for the following: viable

cell counts, calcein-AM staining, propidium iodide (PI) staining, TUNEL assay, DNA microarray, real-time quantitative PCR (qPCR), p38 and JNK inhibition, and siRNA-based gene knockdown. Ninety-six-well culture plates were used for the formazan formation assay. Furthermore, 35 mm glass bottom dishes were used for detecting mitochondrial damage.

3.2.4 Evaluation of cytotoxicity

Cytotoxicity of the cells was evaluated by assessing viable cell counts and formazan formation. To count cells, cells were removed from cell plates by trypsin treatment after washing with PBS three times. These cells were centrifuged at 2 000 g for 2 min and then resuspended in DMEM. A hemocytometer was used to count viable cells not stained with trypan blue. To count the total number of cells, cells were visually counted in eight different areas for each of the four independently prepared rounds of cultures. To visualize whether a cell was dead or alive, cells on each plate were double-stained with calcein-AM and PI using the Cellstain Double Staining Kit (Dojindo, Kumamoto, Japan). Each stained cell was observed under a fluorescence microscope. To determine the ratio of apoptotic cells, harvested cells were fixed in ethanol and then stained with PI and FITC-labeled Annexin V. Fluorescent intensity was measured with flow cytometry (FACS Calibur, BD, NJ, USA). The level of formazan formed from the water-soluble tetrazolium salt (WST-8) was measured using Dojindo's Cell Counting Kit-8.

3.2.5 Observation of internalized CuO-NPs

Cells exposed to CuO-NPs for 24 h were removed from culture plates by trypsin treatment and harvested by centrifugation at 2000 g for 2 min. The cells were fixed with a mixture of 2% paraformaldehyde and 2.5% glutaraldehyde in 0.1 M cacodylate buffer (pH 7.4) for 2 h at room temperature. After a short rinse in the buffer, the samples were postfixed for 1 h in 1% OsO_4 in 0.1 M cacodylate buffer (pH 7.4). The samples were then rinsed in the buffer, dehydrated in a graded series of ethanol, and embedded in Spurr resin (Agar Scientific,

England). Ultrathin sections were cut with an ultramicrotome (EM UC-6, Leica, Wetzlar, Germany) using a diamond knife. Sections were examined with a JEM-2100F (JEOL) for the dark-field TEM image and elemental mapping. Sections were stained with oolong tea extract (Oken Shoji, Tokyo, Japan), Ti blue (Oken Shoji), and lead citrate for observation with a field emission transmission electron microscope (JEM-3000F, JEOL).

3.2.6 Detection of mitochondrial damage

A549 cells were seeded at a concentration of 5 000 cells/cm^2. After culturing for 48 h, CuO-NPs were added to the cells to obtain a concentration of 25 μg/ mL, and the cells were cultured for an additional 4 h. This treatment was followed by the addition of $CuCl_2$ to obtain a concentration of 30 μg/mL, and the cells were further cultured.

To detect mitochondrial damage, cells were stained with JC-1 (5,50,6,60-tetrachloro-1,10,3,30-tetrathylbenzinidazolylcarbocyanin iodide; Invitrogen, CA, USA), and mitochondria were detected using a confocal laser microscope. Damaged mitochondria accumulate less JC-1 and therefore exhibit less fluorescence.

3.2.7 DNA microarray analysis

Cells cultured previously in DMEM for 48 h were further cultured for 24 h in media containing CuO-NPs, released Cu ions, or in DMEM (control medium). Total RNA was then recovered from the cells in each culture using ISOGEN (Nippon Gene, Tokyo, Japan). These RNAs were amplified using Amino Allyl MessageAmp II aRNA Amplification Kit (Ambion, TX, USA) and then labeled with Cy3 and Cy5. Whole Human Genome Microarray Kit 4- 44K (Agilent, CA, USA) was applied to the Cy3- and Cy5-labeled amplified RNAs, which were then competitively hybridized for 18 h at 65 ℃. After washing this DNA microarray, the fluorescence intensity of Cy3 and Cy5 was scanned using GenePix 4000B (Molecular Devise, CA, USA) at 10 μm resolution at three levels, from a low PTM gain value to a high value. Spots in the scanned images were detected using GenePix Pro (Molecular Devise). The foreground

and background median values of each spot were obtained from the median values of the pixels included in each spot area. The difference between the foreground and background values of each spot was established as the signal strength. The standard deviation of the background values was treated as the noise value. Only spots with signal values 3X the noise value or greater were considered valid spots. Data from scans, whose gains were separated into three levels, were globally normalized and merged. Finally, locally weighted scatterplot smoothing (LOWESS) adjustment was applied.

The DNA microarray experiment was carried out twice using RNA obtained from different cultures. For the first trial, RNA obtained from cells cultured in the control medium was labeled with Cy3. RNA obtained from cells cultured in media containing CuO-NPs and released Cu ions was labeled with Cy5. Genes whose Cy5 fluorescence intensity was 2X the fluorescence intensity of Cy3 or greater, or 0.5X the fluorescence intensity of Cy3 or lesser, were extracted as genes with altered expression levels. For the second trial, the roles of Cy3 and Cy5 were switched; that is, RNA obtained from the control cells was labeled with Cy5. Genes with altered expression level as indicated by the ratio of Cy3 to Cy5 fluorescence intensity were extracted. Of these extracted genes, only genes whose ratio of expression levels from the two trials was less than double the margin of error were identified as reproducible genes. The ratio of the expression levels of these genes was set as the average value of the two trials.

Next, these genes were placed into GO biological process categories using PANTHER gene expression analysis/compare gene lists (http://www.pantherdb.org/tools/genexAnalysis.jsp). Significant changes were indicated by categories with over (+) and p value <0.001.

3.2.8 Real-time quantitative PCR

Real-time quantitative PCR (qPCR) was performed to confirm the reproducibility of the ratio of RNA expression levels obtained from independent cultures for certain genes that revealed altered expression levels during the DNA microarray analysis. The primer sequence of each gene for qPCR is shown in Table S10 of reference 11[11]. The expression level of each gene

was set as a value relative to the expression level of the GAPDH gene.

3.2.9 Western blotting

The following primary antibodies were used for Western blotting: anti-GADD45B polyclonal antibody (ab105060, abcam, Cambridge, UK), anti-GADD45G polyclonal antibody (ab96578, abcam,), anti-NR4A1 monoclonal antibody (ab109180, abcam), anti-NR4A3 monoclonal antibody (WH0008013M6, Sigma-Aldrich), anti-CDC2 polyclonal antibody (9122, Cell Signaling Technology, MA, USA), anti-CCNB1 monoclonal antibody (ab72, abcam).

A549 cells were seeded at 5 000 cells/cm^2 in 14.5 cm culture dishes containing DMEM. After 48 h, medium was replaced with media containing CuO-NPs, released Cu ions, or $CuCl_2$ and cultured for another 24 h. Total protein was extracted using RIPA buffer (Thermo Fisher Scientific, MA, USA) after cell washing with PBS buffer. Thirty micrograms of total protein was size fractionated on a precast SDS-polyacrylamide gel (15% acrylamide, Atto Corporation, Tokyo, Japan) and blotted onto an Immobilon-PSQ membrane (Millipore, MA, USA). After 1 h of blocking at room temperature with 3% immunoblot blocking reagent (Millipore), the membrane was incubated overnight at 4 ℃ with a primary antibody. The membrane was then washed three times with PBS buffer containing 0.05% Tween-20 and incubated for 1 h at room temperature or overnight at 4 ℃ with HRP-F(ab')2 goat antirabbit IgG(HtL) (Zymed Laboratories, CA, USA) or HRP goat anti-mouse IgG(HtL) (Zymed Laboratories). Proteins were detected using Immobilon Western chemiluminescent HRP substrate (Millipore).

3.2.10 Inhibition of JNK and p38

A549 cells were cultured in DMEM for 46 h. JIP-1 peptide (GIBCO) or SB239063 (Sigma-Aldrich), inhibitor of JNK and p38, respectively, was added so that the concentration of each reagent was 10 μM. After 2 h, these media were exchanged with media containing CuO-NPs, to which JIP-1 peptide or SB239063 was added to obtain the same concentration. The cells were cultured for another 24 h, and the number of live cells was counted.

3.2.11 Knock-down of GADD45B and NR4A1 using siRNA

The sequences of siRNAs used to knock down genes were the following: GADD45B sense (50-GCACUUAUUCGAACCATT-30) and antisense (50-UGGUUCGAAUAACAAGUGCTT-30); NR4A1 sense (50-GCAUGGUGAAGGAAGUUGUTT-30) and antisense (50-ACAACUUCCUUCACCAUGCTT- 30). A549 cells were cultured in DMEM for 42 h, and each siRNA was added to the control medium to obtain a concentration of 25 μM. The siRNAs were introduced using Lipofectamine RNAiMAX (Invitrogen). After 6 h, the media were exchanged with medium containing CuO-NPs, and each siRNA was transfected. After culturing for 24 h, the number of viable cells was counted. Control cells were transfected with siRNA with the sequence of sense (50-UCUUAAUCGCGUAUAAGGCTT-30) and antisense (50-GCCUUAUACGCGAUUAAGATT-30).

3.2.12 N-acetylcysteine treatment

A549 cells were cultured in a 96-well plate or 35 mm dish for 46 h, and N-acetylcysteine (NAC) was added to the medium to obtain a concentration of 10 mM. After 2 h, the media were exchanged with medium containing CuO-NPs or released Cu ions. The cells were cultured another 24 h to examine recovery from toxicity.

3.2.13 Cell cycle analysis

Cells cultured previously in DMEM for 48 h were cultured for a further 24 h in media containing 25 μg/mL CuO-NPs, released Cu ions, or in DMEM (control medium). These cells were harvested, fixed in ethanol, and then stained with PI. Fluorescence intensity was measured with flow cytometry (FACS Calibur).

3.2.14 Statistics

Differences between samples and control were evaluated using two-tailed Student's

t-test, and post hoc Bonferroni correction was performed for multiple comparisons. The results were considered significant if $p < 0.05$.

3.3 Results and Discussion

3.3.1 Preparing and characterizing medium containing released Cu

The average diameter of CuO-NPs used in this study was 50 nm and the mean aggregate size of the particles after dispersal in medium at a concentration of 25 μg/mL was around 300 nm (Figure 3.1). However, CuO-NPs immediately subsided. The morphology and electronic properties of CuO-NPs have been reported previously [1].

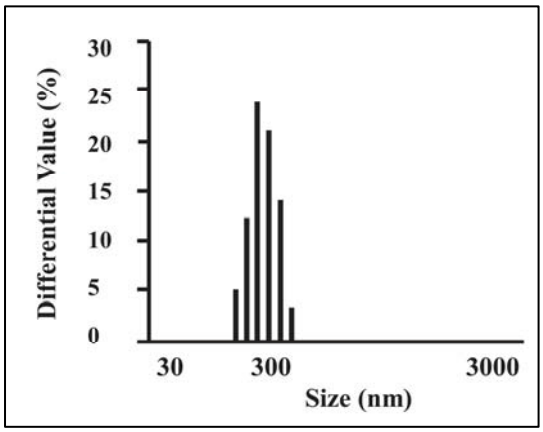

Figure 3.1 Particle size distribution of CuO-NPs (25 μg/ml) in culture medium assessed by using a laser diffraction particle size analyzer.

To investigate the contribution of the released Cu ions to the toxicity of CuO-NPs, we prepared culture medium containing Cu ions released from CuO-NPs (Figure 3.2a). CuO-NPs (25 μg/mL final concentration) were added to the culture medium and incubated at 37 ℃ for 24 h. Then, the medium containing CuO-NPs was centrifuged at 150 000 g for 1 h to remove the CuO-NPs. Inductively coupled plasma optical emission spectrometry (ICPOES) indicated that the Cu concentration in the resulting supernatant was 13.2±1.54μg/mL (11.6-15.0μg/mL, n =5). To examine the presence or absence of CuO-NPs in the supernatant, we analyzed the supernatant using a laser diffraction particle analyzer (DLS). The analysis revealed the presence of NPs in the supernatant (Figure 3.3a). However, the similar pattern of size distribution was

also observed in the culture medium without CuO-NPs after incubation at 37 ℃ for 24 h (Figure 3.3b and Figure 3.2b), suggesting that the NPs in the supernatant are attributed to medium components, not CuO-NPs. In addition, as shown by transmission electron microscopy (TEM) and energy-dispersive spectroscopy (EDS) (Figure 3.3c-f), NPs in the supernatant contained hardly any CuO-NPs. On the other hand, observation of the resulting precipitation that contains CuO-NPs removed from the culture medium, using scanning electron microscope (SEM), revealed CuO-NPs with smaller than original size (Figure 3.3g, h). This implies that CuO-NPs released Cu ions into the culture medium, resulting in smaller size. Therefore, we used the supernatant as the culture medium containing released Cu ions to assess the contribution of the released Cu ions to the toxicity of CuO-NPs. Although CuO-NPs released Cu ions into the medium, they hardly released the ions in water (Figure 3.2c).

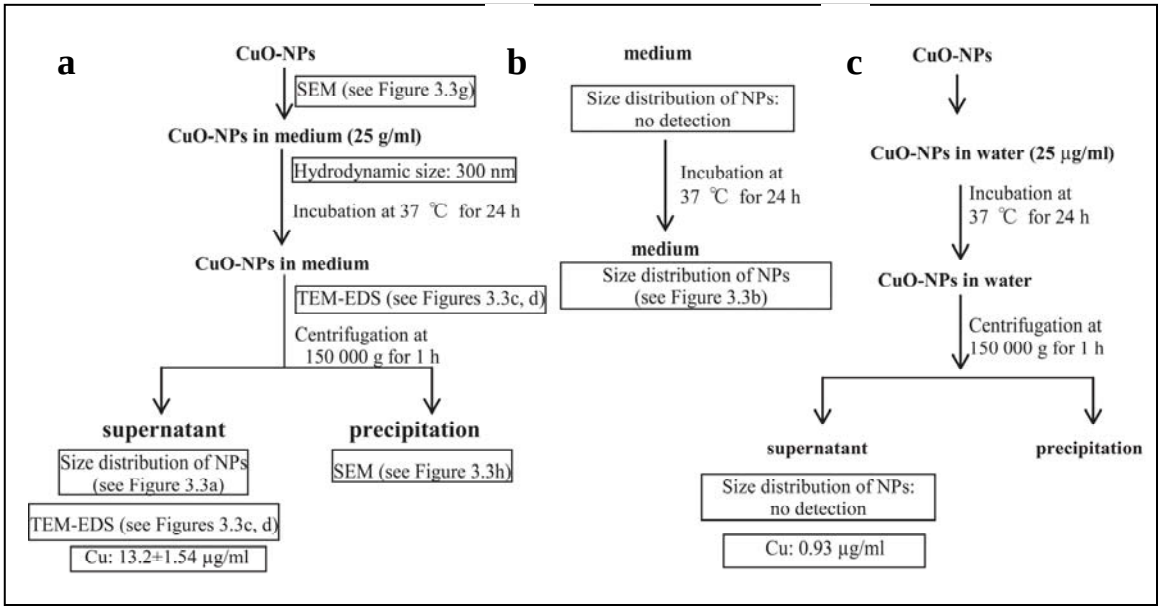

Figure 3.2 Preparation and characterization of medium containing Cu ions released from CuO-NPs. (a) The culture medium with CuO-NPs (25 μg/ml) was incubated at 37 ℃ for 24 , and then centrifuged. The supernatant was used to estimate contribution of Cu ions released from CuO-NPs toxicity. (b) Culture medium without CuO-NPs was incubated at 37 ℃ for 24 h, and then particle size distribution was measured with a laser diffraction size analyzer. (c) CuO-NPs in water were incubated at 37 ℃ for 24 h, and then centrifuged. No particles were detected in the supernatant.

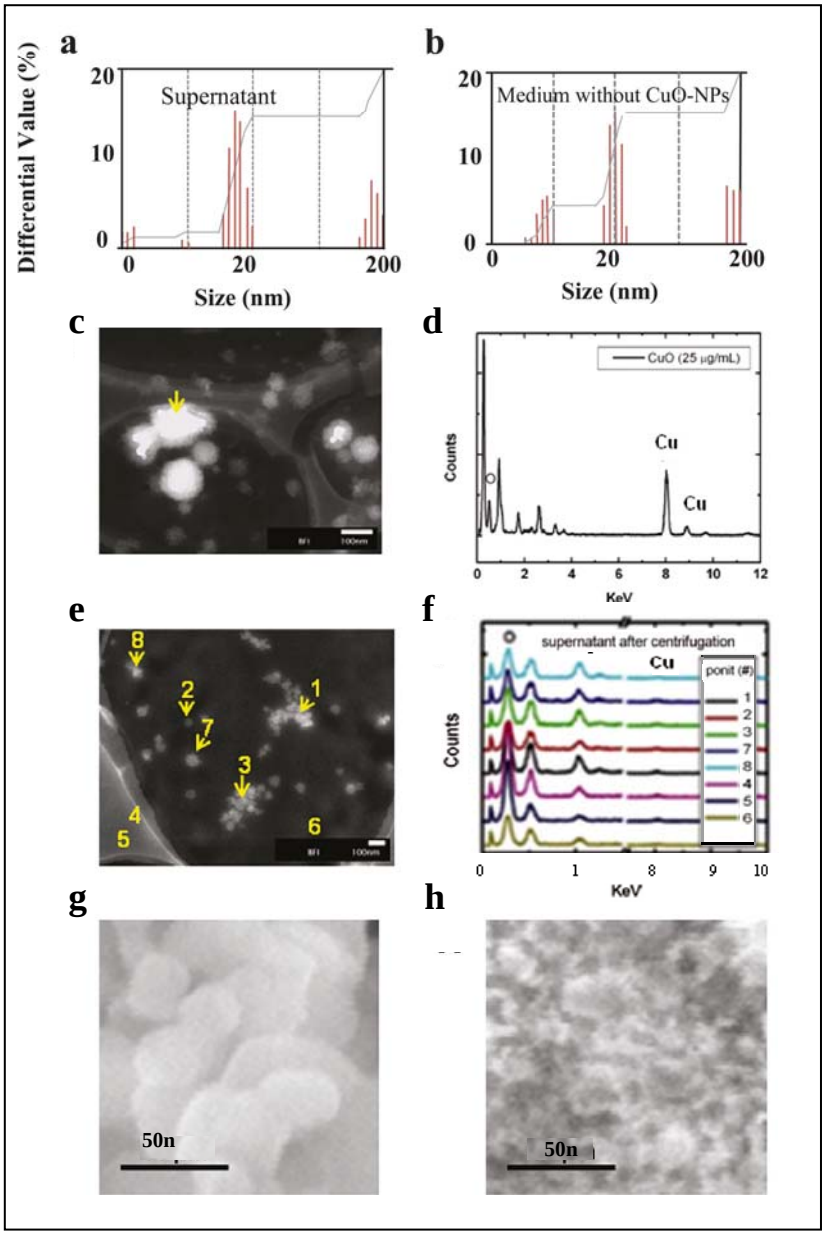

Figure 3.3 Characterization of supernatant for preparation of medium containing Cu ions released from CuO-NPs. (a) Size distribution of NPs in supernatant. (b) Size distribution of NPs in medium without CuO-NPs incubated at 37 ℃ for 24 h. (c) Dark-field TEM image of a CuO-NP sample. A TEM grid was immersed into the cell culture medium that contained 25 μg/mL CuO-NPs and then air-dried. (d) EDS spectrum of the point indicated by the arrow in (c), which suggests the presence of Cu and O. (e) Dark-field TEM image of the supernatant. The CuO-NP suspension was centrifuged at 150 000 g for 1 h. Subsequently, a TEM grid was immersed into the supernatant and then air-dried. (f) EDS spectra of points 1-8 in (e). (g) SEM image of original CuO-NPs. (h) SEM image of CuO-NPs incubated in medium at 37 ℃ for 24 h.

3.3.2 Toxicity of CuO-NPs

The number of viable A549 cells cultured in 25 μg/mL CuO-NPs or the supernatant was 34 and 81% of that of the control culture, respectively (Figure 3.4a and Figure 3.5). This result indicated that released Cu ions are also toxic and may account for part of the toxicity of CuO-NPs. In addition, we used the water-soluble tetrazolium salt (WST) cell proliferation assay, which is based on the production of formazan from WST-8 by mitochondrial dehydrogenases in viable cells, to measure cytotoxicity. The amount of formazan produced by cells cultured in 25 μg/mL CuO-NPs or the supernatant was 20 and 57% of that of the control culture, respectively (Figure 3.4b). This result implies that the CuO-NPs and released Cu ions damaged the mitochondria. This damage occurred after 4 h of exposure to CuO-NPs (Figure 3.6). Furthermore, supplementation of Al_2O_3-NPs with 50 nm in size that were used as nontoxic dummy NPs to the supernatant did not affect the formazan formation of the supernatant (Figure 3.7), suggesting released Cu ions alone damaged mitochondria. Approximately 9% of cells underwent apoptosis in response to CuO-NPs, but we observed few apoptotic cells in culture with the supernatant (Figure 3.4c). These results suggested that CuO-NPs damaged mitochondria and induced apoptosis, and that released Cu ions were responsible for some of the damage to the mitochondria.

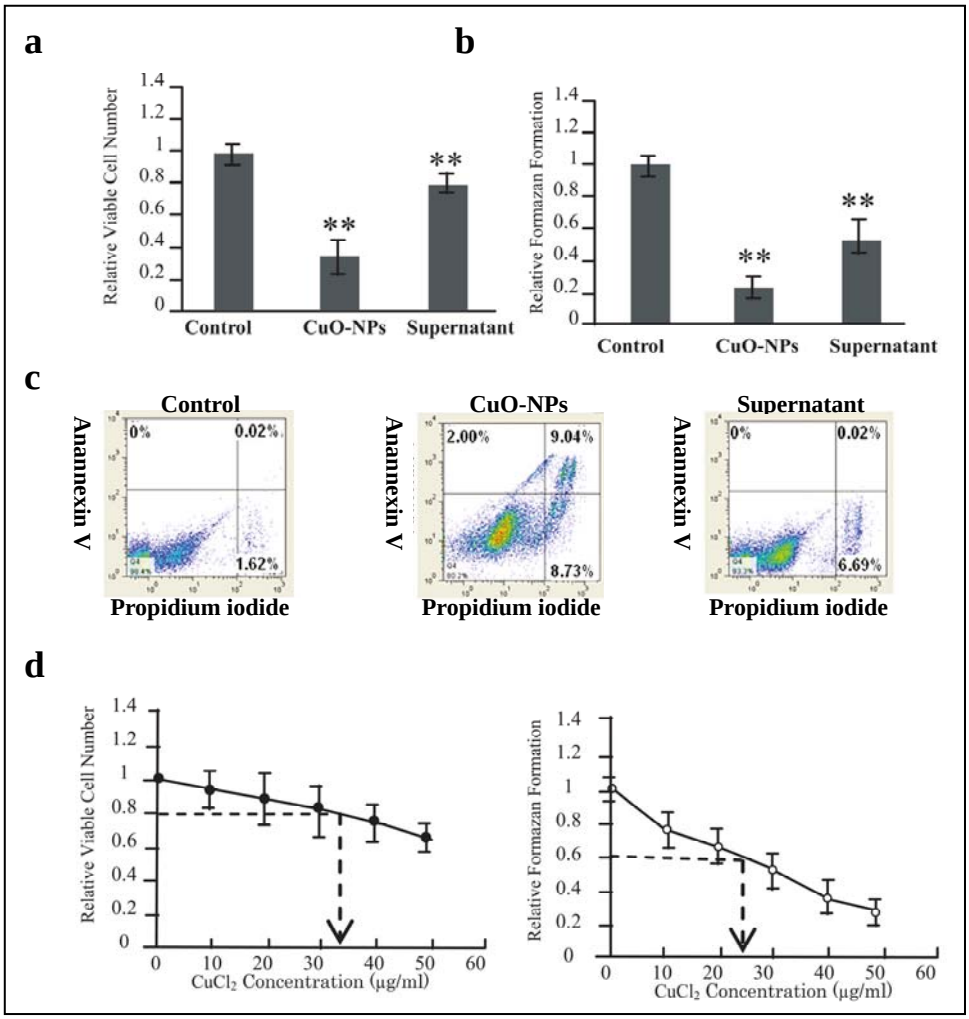

Figure 3.4 Toxicity of CuO-NPs and released Cu ions. (a) Cytotoxicity of CuO-NPs and supernatant as indicated by the number of viable cells. A549 human lung epithelial cells were cultured in media containing 25 μg/mL CuO-NPs or supernatant at 37 ℃ for 24 h, and then the number of viable cells was compared to that of control (untreated) cells (defined as 1). Results are expressed as mean (SE) (n = 4); $^{**}p < 0.05$. (b) Cytotoxicity of CuO-NPs and supernatant as indicated by cell viability in the WST assay. Results are expressed as mean (SE) (n = 8); $^{**}p< 0.05$. (c) Ratio of apoptotic cells determined by using flow cytometry Cells were stained with propidium iodide and FITC-labeled Annexin V; 20 000 cells were analyzed. Apoptotic cells are distributed in the upper right-hand area. Apoptosis was not observed in cells exposed to supernatant. However, about 9% of cells underwent apoptosis in response to CuO-NPs. Living cells in early apoptotic stage are distributed in the upper left-hand area. Therefore, only 2% of cells were in the early apoptotic stage when cells were exposed to CuO-NPs. (d) Cytotoxicity of $CuCl_2$ as indicated by the number of viable cells. Arrow indicates concentration of $CuCl_2$ whose toxicity is similar to that of supernatant. (e) Cytotoxicity of $CuCl_2$ as indicated by cell viability. Arrow indicates concentration of $CuCl_2$ whose toxicity is similar to that of supernatant.

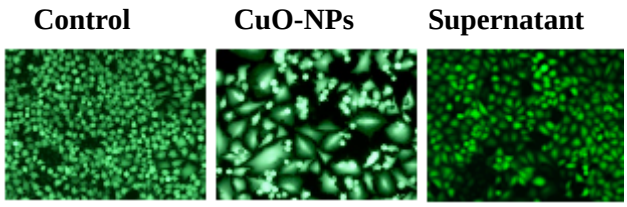

Figure 3.5 Cell viability as indicated by staining of cells that were exposed to CuO-NPs and the supernatant for 24 h with calcein acetoxymethyl ester (calcein-AM). A549 human lung epithelial cells were cultured in media containing 25 μg/mL CuO-NPs or the supernatant at 37 ℃ for 24 h, and then the number of viable cells was compared to that of the control.

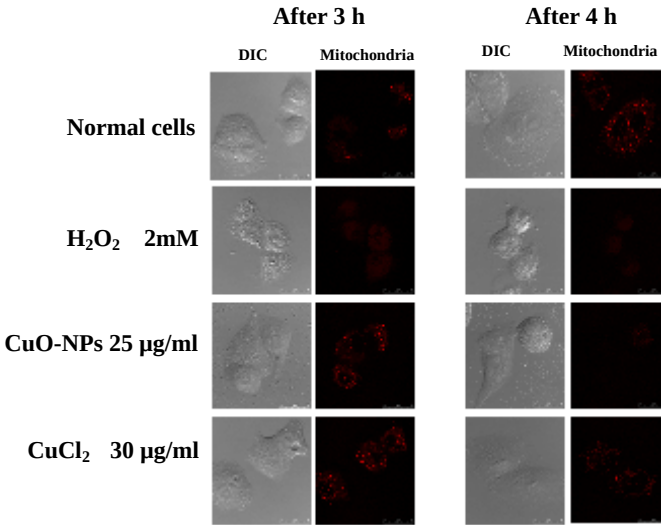

Figure 3.6 Damage to mitochondria by CuO-NPs. Mitochondrial damage in A549 human lung epithelial cells after exposure to H_2O_2 (2 mM), CuO-NPs (25 μg/mL), and $CuCl_2$ (30 μg/mL) was measured by using 5,5′,6,6′-tetrachloro-1,1′,3,3′- tetraethylbenzimidazolylcarbocyanine iodide (JC-1; Invitrogen). The accumulation of JC-1 in mitochondria was measured by excitation at 543 nm and detection of fluorescence at 573–607 nm. Damaged mitochondria accumulated less JC-1, and therefore, exhibited less fluorescence. The mitochondria of cells that were exposed to CuO-NPs were damaged after 4 h. Cells that were exposed to $CuCl_2$ also were damaged after 4 h; however, the damage was not as severe as that from CuO-NPs.

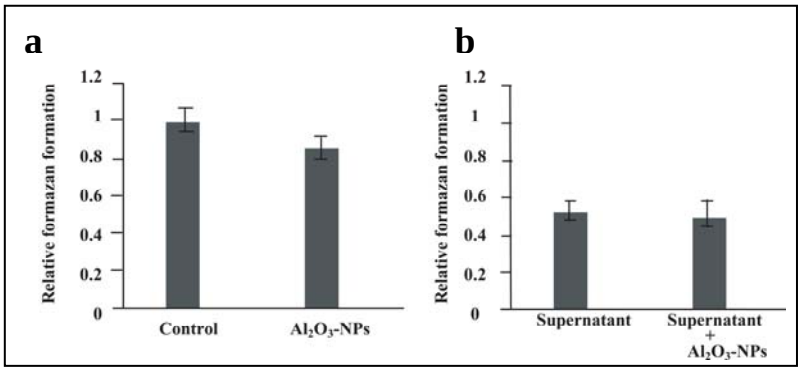

Figure 3.7 Effect of non-toxic dummy Al_2O_3-NPs on supernatant toxicity. (a) Cytotoxicity of Al_2O_3-NPs. The primary size of Al_2O_3-NPs was 50 nm and the hydrodynamic size was around 160 nm. A549 cells cultured for 48 h were exposed to Al_2O_3-NPs at a concentration of 25 μg/ml. After 24 h, a WST assay was performed. (b) Effect of Al_2O_3-NPs on the supernatant toxicity. A549 cells cultured for 48 h were exposed to supernatant and supernatant with Al_2O_3-NPs. The supernatant contained Cu ions released from CuO-NPs. After 24 h, a WST assay was performed. Zeta potential of Al_2O_3-NPs was -20.37 mV. Physicochemical character of Al_2O_3-NPs was previously reported (Xu et al., Biomaterials 2010, 31, 8022-8031).

To confirm the contribution of released Cu ions to the toxicity of CuO-NPs, we examined the cytotoxicity of different concentrations of $CuCl_2$. In cultures with the supernatant, the number of viable cells and the amount of formazan was 81% and 57% of control culture levels (Figure 3.4a, b). The concentration of $CuCl_2$ required for similar toxicity was 25-33 μg/mL (Figure 3.4d, e). This concentration is equivalent to 11.8-15.6 μg/mL Cu ions, which was consistent with the concentration of Cu ions that were released from CuO-NPs. This result showed that the effect of Cu ions that are released from CuO-NPs is similar to that of Cu ions from $CuCl_2$.

Next, we examined the uptake of CuO-NPs into cells using TEM. NP-like structures were observed inside cell (Figure 3.8). To verify whether these NP-like structures are attributed to CuO-NPs, elemental maps were analyzed. The elemental maps clearly showed that CuO-NPs were taken up into cell (Figure 3.9).

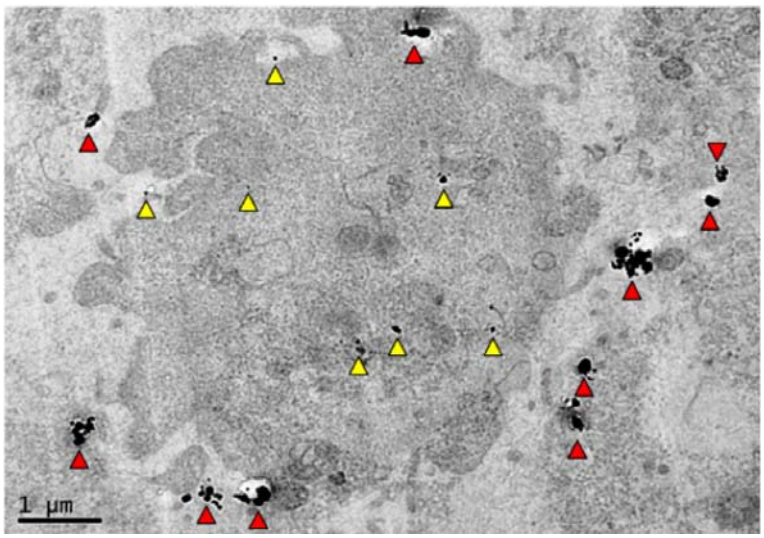

Figure 3.8 Internalized CuO-NPs observed by TEM. Yellow arrowheads indicate single or smaller (<100 nm) aggregated NPs. Red arrowheads indicate larger (> 100 nm) aggregated NPs. Cells were cultured in medium with 25 μg/mL CuO-NPs for 24 h, and then living cells were harvested.

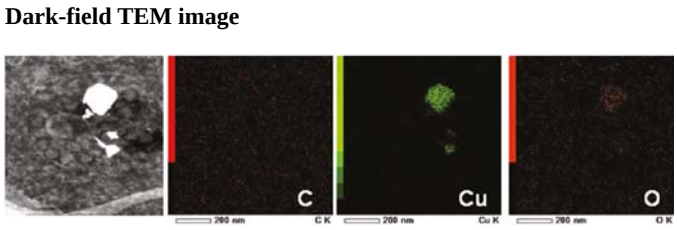

Figure 3.9 Dark-field TEM image and elemental map of NPs inside cells. A549 cells were cultured in medium containing 25 μg/mL CuO-NPs at 37 ℃ for 24 h, and then living cells were harvested for the observation. Elemental map suggests the presence of Cu and O.

3.3.3 Molecular response of cells to CuO-NPs

To elucidate the underlying molecular mechanism of CuO-NP toxicity, comprehensive gene expression analysis was performed using DNA microarray. We exposed A549 cells to 25 μg/mL CuO-NPs for 24 h and then identified genes that demonstrated greater than 2-fold change in expression level compared with those in control cells. Our results revealed that CuO-NPs upregulated the expression of 648 genes and downregulated the expression of 562 genes. These data have been deposited in the Gene Expression Omnibus database with accession code GE33278. By classifying these genes into GO functional categories, we obtained the following statistically significant categories ($p < 0.001$): CuO-NPs upregulated genes that affect "nucleobase, nucleoside, nucleotide, and nucleic acid metabolic processes" and "response to stress" and downregulated genes that affect "cell cycle", "mitosis", "cytokinesis", "chromosome segregation", "cellular component organization", and "cellular component morphogenesis" (Figure 3.10; Table S1-S6 of reference 11) [11]. The upregulated 31 genes in the response to stress category included genes that encode heat shock proteins (HSPs) (Table S2 of reference 11) [11] and proteins involved in mitogen-activated protein kinase (MAPK) pathways, such as growth arrest and DNA damage-inducible 45 β and γ (GADD45B/GADD45G) and nuclear receptors 4A1 and 3 (NR4A1/NR4A3) (Figure3.10a and Table3.1). We confirmed the upregulation of GADD45B/GADD45G and NR4A1/NR4A3 at protein level by using Western blot analysis (Figure 3.11).

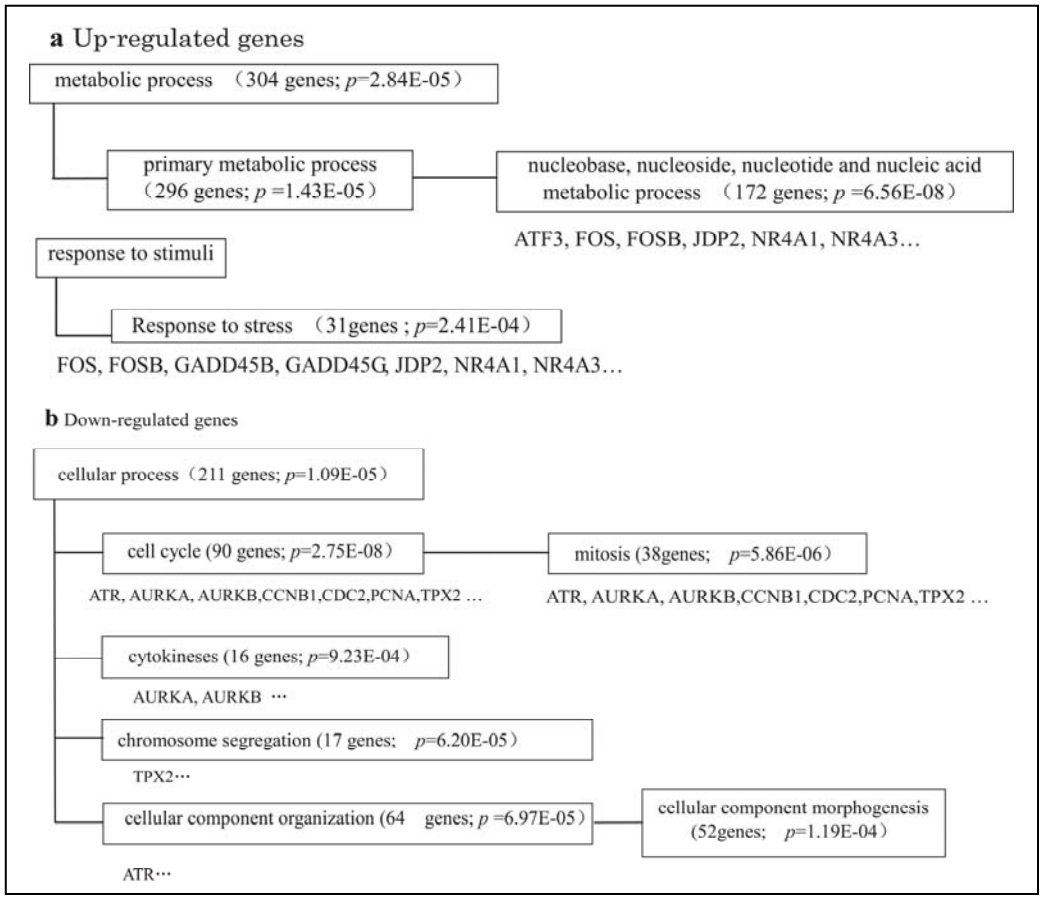

Figure 3.10 Gene ontology classification of genes that were upregulated or downregulated by CuO-NPs. A549 cells were exposed to 25 μg/mL CuO-NPs for 24 h, and then DNA microarray analysis was used to identify genes that demonstrated a 2-fold or greater change in expression level compared with control cells. These genes were grouped into statistically significant GO functional categories ($p< 0.001$). (a) Functional categories of genes upregulated by CuO-NPs. The numbers within parentheses indicate the number of genes in each category. (b) Functional categories of genes downregulated by CuONPs. Representative genes are shown in each category. The gene list for each category is included in Supporting Information (Table S1-S6 of reference 11) [11].

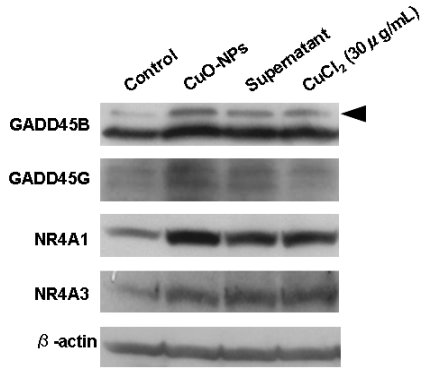

Figure 3.11 Western blotting analysis to confirm the change of gene expression. A549 cells were cultured for 48 h, and then exposed to 25 μg/mL CuO-NPs, supernatant and 30 μg/mL $CuCl_2$ for 24 h.

Table 3.1 Fold change of gene expression level mainly discussed in this study

	Fold-change (log_2 ratio)[a]						
	CuO-NP (25 µg/mL)		**supernatant (contained about 15 µg Cu/mL)**		**CuCl2 (30 µg/mL)**	**CuCl2 (60 µg/mL)**	
Gene name	**DNA microarray**	**qPCR**	**DNA microarray**	**qPCR**	**qPCR**	**qPCR**	**GO category**
GADD45A	0.24	0.55 _	-0.76	0.68	0.14	1.07	response to stress
GADD45B	2.96	3.00	-0.02	0.30	-0.42	1.52	response to stress
GADD45G	3.59	3.22	NR	0.61	0.38	1.70	response to stress
PCNA	-1.37	-0.87	NR	-0.28	-0.05	0.23	cell cycle
CDC2	-1.41	-1.48	-1.16	-1.08	-1.40	1.22	cell cycle
CCNB1	-1.74	-2.14	-1.33	-1.51	-1.27	1.46	cell cycle
CDKN1A	0.30	0.78	-0.08	0.63	-0.07	0.49	cell cycle
FOS	4.48	1.06	NR	-0.14	0.37	0.61	nucleobase, nucleoside, nucleotide and nucleic acid metabolic process; response to stress
FOSB	5.70	3.97	NR	0.68	0.57	3.43	nucleobase, nucleoside, nucleotide and nucleic acid metabolic process; response to stress
ATF3	4.22	1.23	NR	-0.01	0.07	1.14	nucleobase, nucleoside, nucleotide and nucleic acid metabolic process
JDP2	1.13	-0.67	NR	-0.19	-0.36	_0.41	Process nucleobase, nucleoside, nucleotide and nucleic acid metabolic
ATR _	1.11	-0.83	-0.20	-0.48 _	-0.33	0.51	cell cycle; cellular component organization
TP53	NR	-1.10	NR	-1.12	-0.04	0.15	induction of apoptosis; cell cycle; Nucleobase, nucleoside, nucleotide and nucleic acid metabolic process
NR4A1	5.28	2.82	2.71	1.25	0.89	2.09	nucleobase, nucleoside, nucleotide and nucleic acid metabolic process; response to stress
R4A2	NR	1.12	NR	-0.96	0.07	0.33	nucleobase, nucleoside, nucleotide and nucleic acid metabolic process; response to stress
NR4A3	3.06	1.08	NR	0.94	1.55	2.96	nucleobase, nucleoside, nucleotide and nucleic acid metabolic process; response to stress
AURKA	-1. 21	-1.62	-0.91	-1.34	-0.59	1.12	cell cycle; cytokinesis
AURKB _	1.13	-1.76	-0.81	-1.18	-0.96	1.37	cell cycle; cytokinesis
TPX2	-1.25	-2.13	-1.17	-1.63	-1.16	2.11	cell cycle; chromosome segregation

[a] Fold-change is represented by logarithmic ratio (log2 ratio) to expression level in control. NR: Not reproducible.

The upregulation of many HSPs suggested that CuO-NPs stimulate protein denaturation. GADD45B and GADD45G are members of the GADD45 family of proteins that are induced by genotoxic stresses and various apoptotic cytokines [12-14] and are involved in cell cycle arrest [15-20], DNA repair [21-23], cell survival [23-28] and apoptosis [29-38]. These functions are mediated by proliferating cell nuclear antigen (PCNA), cell division control 2 (CDC2), cyclin B1 (CCNB1), and cyclindependent kinase inhibitor 1A (CDKN1A; also known as p21), which are classified in the GO cell cycle category. PCNA is involved in DNA repair and the transition from the G1 to the S phase of the cell cycle [21-23]. In contrast, CDKN1A inhibits PCNA and blocks the transition from the G1 to the S phase of the cell cycle [21, 39]. The CDC2-CCNB1 complex is required for the transition from theG2 to the M phase [40-41]. Although CuO-NPs did not affect the expression of CDKN1A, they downregulated the expression of PCNA, CDC2, and CCNB1 (Figure 3.10b and Table 3.1), this suggests that CuO-NPs induce cell cycle arrest in the G1 and G2 phases. In addition, CuO-NPs downregulated the expression of genes that encode aurora kinase A and B (AURKA/AURKB) and target protein for XKlp2 (TPX2) (Figure 3.10b and Table 3.1), this peak during the G2/M transition and are involved in the assembly and maintenance of the spindle [42] .

To confirm that CuO-NPs cause cell cycle arrest, we isolated cells that survived exposure to CuO-NPs and cultured them in fresh culture medium that did not contain CuO-NPs. However, these cells did not proliferate for 72 h (Figure 3.12a). When we harvested these cells and cultured them again in fresh culture medium that did not include CuO-NPs for an additional 72 h, their proliferative capacity was restored; however, their rate of proliferation lagged behind that of control cells (Figure 3.12b). These results indicated that the surviving cells were in a state of cell cycle arrest after exposure to CuO-NPs. Since cell cycle arrest is thought to provide time for cells to repair damaged DNA, it is likely that CuO-NPs compromise cell survival.

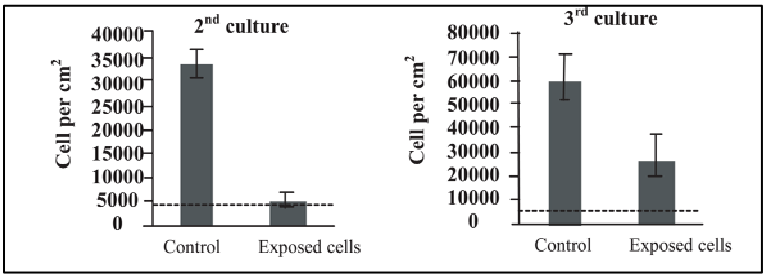

Figure 3.12 Cell cycle arrest due to CuO-NPs. Cells that were exposed to 25 μg/mL CuO-NPs were isolated, and then seeded in fresh culture medium that did not contain CuO-NPs at a density of 5000 cells/cm^2. The left graph shows the number of cells after 72 h. The dotted line shows the number of cells at the time of the seeding. Cell proliferation was not observed. However, when the cells were harvested and seeded in fresh culture medium for an additional 72 h, cell proliferation resumed (right graph). Therefore, cell cycle arrest occurred after the cells were exposed to CuO-NPs.

The expression of GADD45B and GADD45G has been reported to activate the c-Jun N-terminal kinase (JNK) and p38 pathways via MAP 3 kinase 1 (MTK1) [29, 43-44]. In addition, activation of these pathways induces the activation of the constituent proteins of the activator protein 1 (AP-1) transcription factor complex, such as c-Jun, JunD, and activating transcription factor 2 (ATF2) [45-46]. AP-1 is involved in both apoptosis and cell survival [47-48]. To examine how the JNK or p38 pathway is involved in themolecular response to CuO-NPs exposure, we treated cells with CuO-NPs and either a JNK interacting protein 1 (JIP-1) peptide or SB239063, which are inhibitors of JNK and p38, respectively. Although the JIP-1 peptide did not have any effect on the number of viable cells, SB239063 markedly reduced the number of viable cells relative to treatment with CuO-NPs alone (Figure 3.13a Figure 3.14). Similar to SB239063, when GADD45B in cells exposed to CuO-NPs was knocked down with small interfering RNA (siRNA) (Figure 3.15), they were more sensitive to CuO-NPs than cells with normal GADD45B expression, and the number of viable cells decreased (Figure 3.13b and Figure 3.16). Together, these results suggest that the upregulation of GADD45B/GADD45G due to CuO-NPs promotes cell survival by activating the p38 pathway. The activation of the p38 pathway in turn activates ATF2, which interacts with FOS, FOSB, and ATF3 in the AP-1 complex. In addition, we observed the upregulation of these proteins by CuO-NPs (Figure 3.10a and Table 3.1), which strongly suggested that the underlying mechanism of cell survival involved the p38 pathway.

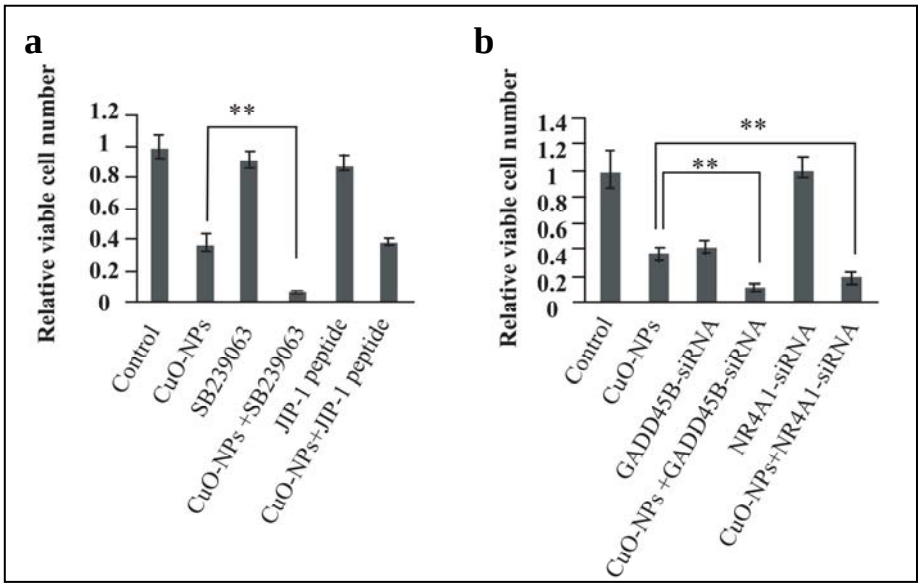

Figure 3.13 Changes in the number of viable cells due to disruption of mitogen-activated protein kinase (MAPK) pathways. After culturing A549 cells for 42 h, p38 or c-Jun N-terminal kinase (JNK) inhibitors or siRNA were added and incubated for 6 h. Subsequently, CuO-NPs were added to a final concentration of 25 μg/mL and then cultured for 24 h. (a) Effects of SB239063 and JNK interacting protein 1 (JIP-1), which are inhibitors of p38 and JNK, respectively, on the number of viable cells. SB239063 increased the cytotoxicity of CuO-NPs (n = 3); $^{**}p < 0.05$. (b) Effect of siRNA knockdown on the expression of GADD45B and NR4A1 on the cytotoxicity of CuO-NPs. Knockdown of the expression of these genes markedly increased the cytotoxicity of CuO-NPs (n = 3); $^{**}p < 0.05$. The knockdown efficiency for each gene is shown in Figure 3.15.

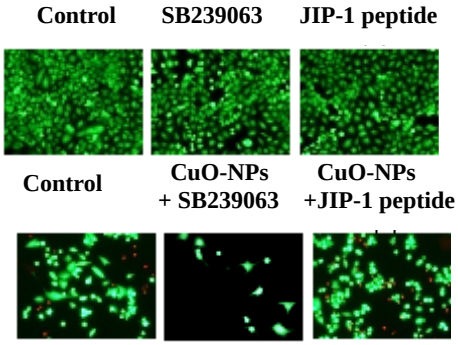

Figure 3.14 Effects of SB239063 and JNK interacting protein 1 (JIP-1), which is inhibitors of p38 and JNK, respectively. Double staining with calcein acetoxymethyl ester (calcein-AM) and propidium iodide (PI). SB239063 and CuO-NPs (CuO-NPs + SB239063) decreased the number of viable cells more than CuO-NPs alone. In the presence of SB239063, many cells that were exposed to CuO-NPs detached from the culture dish.

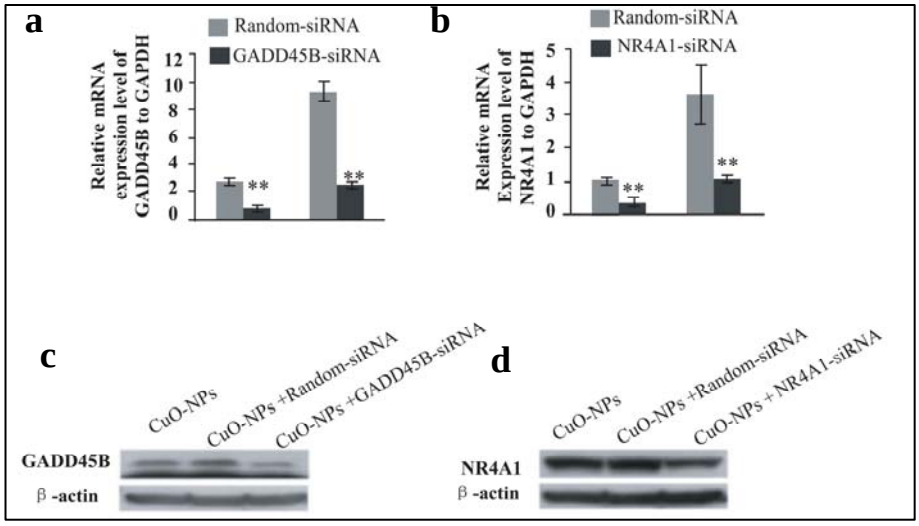

Figure 3.15 siRNA knockdown efficiency of GADD45B and NR4A1. (a) mRNA expression level of GADD45B. (b) Western blotting. The concentration of CuO-NPs was 25 μg/mL. GADD45B siRNA suppressed the expression at protein level. (c) mRNA expression level of NR4A1. (d) Western blotting. NR4A1 siRNA suppressed expression of NR4A1 at protein level.

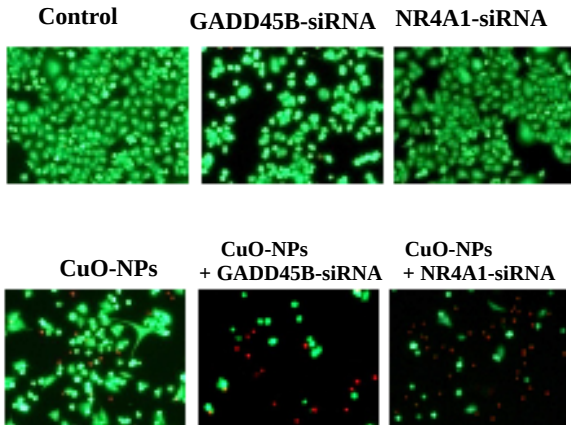

Figure 3.16 Effect of siRNA knockdown on the expression of GADD45B and NR4A1 on the cytotoxicity of CuO-NPs. Double staining with calcein-AM and PI. Knockdown of GADD45B and NR4A1 decreased the number of viable cells after cells were exposed to CuO-NPs. The number of dead cells as indicated by PI staining is not accurate because it included dead cells that detached from the surface of the culture dish.

CuO-NPs also upregulated NR4A1 and NR4A3. These nuclear receptors are involved in both cell survival and apoptosis and are activated via the mitogen-activated protein kinase/extracellular signal regulated kinase 5 (MEK5/ERK5) pathways [49-50]. When NR4A1 in cells exposed to CuO-NPs was knocked down with siRNA (Figure 3.15), A549 cells were more sensitive to CuO-NPs than cells with normal NR4A1 expression, and the number of viable cells decreased (Figure 3.13b and Figure 3.16). These results indicated that the upregulation of NR4A1 is also involved in cell survival after exposure to CuO-NPs.

DNA damage is well-known to activate p53, which induces checkpoint arrest in the G1 and G2/M phases of the cell cycle and apoptosis in cells that cannot recover from DNA damage [51]. The checkpoint function of p53 is activated by the phosphorylation of ataxia telangiectasia mutated (ATM), ataxia telangiectasia and Rad3-related protein (ATR), and checkpoint kinase 1 (Chk1). Subsequently, activated p53 induces the expression of GADD45A and CDKN1A [31, 52-55]. Although CuO-NPs downregulated ATR, they did not affect the expression of GADD45A or CDKN1A (Table 3.1). Therefore, we concluded that p53 does not play a major role in the response of cells exposed to CuO-NPs.

3.3.4 Contribution of released Cu from CuO-NPs at molecular level

In addition to the genes that demonstrated altered expression in response to CuO-NPs, we identified genes that were altered in response to the Cu ions released from CuO-NPs into culture medium to determine their contribution to the molecular response to CuO-NP exposure. Cells exposed to the supernatant for 24 h upregulated 108 genes (Figure 3.17a). Of these 108 genes, 54 were also found in the list of 648 genes upregulated by CuO-NPs (Figure 3.17a and Table S7 of reference 11) [11]. Therefore, of 648 genes upregulated by CuO-NPs, 594 upregulated genes were induced by CuO-NPs themselves, but 54 upregulated genes were attributable to Cu ions released from CuO-NPs into the culture medium. After classifying these 54 shared genes into GO functional categories, we did not identify any statistically significantly enriched categories. This finding suggests that released Cu ions do not contribute to changes in

cellular functions related to nucleobase, nucleoside, nucleotide, and nucleic acid metabolic processes or response to stress, categories found to be enriched in the classification of genes upregulated by CuO-NPs. The changes in these two functions were specifically induced by CuO-NPs themselves. However, NR4A1 and NR4A3, which are involved in response to stress, were upregulated by both CuO-NPs and the supernatant (Table 3.1 and TableS7 of reference 11) [11], suggesting that these genes were induced by released Cu from the CuO-NPs.

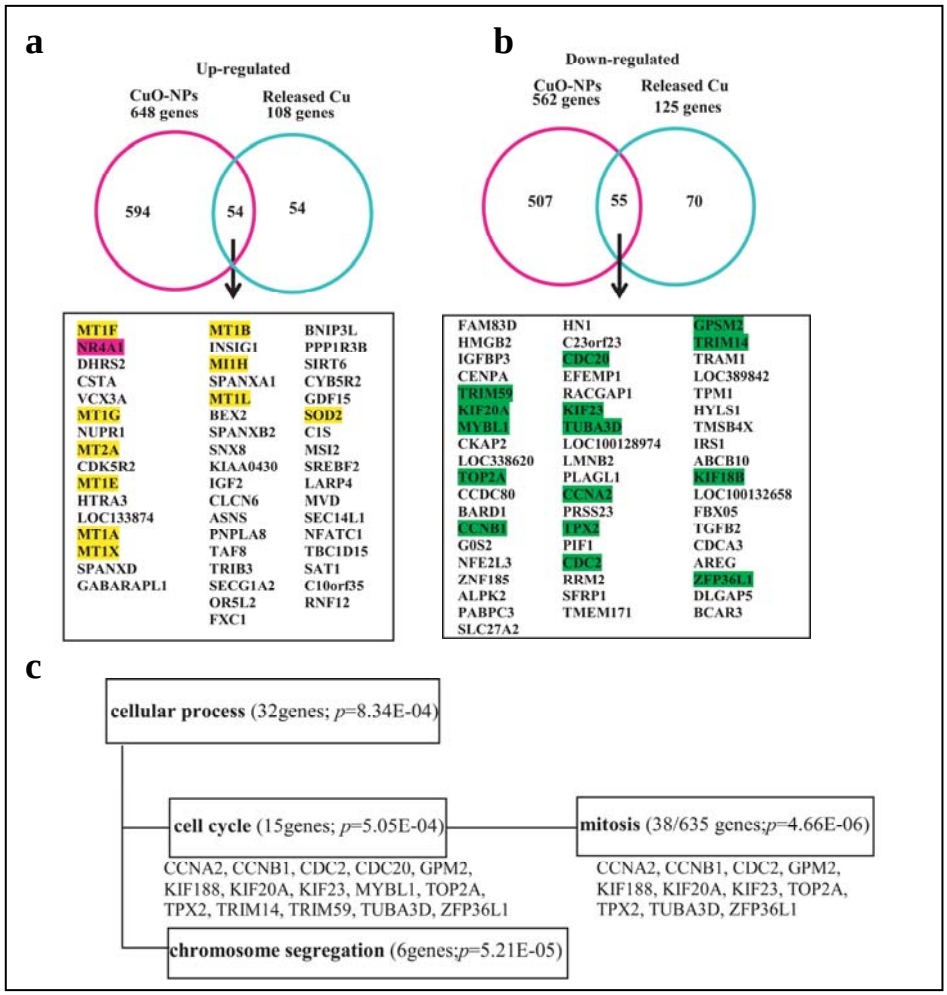

Figure 3.17 Gene expression altered by both CuO-NPs and released Cu ions. (a) Genes upregulated by both CuO-NPs and supernatant. Of 108 genes that were upregulated in response to supernatant, 54 genes were also upregulated by CuO-NPs. (b) Genes downregulated by both CuO-NPs and supernatant. Of 125 genes that were downregulated in response to supernatant, 55 genes were also downregulated by CuO-NPs. The names of the common genes are boxed. Yellow, orange, and green highlighting of gene names indicate ROS scavenger genes, MAPK-related gene, and cell cycle-related genes, respectively. (c) Gene ontology classification of genes that were downregulated by both CuO-NPs and supernatant. Categories with p 0.001 were considered statistically significant functional categories. The numbers within parentheses indicate the number of genes in each category. Gene names are listed under each category.

We identified genes encoding super oxide dismutase 2 (SOD2), which functions as a ROS quencher and 9 genes for metallothionein isomers (MT1A, MT1B, MT1E, MT1F, MT1G, MT1H, MT1L, MT1X, and MT2A) among the 54 common genes upregulated by both CuO-NPs and the supernatant (Figure 3.17a and Table S7 of reference 11) [11]. Since MT isomers help protect cells from oxidative stress due to excess metal ions, such as cadmium, zinc, and copper [56-59], the released Cu ions may generate ROS. To examine whether CuO-NPs and Cu ions induce ROS in A549 cells, we pretreated cells with N-acetylcysteine (NAC), which is a ROS scavenger. NAC protected cells exposed to supernatant from mitochondrial damage (Figure 3.18a). NAC also partially protected cells exposed to CuO-NPs from mitochondrial damage and cell death (Figure 3.18b). These findings imply that ROS generation by Cu ions released from CuO-NPs is one of the causes of CuO-NPs toxicity.

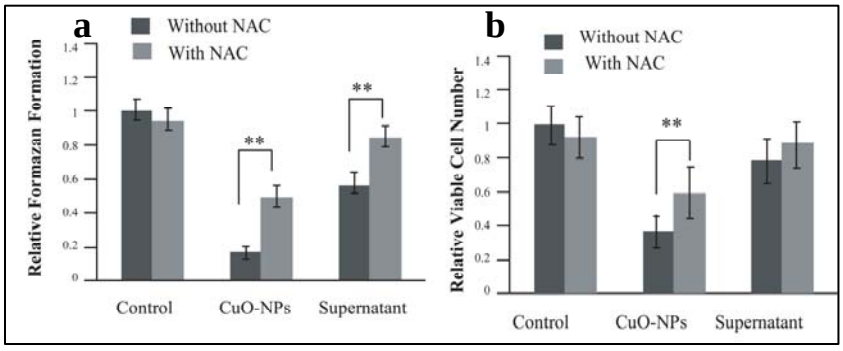

Figure 3.18 Effect of pretreatment of cells with NAC, a scavenger of ROS. (a) NAC decreased mitochondrial damage of cells exposed to CuO-NPs and supernatant (n = 8); $^{**}p < 0.05$. (b) NAC increased the number of living cells exposed to CuO-NPs and supernatant (n = 3); $^{**}p < 0.05$.

The supernatant also downregulated 125 genes (Figure 3.17b). Of these genes, 55 genes were also among the 562 genes downregulated by CuO-NPs (Figure 3.17b and Table S8 of reference 11) [11]. Therefore, of 562 genes downregulated by CuO-NPs, 507 genes were specifically downregulated by CuO-NPs themselves, but 55 genes were downregulated by Cu ions released from CuO-NPs. After classifying these 55 shared downregulated genes into GO categories, we identified statistically significantly enriched functional categories including cell cycle, mitosis, and chromosome segregation (Figure 3.17c and TableS9 of reference 11) [11]. These categories were also identified in the classification of genes downregulated by CuO-NPs (Figure 3.10b), suggesting that changes in these cellular functions by CuO-NPs were attributable to Cu ions released from CuO-NPs into culture medium.

Among genes downregulated by CuO-NPs, CDC2, CCNB1, PCNA, AURKA/AURKB, and TPX2 were classified into GO categories cell cycle, mitosis, or chromosome segregation (Figure 3.10b). Downregulation of CDC2, CCNB1, AURKA/AURKB, and TPX2 has been reported to induce cell cycle arrest in the G2 phase [40, 42-43] , and downregulation of PCNA led to cell cycle arrest in the G1 phase [21, 39]. Among these genes, CDC2, CCNB1, AURKA/AURKB, and TPX2 were also downregulated by the supernatant, but PCNA was not changed by the supernatant (Table 3.1). We observed a marked increase in the number of cells in the G2/M phase upon exposure to CuO-NPs and the supernatant compared with control cells (Figure 3.19). In addition, an increase in the G1 population accompanied by a decrease in the S phase population was observed in the cells exposed to CuO-NPs compared to the cells exposed to the supernatant (Figure 3.19). Therefore, released Cu ions are responsible for the cell cycle arrest in the G2 phase induced by CuO-NPs, while cell cycle arrest in the G1 phase is attributable to CuO-NPs themselves. This observation corresponds to the results of gene expression analysis.

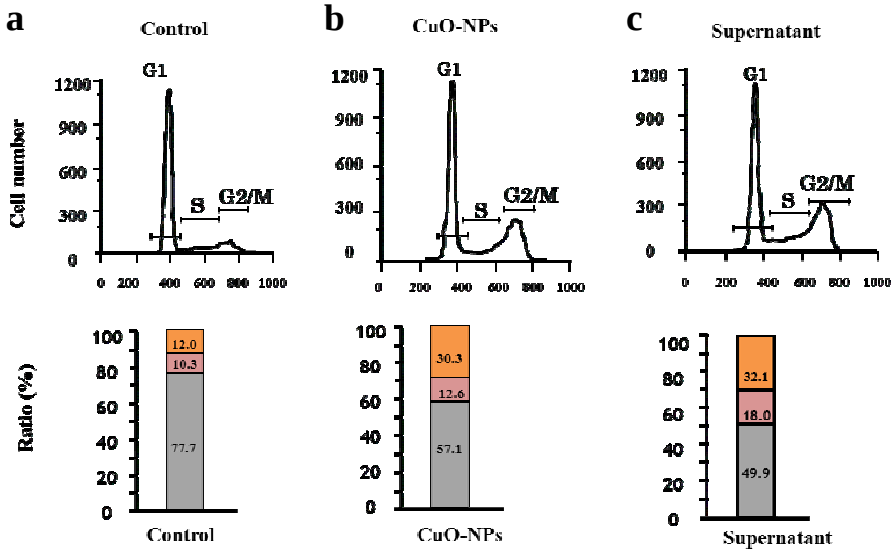

Figure 3.19 Cell cycle analysis in A549 cells determined by flow cytometry. A549 cells cells were cultured for 48 h and then were exposed to CuO-NPs and supernatant for another 24 h. Viable cells were harvested and stained with PI. (a) Control cells. These cells were under confluent. (b) Cells exposed to 25 μg/mL CuO-NPs for 24 h. (c) Cells exposed to supernatant for 24 h.

A question remains: what causes the toxicity of CuO-NPs themselves? One possibility is the effect of Cu ions released from CuO-NPs taken up into cells. When Cu ions are released from internalized CuO-NPs, the intracellular concentration of Cu ions increased. Indeed, in cells cultured in medium containing 60 μg/mL $CuCl_2$, which has a Cu ion concentration twice of that released from CuO-NPs into culture medium, the expression levels of GADD45B, GADD45G, FOSB, and ATF3, which were induced by CuO-NPs but not Cu ions released from CuO-NPs into culture medium, were upregulated (Table 3.1). These results suggest that the changes in gene expression due to CuO-NP exposure might not be due to the nanoparticles themselves but rather to the high concentration of Cu ions that are released from internalized CuO-NPs.

3.3.5 Proposed mechanism for cellular response to CuO-NPs

We propose a model for cellular responses to the toxicity of CuO-NPs on the basis of these results (Figure 3.20). In this model, CuO-NPs damage both mitochondria and DNA, and Cu ions that are released into the culture medium contribute to the mitochondrial damage. In addition, released Cu ions generate ROS and lead to cell cycle arrest at the G2 phase by altering the expression of various cell cycle genes such as CDC2, CCNB1, TPX2, AURKA, and AURKB. Moreover, CuO-NPs induce the expression of many HSPs and strongly arrest the cell cycle at the G1 phase by downregulating PCNA. Furthermore, cells that are exposed to CuO-NPs avoid cell death by activating the p38 pathway via upregulation of GADD45B and GADD45G. We observed numerous CuO-NPs in dead cells compared to viable cells (Figure 3.21), suggesting that the difference in the amount of CuO-NPs that are absorbed into individual cells may determine their fate.

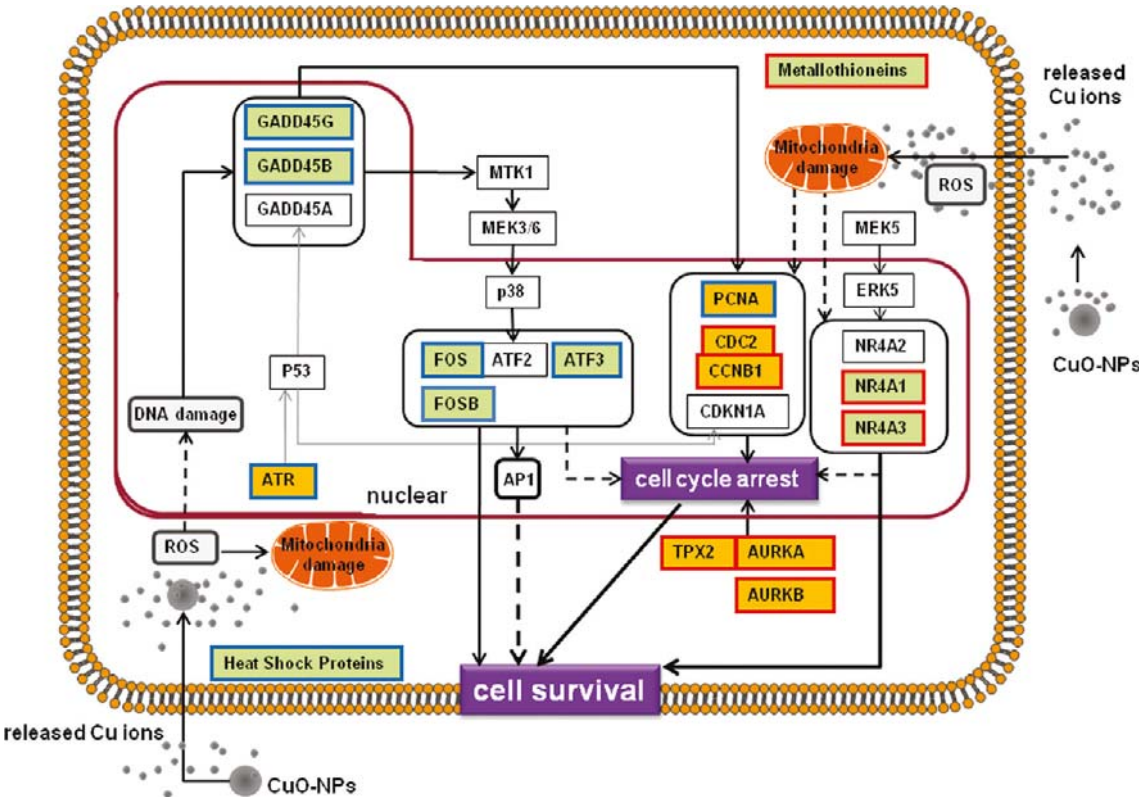

Figure 3.20 Model of the molecular responses of cells exposed to CuO-NPs. The boxes outlined in blue and red indicate genes that are induced by CuO-NPs and released Cu ions, respectively. Orange and light green boxes indicate downregulated and upregulated genes, respectively. The solid black lines indicate pathways that are induced by CuO-NPs or released Cu ions, while the dotted lines indicate inferred pathways. The gray lines indicate pathways that are not induced by CuO-NPs. Cells that survive exposure to CuO-NPs halt their cell cycle progression via downregulation of PCNA, CDC2, CCNB1, tTPX2, AURKA, and AURKB. Cell death is also prevented by the induction of NR4A1, NR4A3, GADD45B, and GADD45G. In addition, Cu ions that are released into the culture medium downregulate CDC2, CCNB1, TPX2, AURKA, and AURKB and upregulate NR4A1 and NR4A3. However, the expression of PCNA is only downregulated by CuO-NPs. The expression of GADD45B and GADD45G activates the p38 pathway to prevent cell death. Furthermore, CuO-NPs upregulate the expression of FOS, FOSB, and ATF3. These products dimerize with ATF2, which is activated by the p38 pathway, to form the AP-1 transcription factor complex. It is not known whether activation of the p38 pathway and upregulation of NR4A1/NR4A3 are involved in cell survival via cell cycle arrest. The induced expression of GADD45B and GADD45G is thought to be due to the absorption of Cu ions that are released from CuO-NPs into cells.

Finally, we examined toxicity of CuO-NPs using primary human lung epithelial cells. CuO-NPs and Cu ions also showed a toxic effect on primary cells (Figure 3.22). In addition, primary cells upregulated expression of genes involved in MAPK pathways such as GADD45B/GADD45G and NR4A1/NR4A3, which is similar to that in A549 cells (Figure 3.22). However, expression of several genes related to cell cycle regulation such as PCNA, CDC2, and AURKB showed a different pattern from that of A549 cells.

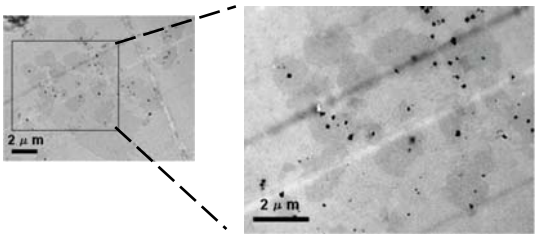

Figure 3.21 CuO-NPs in dead cell observed by TEM. Black dots indicate aggregates of CuO-NPs. Cells were cultured in medium with 25 μg/mL CuO-NPs for 24 h, and then dead cells detached from culture dish were harvested. Right panel is a magnified image of leaflet in left panel.

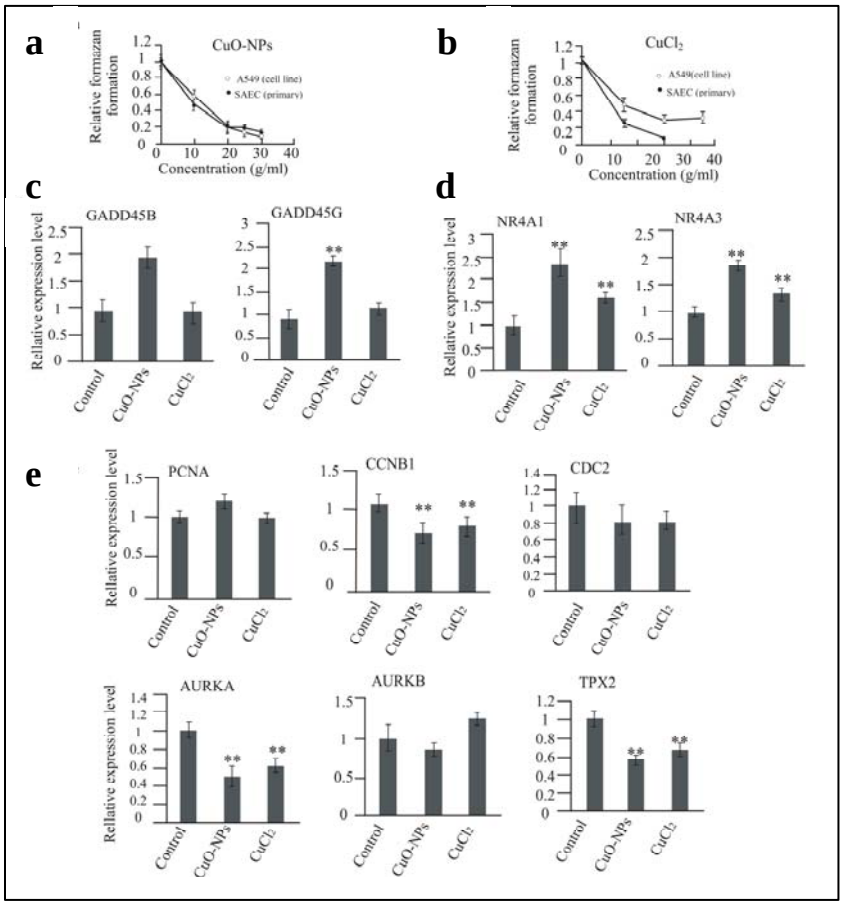

Figure 3.22 Cytotoxicity of CuO-NPs and Cu ions to primary human lung epithelial cells and change of gene expression. (a) Comparison of CuO-NPs toxicity between primary human epithelial cells (SAEC) and A549 cells. (b) Comparison of Cu ion toxicity between SAEC and A549 cells. (c-e) Expression level of genes in SAEC. Genes in (c) upregulated in CuO-NPs but not in 30 μg/mL $CuCl_2$ in A549 cells. SAEC cells showed similar pattern. Genes in (d) upregulated in both CuO-NPs and 30 μg/mL $CuCl_2$ in A549 cells. SAEC cells showed similar pattern. Genes in (e) downregulated in both CuO-NPs and 30 μg/mL $CuCl_2$ in A549 cells. SAEC cells showed similar pattern in CCNB1, AURKA and TPX2, but not PCNA, CDC2 and AURKB. For gene expression analysis, SAEC cells were exposed to media containing 25 μg/mL CuO-NPs or 30 μg/mL $CuCl_2$ for 24 h.

This study demonstrated that change of gene expression in A549 cells exposed to CuO-NPs is similar to that of cells exposed to $CuCl_2$, which suggests that Cu ions that are released from CuO-NPs inside and outside cells may be the primary cause of their cytotoxicity. However, our model established using A549 cells does not completely explain the molecular responses to the toxic effects of CuO-NPs. For example, although CuO-NPs down-regulated PCNA, a high concentration of $CuCl_2$ did not have a similar effect. In addition, our model does not entirely apply to primary human lung epithelial cells because some of genes showed different expression patterns from that of A549 cells. Further studies are needed to elucidate the differences in molecular mechanism of primary cells from that of A549 cells demonstrated in this study.

3.4 Conclusions

CuO-NPs showed strong cytotoxicity to carcinomaderived human lung epithelial A549 cells *in vitro*. CuO-NPs upregulated genes, which involved in MAPK pathways such as GADD45B/GADD45G and NR4A1/NR4A3, while downregulated genes which involved in cell cycle progression. Of these changes in gene expression, upregulation of NR4A1/NR4A3 and downregulation of genes related to cell cycle progression were attributed to Cu ions released from CuO-NPs into culture medium. Although GADD45B/GADD45G were not induced by Cu ions released into culture medium, higher concentration of Cu ions prepared from $CuCl_2$ enhanced the expression. The results indicated that change of gene expression involved in MAPK pathways and cell cycle progression in cells exposed to CuO-NPs was similar to that in cells exposed to Cu ions.

3.5 References

1. Xu M. S.; Fujita D.; Kajiwara S.; Minowa T.; Li X. L.; Takemura T.; Iwai H.; Hanagata N. Contribution of physicochemical characteristics of nano-oxides to cytotoxicity. *Biomaterials* **2010**, *31,* 8022-8031.

2. Hanagata N.； Xu, M.; Takemura, T.; Zhuang, F. Cellular response to ZnO nanoparticle toxicity inferred from global gene expression profiles. *Nano Biomedicine* **2010**, *2,* 153-169.

3. Gabbay J.; Borkow, G.; Mishal, J.; Magen, E.; Zatcoff, R.; Shemer-Avni, Y., Copper oxide impregnated textiles with potent biocidal activity. In *J. Ind. Textiles*, **2006**; Vol. *35*, pp 323-335.

4. Chang H.; Jwo C. S.; Lo C. H.; Tsung T. T.; Kao M. J.; Lin H. M. Rheology of CuO nanoparticle suspension prepared by ASNSS. *Rev Adv Mater Sci* **2005**, *10,* 128-132.

5. Zhou K. B.; Wang R. P.; Xu B. Q.; Li Y. D. Synthesis, characterization and catalytic properties of CuO nanocrystals with various shapes. *Nanotechnology* **2006**, *17,* 3939-3943.

6. Cioffi N.; Ditaranto N.; Torsi L.; Picca R. A.; Sabbatini L.; Valentini A.; Novello L.; Tantillo G.; Bleve-Zacheo T.; Zambonin P. G. Analytical characterization of bioactive fluoropolymer ultra-thin coatings modified by copper nanoparticles. *Anal Bioanal Chem* **2005**, *381,* 607-616.

7. Xu L. M.; Takemura T.; Xu M. S.; Hanagata N. Toxicity of silver nanoparticles as assessed by global gene expression analysis. *Mater Express* **2011**, *1,* 74-79.

8. Ahamed M.; Siddiqui M. A.; Akhtar M. J.; Ahmad I.; Pant A. B.; Alhadlaq H. A. Genotoxic potential of copper oxide nanoparticles in human lung epithelial cells. *Biochem Bioph Res Co* **2010**, *396,* 578-583.

9. Midander K.; Cronholm P.; Karlsson H. L.; Elihn K.; Moller L.; Leygraf C.; Wallinder I. O. Surface characteristics, copper release, and toxicity of nano- and micrometer-sized copper and copper(II) oxide particles: A cross-disciplinary study. *Small* **2009**, *5,* 389-399.

10. Karlsson H. L.; Cronholm P.; Gustafsson J.; Moller L. Copper oxide nanoparticles are highly toxic: A comparison between metal oxide nanoparticles and carbon nanotubes. *Chem Res Toxicol* **2008**, *21,* 1726-1732.

11. Hanagata N.; Zhuang F.; Connolly S.; Li J.; Ogawa N.; Xu M. S. Molecular responses of human lung epithelial cells to the toxicity of copper oxide nanoparticles inferred from whole genome expression analysis. *Acs Nano* **2011**, *5,* 9326-9338.

12. Zhan Q. M.; Lord K. A.; Alamo I.; Hollander M. C.; Carrier F.; Ron D.; Kohn K. W.; Hoffman B.; Liebermann D. A.; Fornace A. J. The gadd and MyD genes define a novel set of mammalian genes encoding acidic proteins that synergistically suppress cell-growth. *Mol Cell Biol* **1994**, *14,* 2361-2371.

13. Fornace A. J.; Jackman J.; Hollander M. C.; Hoffmanliebermann B.; Liebermann D. A. Genotoxic-stress-response genes and growth-arrest genes - gadd, MyD, and other genes induced by treatments eliciting growth arrest. *Ann Ny Acad Sci* **1992**, *663,* 139-153.

14. Fornace A. J.; Nebert D. W.; Hollander M. C.; Luethy J. D.; Papathanasiou M.; Fargnoli J.; Holbrook N. J. Mammalian genes coordinately regulated by growth arrest signals and DNA-damaging agents. *Mol Cell Biol* **1989**, *9,* 4196-4203.

15. Zhang W.; Bae I.; Krishnaraju K.; Azam N.; Fan W.; Smith K.; Hoffman B.;

Liebermann D. A. CR6: A third member in the MyD118 and Gadd45 gene family which functions in negative growth control. *Oncogene* **1999**, *18,* 4899-4907.

16. Beadling C.; Johnson K. W.; Smith K. A. Isolation of interleukin-2-induced immediate-early genes. *Proc Natl Acad Sci U S A* **1993**, *90,* 2719-2723.

17. Liebermann D. A.; Hoffman B. MyD genes in negative growth control. *Oncogene* **1998**, *17,* 3319-3329.

18. Vairapandi M.; Balliet A. G.; Hoffman B.; Liebermann D. A. GADD45b and GADD45g are cdc2/cyclinB1 kinase inhibitors with a role in S and G2/M cell cycle checkpoints induced by genotoxic stress. *J Cell Physiol* **2002**, *192,* 327-338.

19. Wang X. W.; Zhan Q.; Coursen J. D.; Khan M. A.; Kontny H. U.; Yu L.; Hollander M. C.; O'connor P. M.; Fornace A. J., Jr.; Harris C. C. GADD45 induction of a G2/M cell cycle checkpoint. *Proc Natl Acad Sci U S A* **1999**, *96,* 3706-11.

20. Jin S. Q.; Antinore M. J.; Lung F. T.; Dong X.; Zhao H. C.; Fan F. Y.; Colchagie A. B.; Blanck P.; Roller P. P.; Fornace A. J.; Zhan Q. M. The GADD45 inhibition of Cdc2 kinase correlates with GADD45-mediated growth suppression. *J Biol Chem* **2000**, *275,* 16602-16608.

21. Vairapandi M.; Balliet A. G.; Fornace A. J., Jr.; Hoffman B.; Liebermann D. A. The differentiation primary response gene MyD118, related to GADD45, encodes for a nuclear protein which interacts with PCNA and p21WAF1/CIP1. *Oncogene* **1996**, *12,* 2579-94.

22. Smith M. L.; Chen I. T.; Zhan Q.; Bae I.; Chen C. Y.; Gilmer T. M.; Kastan M. B.; O'connor P. M.; Fornace A. J., Jr. Interaction of the p53-regulated protein Gadd45 with proliferating cell nuclear antigen. *Science* **1994**, *266,* 1376-80.

23. Smith M. L.; Ford J. M.; Hollander M. C.; Bortnick R. A.; Amundson S. A.; Seo Y. R.; Deng C. X.; Hanawalt P. C.; Fornace A. J., Jr. p53-mediated DNA repair responses to UV radiation: studies of mouse cells lacking p53, p21, and/or gadd45 genes. *Mol Cell Biol* **2000**, *20,* 3705-14.

24. Smith M. L.; Kontny H. U.; Zhan Q. M.; Sreenath A.; Oconnor P. M.; Fornace A. J. Antisense GADD45 expression results in decreased DNA repair and sensitizes cells to uv-irradiation or cisplatin. *Oncogene* **1996**, *13,* 2255-2263.

25. Gupta M.; Gupta S. K.; Balliet A. G.; Hollander M. C.; Fornace A. J.; Hoffman B.; Liebermann D. A. Hematopoietic cells from Gadd45a- and Gadd45b-deficient mice are sensitized to genotoxic-stress-induced apoptosis. *Oncogene* **2005**, *24,* 7170-9.

26. Gupta M.; Gupta S. K.; Hoffman B.; Liebermann D. A. Gadd45a and Gadd45b protect hematopoietic cells from UV-induced apoptosis via distinct signaling pathways, including p38 activation and JNK inhibition. *J Biol Chem* **2006**, *281,* 17552-8.

27. De Smaele E.; Zazzeroni F.; Papa S.; Nguyen D. U.; Jin R. G.; Jones J.; Cong R.; Franzoso G. Induction of gadd45 beta by NF-kappa B downregulates pro-apoptotic JNK signalling. *Nature* **2001**, *414,* 308-313.

28. Amanullah A.; Azam N.; Balliet A.; Hollander C.; Hoffman B.; Fornace A.; Liebermann D. Cell signalling (communication arising): Cell survival and a Gadd45-factor deficiency. *Nature* **2003**, *424,* 741-742.

29. Takekawa M.; Saito H. A family of stress-inducible GADD45-like proteins mediate activation of the stress-responsive MTK1/MEKK4 MAPKKK. *Cell* **1998**, *95,* 521-530.

30. Selvakumaran M.; Lin H. K.; Miyashita T.; Wang H. G.; Krajewski S.; Reed J. C.;

Hoffman B.; Liebermann D. Immediate early up-regulation of bax expression by p53 but Not TGF-beta-1 - a paradigm for distinct apoptotic pathways. *Oncogene* **1994**, *9,* 1791-1798.

31. Selvakumaran M.; Lin H. K.; Sjin R. T. T.; Reed J. C.; Liebermann D. A.; Hoffman B. The novel primary response gene MyD118 and the protooncogenes myb, myc, and bcl-2 modulate transforming growth factor-beta-1-induced apoptosis of Myeloid-leukemia cells. *Mol Cell Biol* **1994**, *14,* 2352-2360.

32. Zhang W.; Hoffman B.; Liebermann D. A. Ectopic expression of MyD118/GADD45/CR6 (Gadd45 beta/alpha/gamma) sensitizes neoplastic cells to genotoxic stress-induced apoptosis. *Int J Oncol* **2001**, *18,* 749-757.

33. Yoo J.; Ghiassi, M.; Jirmanova, L.; Balliet, A. G.; Hoffman, B.; Fornace, A.J., Jr.; Liebermann, D. A.; Bottinger, E. P.; Roberts, A. B. TGF-beta-induced apoptosis is mediated by Smad -dependent expression of GADD45B through p38 activation. *J. Biol. Chem.* **2003**, *278,* 43001-43007.

34. Vairapandi M.; Azam N.; Balliet A. G.; Hoffman B.; Liebermann D. A. Characterization of MyD118, Gadd45, and proliferating cell nuclear antigen (PCNA) interacting domains. *J Biol Chem* **2000**, *275,* 16810-16819.

35. Azam N.; Vairapandi M.; Zhang W.; Hoffman B.; Liebermann D. A. Interaction of CR6 (GADD45 gamma) with proliferating cell nuclear antigen impedes negative growth control. *J Biol Chem* **2001**, *276,* 2766-2774.

36. Harkin D. P.; Bean J. M.; Miklos D.; Song Y. H.; Truong V. B.; Englert C.; Christians F. C.; Ellisen L. W.; Maheswaran S.; Oliner J. D.; Haber D. A. Induction of GADD45 and JNK/SAPK-dependent apoptosis following inducible expression of BRCA1. *Cell* **1999**, *97,* 575-586.

37. Kojima S.; Mayumi-Matsuda K.; Suzuki H.; Sakata T. Molecular cloning of rat GADD45 gamma, gene induction and its role during neuronal cell death. *Febs Lett* **1999**, *446,* 313-317.

38. Hildesheim J.; Bulavin D. V.; Anver M. R.; Alvord W. G.; Hollander M. C.; Vardanian L.; Fornace A. J. Gadd45a protects against UV irradiation-induced skin tumors, and promotes apoptosis and stress signaling via MAPK and p53. *Cancer Res* **2002**, *62,* 7305-7315.

39. Cazzalini O.; Perucca P.; Riva F.; Stivala L. A.; Bianchi L.; Vannini V.; Ducommun B.; Prosperi E. p21CDKN1A does not interfere with loading of PCNA at DNA replication sites, but inhibits subsequent binding of DNA polymerase delta at the G1/S phase transition. *Cell Cycle* **2003**, *2,* 596-603.

40. O'connor P. M. Mammalian G1 and G2 phase checkpoints. *Cancer Surv* **1997**, *29,* 151-82.

41. Elledge S. J. Cell cycle checkpoints: preventing an identity crisis. *Science* **1996**, *274,* 1664-72.

42. Kufer T. A.; Sillje H. H. W.; Korner R.; Gruss O. J.; Meraldi P.; Nigg E. A. Human TPX2 is required for targeting Aurora-A kinase to the spindle. *J. Cell Biol.* **2002**, *158,* 617-623.

43. Lu B. F.; Yu H.; Chow C. W.; Li B. Y.; Zheng W. P.; Davis R. J.; Flavell R. A. GADD45 gamma mediates the activation of the p38 and JNK MAP kinase pathways and cytokine production in effector T(H)1 cells. *Immunity* **2001**, *14,* 583-590.

44. Yang J. F.; Zhu H.; Murphy T. L.; Ouyang W. J.; Murphy K. M. IL-18-stimulated

GADD45 beta required in cytokine-induced, but not TCR-induced, IFN-gamma production. *Nat. Immunol.* **2001**, *2,* 157-164.

45. Angel P.; Karin M. The role of Jun, Fos and the AP-1 complex in cell-proliferation and transformation. *Biochim Biophys Acta* **1991**, *1072,* 129-57.

46. Karin M.; Liu Z. G.; Zandi E. AP-1 function and regulation. *Curr. Opin. Cell Biol.* **1997**, *9,* 240-246.

47. Shaulian E.; Karin M. AP-1 in cell proliferation and survival. *Oncogene* **2001**, *20,* 2390-2400.

48. Shaulian E.; Karin M. AP-1 as a regulator of cell life and death. *Nat Cell Biol* **2002**, *4,* E131-E136.

49. Li Q. X.; Ke N.; Sundaram R.; Wong-Staal F. NR4A1, 2, 3 - an orphan nuclear hormone receptor family involved in cell apoptosis and carcinogenesis. *Histol Histopathol* **2006**, *21,* 533-540.

50. Moll U. M.; Marchenko N.; Zhang X. K. p53 and Nur77/TR3 - transcription factors that directly target mitochondria for cell death induction. *Oncogene* **2006**, *25,* 4725-4743.

51. Giono L. E.; Manfredi J. J. The p53 tumor suppressor participates in multiple cell cycle checkpoints. *J Cell Physiol* **2006**, *209,* 13-20.

52. Kastan M. B.; Zhan Q. M.; Eldeiry W. S.; Carrier F.; Jacks T.; Walsh W. V.; Plunkett B. S.; Vogelstein B.; Fornace A. J. A mammalian-cell cycle checkpoint pathway utilizing p53 and GADD45 is defective in ataxia-telangiectasia. *Cell* **1992**, *71,* 587-597.

53. Guillouf C.; Grana X.; Selvakumaran M.; Deluca A.; Giordano A.; Hoffman B.; Liebermann D. A. Dissection of the genetic programs of p53-mediated G1 growth arrest and apoptosis - blocking p53-induced apoptosis unmasks G1 arrest. *Blood* **1995**, *85,* 2691-2698.

54. Vogelstein B.; Lane D.; Levine A. J. Surfing the p53 network. *Nature* **2000**, *408,* 307-310.

55. Vousden K. H. p53: Death star. *Cell* **2000**, *103,* 691-694.

56. Andrews G. K. Regulation of metallothionein gene expression by oxidative stress and metal ions. *Biochem Pharmacol* **2000**, *59,* 95-104.

57. Huang Y. C. T.; Li Z. W.; Carter J. D.; Soukup J. M.; Schwartz D. A.; Yang I. V. Fine ambient particles induce oxidative stress and metal binding genes in human alveolar macrophages. *Am J Resp Cell Mol* **2009**, *41,* 544-552.

58. Min K. S.; Morishita F.; Tetsuchikawahara N.; Onosaka S. Induction of hepatic and renal metallothionein synthesis by ferric nitrilotriacetate in mice: the role of MT as an antioxidant. *Toxicol Appl Pharm* **2005**, *204,* 9-17.

59. Kumar A.; Gabbay J. S.; Nikjoo R.; Heller J. B.; O'hara C. M.; Sisodia M.; Garri J. I.; Wilson L. S.; Kawamoto H. K., Jr.; Bradley J. P. Improved outcomes in cleft patients with severe maxillary deficiency after Le Fort I internal distraction. *Plast Reconstr Surg* **2006**, *117,* 1499-509.

Chapter 4 Summary

Nowadays, human exposure to the engineered nanoparticles has become inevitable since nanoparticles are more and more widely used in various industries and products. Among the nanomaterials, metal oxide nanoparticles are widely applied because of their unique properties, but the toxicity of them has also been reported by both *in vitro* and *in vivo* assessments. For the recent controversial reports on the mechanism of zinc oxide nanoparticles (ZnO-NPs) cytotoxicity and the dramatic cytotoxicity of copper oxide nanoparticles (CuO-NPs), we focused on the study on the molecular mechanism of human lung epithelial cells (A549 cells) in response of exposure to them. By analyzing the global gene expression with micro array technology, we proved the ROS was critical not only in toxicity of the transient metal oxide nanoparticles (CuO-NPs) but also in the toxicity of semiconductor metal oxide nanoparticles (ZnO-NPs). Furthermore, we discovered that CuO-NPs and ZnO-NPs produced ROS and killed the cells in the different ways.

In chapter 1, general information on the nanomaterials and the nanotoxicity was introduced to clarify the concepts in present study. Also, the origin of the healthy risk concern about the nanomaterials and the new anxiety raised by the nanotechnology were combed to explain the necessity of our study. The development of nanotoxicity research was summarized and the discrepancies of these studies on nanotoxicity were discussed to explain the object of the present study.

In chapter 2, to clarify the controversial report on the cytotoxicity of ZnO-NPs, we tried to identify the respective contributions of the released zinc and the solid particles to the cytotoxicity of ZnO-NPs, we exposed A549 cells to the ZnO-NPs suspensions, their extractions collected with centrifugation and the medium containing zinc chloride ($ZnCl_2$), then we assayed the cytotoxicity with water soluble tetrazolium salts (WSTs) and the intracellular reactive oxygen species (ROS) with the 2`,7`- dichlorodihydrofluorescin diacetate (DCFH-DA). Only

the ZnO-NPs suspension brought about the cytotoxicity and the increase of intracellular ROS; the extractions and $ZnCl_2$ had no effect on the cells. However the subsequent global gene expression analysis revealed that “cadmium binding category” was the only one gene functional category which was up-regulated not only by $ZnCl_2$ medium also by ZnO-NPs suspension. This category consisted of metallothioneins (MTs), the important zinc-toxicity neutralizing proteins. We inhibited the over expression of MTs with the corresponding siRNA, and found that the released zinc contributed to the ZnO-NPs cytotoxicity. We conclude that both of the solid particles and the released zinc contribute to the ZnO-NPs cytotoxicity, further we propose the synergic relationship of them through disabling the MTs via ROS.

In chapter 3, the toxicity mechanism of CuO-NPs was discussed with global gene expression analysis because CuO-NPs were proved to be the most toxic nanoparticles among the most widely used nanomaterials. With the same analysis methods, this study proposes a molecular mechanism for lung epithelial A549 cell response to CuO-NPs related to Cu ions released from CuO-NPs with the same analysis methods as in previous ZnO-NPs research. Cells that survived the exposure to CuO-NPs arrested the cell cycle as a result of the down-regulation of proliferating cell nuclear antigen (PCNA), cell division control 2 (CDC2), cyclin B1 (CCNB1), target protein for Xklp2 (TPX2), and aurora kinase A (AURKA) and B (AURKB). Furthermore, cell death was avoided through the induced expression of nuclear receptors (NR4A1 and NR4A3) and growth arrest and DNA damage-inducible 45 β and γ (GADD45B and GADD45G, respectively). The down-regulation of CDC2, CCNB1, TPX2, AURKA, and AURKB, the expressions of which are involved in cell cycle arrest, was attributed to Cu ions released from CuO-NPs into medium. NR4A1 and NR4A3 expression was also induced by Cu ions released into the medium. The expression of GADD45B and GADD45G activated the p38 pathway that was involved in escape from cell death. The upr-egulation of GADD45B and GADD45G was not observed with Cu ions released into medium but was observed in cells exposed to CuO-NPs. However, because the expression of the genes was also induced by Cu ion

concentrations higher than that released from CuO-NPs into the medium, the expression appeared to be triggered by Cu ions released from CuO-NPs taken up into cells. We inferred that, for cells exposed to CuO-NPs, those able to make such a molecular response survived and those unable to do so eventually die.

Achievements

Publications

1) Fei Zhuang, Nobutaka Hanagata. Synergic toxicity of solid particles and released zinc of zinc oxide nanoparticles to human lung epithelial cells. Nano Medicine 20102; 4(2): 90-102.

2) Nobutaka Hanagata, **Fei Zhuang,** Sarah Connolly, Jie Li, Nobuhiro Ogawa, Mingshen Xu. Molecular responses of human lung epithelial cells to the toxicity of copper oxide nanoparticles inferred from whole genome expression analysis. ACS Nano 2011; 5: 9326-9338.

3) Nobutaka Hanagata, Mingsheng Xu, Taro Takemura, **Fei Zhuang**. Cellular Response to ZnO nanoparticle toxicity inferred from global gene expression profiles. Nano Medicine 2010; 2(2): 153-169.

4) Fei Zhuang, Biao Ding; Biological Evaluation within a Risk Management Process. Chinese Journal of Medical Instrumentation, 2007, 31(04): 280-283.

5) Fei Zhuang, Qiqing Zhang;The progress of identification and isolation of epidermal stem cells [J]. Biomedical Engineering Foreign Medical Sciences 2004; 27(2): 108 – 111.

Presentations

1) 庄菲 花方信孝 Response of human epithelial cells to the exposure to zinc oxide nanoparticles. 6th Annual Meeting of Nano Biomedical Society, Jul. 2012.

2) 庄菲 花方信孝 Response of human epithelial cells to the exposure to copper oxide nanoparticles.北海道大学生命科学融合生命科学若手シンポジウム 平成 23 年 3 月、札幌

Acknowledgments

There are numerous people I would like to thank for getting me to this point. During my Ph. D. study, I got a lot of lot of help and cheers both in the academic field and daily life. Hopefully I can express my gratitude to you all in person.

First of all, I would like to express my sincere gratitude to my supervisor Prof. Nobutaka Hanagata for the continuous help, support an scientific guiding during my Ph.D. study. He took me into his field, gave me an interesting research topic to work on and helped me improve in the scientific field. His patience and understanding really supported supported me during the study. I have learned so many things during the discussion and talking with him. The successful accomplishment of the present htesis is mainly attributed to his guide and valuable advice.

I am very grateful to my supervisor, associate Prof. Tomohiko YAMAZAKI, for his constant support during my Ph. D. study. He gave me a lot of help and care in my daily life.

I would like to express my special gratitude to Ms. Akemi Hoshikawa, for her kindness in helping me solving all problems in my work and daily life. She is such an elegant lady and always ready to support me when I need help. Without her help, I probably would not adapt myself to the life and work in Japan.

I want to thank all the fantastic people in the Biosystem and Biomolecule Control Group for the pleasant working environment and helpful discussion. Dr. Yoshihisa Kaizuka, Dr. Song Chen, Ms. Ling zhang, Mr. Huijie Zhang, Ms. Fei Zhuang, Ms. Suwarti , thank you all.

I would like to thank Dr. Takashi MINOWA, Ms. Hiromi, Dr. Tairo TAKEMURA, MORITA, Dr. Jie LI, Dr. Xianglan LI, Ms. Shoko KAJIWARA, and from Nano Invitation Center of National Institute for Materials Science, for their supporting and suggestions during my research.